2014

Predicted Risk of Post-Irradiation Cerebral Necrosis in Pediatric Brain Cancer Patients: A Treatment Planning Comparison of Proton Therapy vs. Photon Therapy

Derek Freund
Louisiana State University and Agricultural and Mechanical College, dfreun1@lsu.edu

Recommended Citation

Freund, Derek, "Predicted Risk of Post-Irradiation Cerebral Necrosis in Pediatric Brain Cancer Patients: A Treatment Planning Comparison of Proton Therapy vs. Photon Therapy" (2014). *LSU Master's Theses*. 3389.
https://digitalcommons.lsu.edu/gradschool_theses/3389

PREDICTED RISK OF POST-IRRADIATION
CEREBRAL NECROSIS
IN PEDIATRIC BRAIN CANCER PATIENTS:
A TREATMENT PLANNING COMPARISON OF
PROTON THERAPY
VS.
PHOTON THERAPY

A Thesis

Submitted to the Graduate Faculty of the
Louisiana State University and
Agricultural and Mechanical College
in partial fulfillment of the
requirements for the degree of
Master of Science

in

The Department of Physics and Astronomy

by
Derek H. Freund
B.S., University of Missouri – Columbia, 2001
B.A., University of Missouri – St. Louis, 2009
December 2014

This work is dedicated to my wife, Andrea
Without whom none of this would be possible
And son, Liam
The joy of my life

Acknowledgments

I would like to thank my advisor, Dr. Rui Zhang, for taking time out of his busy schedule to help me on this project. I would also like to express my gratitude to the other members of my advisory committee: Drs. Wayne Newhauser, Oleg Vassiliev, Mary Ella Sanders, and John DiTusa. Additionally I would like to thank Dr. Shiao Woo who has consulted on this project. Their feedback into this project and assistance along the way helped move this project to completion.

I would like to thank the dosimetrists at Mary Bird Perkins Cancer Center: Frank Apollo, Eddie Singleton, and Chad Dunn for taking the time to field question and better understand the delicate art of treatment planning.

Additionally I would like to thank my classmates: Margaret Hernandez, Melissa Lamberto, Ben Rusk, Bart Morris, Tony Mazza, and Chris Schneider. We have been an inseparable crew over the last few years and I will miss you all fondly. Particularly I would like to thank Margaret Hernandez who had a project very similar to mine and with whom I was able to talk out some of the issues we were having.

I would like to thank Dr. Thomas Merchant for some helpful discussions about risk models and insight that he had in this project.

I would like to thank Yvonne Thomas, Katie Bailey, Susan Hammond, and Page Barcia who have graciously helped in administrative aspects of my graduate career.

Finally I would like to thank my wife, Andrea who has sacrificed so much over the years to get us here and has brought into our life my proudest achievement, my son Liam. Without you, Andrea, I never would have made it here. I love you both very much!

iii

Table of Contents

List of Tables

List of Figures

Abstract

Purpose: To predict the risk of radiation necrosis in a cohort of pediatric patients with glioma and ependymoma and compare the predicted risk between volumetric modulated arc photon therapy (VMAT), passively scattered proton therapy (PSPT) and intensity modulated proton therapy (IMPT).

Methods: Thirteen pediatric patients with varying age and sex were selected for this study. A radiation oncologist contoured a clinical treatment volume (CTV) on 8 patients selected for glioma in the cerebral hemisphere and 5 with ependymoma located in the posterior fossa. A 1 cm margin was added to the CTV to define the planning treatment volume (PTV). VMAT plans were constructed using Phillips Pinnacle treatment planning system. PSPT and IMPT plans were constructed using Varian Eclipse. Plans were compared using several dose metrics to ensure consistency between plan coverage. Normal tissue complication probability (NTCP) with radiation necrosis as an endpoint was calculated using the Lyman Kutcher Burman probit model. The ratio of risk was calculated between protons and photons and compared to a value of 1 using the student t-test and Wilcoxon signed rank test. Sensitivity tests were performed to determine if the predicted risk of necrosis was sensitive to positional errors, proton range errors and selection of risk models.

Results: PSPT plans resulted in an average ratio of risk of 0.44 ($p<0.00001$) and 0.62 ($p<0.02$) for glioma and ependymoma patients compared to VMAT respectively. IMPT plans resulted in an average ratio of risk of 0.33 ($p<0.00001$) and 0.32 ($p<0.00001$) for glioma and ependymoma plans compared to VMAT respectively.

Conclusion: Both PSPT and IMPT plans statistically significantly reduced the predicted risk of radiation necrosis using the LKB NTCP risk model. Sensitivity analysis upheld these qualitative findings.

Chapter 1   : Introduction

1.1   Background

Cancer of the brain and central nervous system (CNS) is the second most common of all pediatric cancers. At a rate of 5.1 out of every 100,000 cases per year, its incidence is second only to leukemia and there are approximately 4300 new cases of primary malignant and non-malignant brain and CNS tumors expected every year within the United States (Dolecek *et al.*, 2012). Due to improved medical techniques, the cure rate for these diseases has steadily increased. The research focus has shifted to disease and treatment related side effects. The focus of this work is to compare the predicted risks of radiation-induced necrosis of the brain using several contemporary types of radiotherapy.

1.2   Pediatric Brain Cancer Epidemiology

The Surveillance Epidemiology and End Result (SEER) program reported that astrocytomas make up 52% of pediatric brain cancers, followed by Primitive Neuroectodermal Tumors (PNET) (21%), other gliomas (15%) and Ependymomas (9%) (Ries *et al.*, NIH Pub. No. 99-4649). These main types of pediatric brain tumors are broadly classified as tumors of the neuroepithelial tissue because of their involvement of the epithelium or covering of the external surface of the nerves (Louis *et al.*, 2007). These tumor types can further be classified by their grade and location in the brain. Cerebral tumors are those that the primary tumor site is located above the cerebellar tentorium. The tentorium is an extension of the dura mater into the space between the cerebellum and the inferior occipital lobes in the brain. Cerebral tumors are supratentorial because they are located above this demarcation, whereas cerebellar tumors are infratentorial because the primary tumor lies within the cerebellum in the posterior fossa.

Astrocytomas are a type of glioma that arise in the astrocyte cells of the brain (Halperin *et al.*, 2010). A majority of these tumors in children are pilocytic astrocytomas which are considered low grade by the World Health Organization (WHO) grading system, and will not spread far from the primary tumor site (Pizzo and Poplack, 1997). These low-grade pilocytic astrocytomas can be found supratentorially in the brain or infratentorially in the cerebellum. High-grade astrocytomas such as anaplastic astrocytoma (WHO grade III) and glioblastoma (WHO grade IV) are less common among children and are typically found supratentorially (Pizzo and Poplack, 1997; Louis *et al.*, 2007).

PNET is a broad classification of tumors that involve the neuroectoderm of the brain. This tumor classification includes neuroblastoma, pineoblastoma and medulloblastoma, although medulloblastomas comprise more than half of the primitive neuroectodermal tumors that are seen in pediatrics (De Laney and Kooy, 2008). Medulloblastomas are often found medially in the cerebellum in a region known as the vermis that resides in the posterior fossa of the cranium. Medulloblastoma is one of the most common malignant primary brain tumors in pediatrics and has a tendency to seed new tumors via the cerebrospinal fluid requiring radiation treatments of the entire craniospinal cavity (De Laney and Kooy, 2008; Pizzo and Poplack, 1997).

Ependymomas are a type of tumor that occur in the ependymal cells of the CNS. In children a majority of these occur intercranially within the posterior fossa in the lining of the 4th cerebral ventricle (Pizzo and Poplack, 1997; De Laney and Kooy, 2008; Schild *et al.*, 1998). Although most are infratentorial in children they can occur supratentorially or

spread contiguously above the tentorium or into adjacent brain tissue (Pizzo and Poplack, 1997).

1.3   Standards of Care

Standards of care for selected pediatric brain cancers considered in this work will be discussed for proton and photon radiotherapies in this section.

1.3.1   Astrocytoma

1.3.1.1   Low Grade

Most of the low-grade gliomas that are located supratentorially in children are astrocytomas. Treatment for these tumors often depends on the amount of surgical resection that can be achieved. If gross total resection can be achieved, then many times no other treatment may be necessary. If the tumor cannot be completely resected, then radiation therapy and/or chemotherapy may be used(Pizzo and Poplack, 1997).

When radiation therapy is used the typical prescription is 50-60 Gy in 1.8-2Gy/fraction to the Gross Tumor Volume (GTV) plus a geometric expansion of 2 cm to account for subclinical disease and patient setup error (Pizzo and Poplack, 1997).

1.3.1.2   High grade

High-grade anaplastic astrocytomas are typically seen in the cerebral hemispheres in children. Due to the aggressive nature of these tumors gross total resection is often not possible due to the danger of increased neurological morbidity (Pizzo and Poplack, 1997). Often surgery is followed by radiation therapy to a dose of 50-60 Gy in 1.8-2 Gy/fraction to the GTV plus a geometric expansion of 2-4 cm (Pizzo and Poplack, 1997).

1.3.2   Ependymoma

Ependymomas are often located infratentorially, making gross total resection much more difficult due to the proximity of the brainstem (Halperin *et al.*, 2010). Most often, surgery is followed by radiation therapy. For photon therapy, the prescription is typically 50-55 Gy in 1.8-2 Gy/fraction to the planned treatment volume (PTV) which includes the GTV plus a geometric expansion of 1-2 cm (Halperin *et al.*, 2010). Proton therapies have been administered up to 59.4 Gy-RBE to the PTV which includes the GTV plus 2-5 cm expansion (De Laney and Kooy, 2008).

1.4   Side Effects of Radiotherapy

The potential risk of injury from CNS irradiation can include acute effects and late effects. Acute affects are seen early and can include alopecia, erythema, otitis, tinnitus, or even temporary demyelination (Pizzo and Poplack, 1997). Alternatively late effects onset more than 6 months after treatment, tends to be more severe and include spinal myelopathy, endocrine and cognitive dysfunction, secondary cancers, and radiation induced necrosis (Haas-Kogan *et al.*, 2010). With approximately 72% and 73% five-year survival rate after treatment of patients with primary brain and CNS tumors between the ages 0-14 and 0-19, respectively, the risk of late effects when treating pediatric patients with radiation is a major concern (Ostrom *et al.*, 2013). The primary focus of this investigation is to predict the risk of the late effect of radiation-induced necrosis.

1.5   Radiation necrosis

Radiation induced necrosis (RIN) is a late effect that can have a latency of as little as 3 month or as long as 13 year after treatment (Fink *et al.*, 2012). Little is known about the mechanism by which radiation-induced necrosis occurs but it has been suggested by

4

Fink *et al.* (2012) that it may be a result of ischemia resulting from vascular endothelial injury or from the loss of or injury to oligodendrocytes. Due in part to a long latency, difficulty of diagnosis, and apparently low incidence, the true incidence of RIN is poorly known (Chao *et al.*, 2013). Some reports indicate that depending on the treatment protocol the actual incidence could be anywhere from 3-24% (Ruben *et al.*, 2006).

Necrosis varies in severity from asymptomatic radiographic changes, cognitive dysfunction, stroke to death. Current treatments include surgery, corticosteroids, anticoagulants, hyperbaric oxygen therapy, laser interstitial thermal therapy and VEGF inhibitors (Bennett *et al.*, 2005; Ashamalla *et al.*, 1996; Chuba *et al.*, 1997; Delanian and Lefaix, 2007; Gonzalez *et al.*, 2007; Wong *et al.*, 2008; Whelan and Helms, 2012). Treatment of necrosis is, at most, effective in treating the symptoms but to date little has done to treat the cause of necrosis. Additionally some of the mostly widely used treatments, such as corticosteroids, have risks associated with prolonged use and others have too few studies to support their widespread use or have been shown to have little effect (Delsigne, 2012; Bennett *et al.*, 2012).

Although there are many unknowns, we do know that risk of necrosis is associated with the total dose that is given to the patient, the total volume irradiated, and the fraction size (Lawrence *et al.*, 2010; Lee *et al.*, 1998; Fink *et al.*, 2012; Murphy *et al.*, 2012). Other potential risk factors include concurrent chemotherapy, age at exposure, treatment modality, etc. (Lee *et al.*, 2011; Lawrence *et al.*, 2010). To date little has been done to explore the difference between photon and proton treatment modalities and their effect on risk reduction for radiation necrosis as an endpoint.

Recent retrospective studies have assessed some of these risk parameters. A recent study on the quantitative analysis of normal tissue effects in the clinic (QUANTEC) looked at the radiation dose-volume effects in the brain (Lawrence *et al.*, 2010). Their result indicates that the dose to cause radiation is high with a predicted 5% and 10% risk of symptomatic necrosis to occur at 72 Gy and 90 Gy given in 2 Gy/fraction increments (Lawrence *et al.*, 2010). Additionally they added that fractions sizes greater than 2 Gy increased the risk. Another recent study by Murphy *et al.* (2012) found that the percentage of the infratentorial brain receiving 50, 52 and 54 Gy were significant predictors of risk for necrosis for pediatric being treated for craniopharyngioma. Also Ruben *et al.* (2006) found that the risk of necrosis increases with increasing dose, fraction size and the addition of chemotherapy.

All of the above studies were based on patients treated with photon therapy. Boehling *et al.* (2012) compared intensity modulated photon therapy (IMRT) with intensity modulated proton therapy (IMPT) for pediatrics with craniopharyngioma and found IMPT spared dose to the cerebral vasculature compared to IMRT. Other studies have found similar effects of normal tissue sparing for pediatric medulloblastoma when comparing passively scattered proton therapy (PSPT) to conventional photon therapy (Howell *et al.*, 2012).

1.6   Significance and Objective

Although the expected incidence of radiation-induced necrosis may be low it is a severe and potentially lethal late effect that can extremely impact these patients quality of life. Volumetric modulated arc therapy (VMAT) is a rotational arc photon therapy that can provide a highly conformal dose to the tumor but also increase the volume of normal

tissue surrounding the treatment area that receives low dose (Myrehaug *et al.*, 2012; Qi *et al.*, 2012). Passively scattered (PSPT) and intensity modulated proton therapy (IMPT) can also provide highly conformal dose distributions but reduce the volume of brain tissue receiving low dose (Boehling *et al.*, 2012). However, due to competing dose heterogeneity effects that are often seen in proton therapy there may be significant hotspot formation (Urie *et al.*, 1984). These competing dose and volume effects are not well understood and need to be better quantified. To date there have been no studies comparing the effectiveness of Volumetric modulated arc photon therapy to passively scattered and intensity modulated protons therapy to reduce the predicted risk of necrosis in pediatrics following radiation. The objective of this study is to predict the ratio of risk of radiation-induced necrosis in a cohort of pediatric patients between VMAT and PSPT and between VMAT and IMPT.

1.7   Hypothesis

Due to the reduction in irradiated volume that protons confer and additional dose inhomogeneities that may result in hotspot formation we hypothesized that: For a clinically representative cohort of pediatric brain cancer patients, passively scattered and intensity modulated proton therapy plans will offer no statistical difference in the predicted risk of radiation-induced necrosis of the brain using existing risk models compared to VMAT.

To test this hypothesis, we performed the following specific aims:

Aim 1: Evaluate and compare VMAT, PSPT and IMPT plans on the basis of dosimetric endpoints for the PTV and whole brain.

<u>Aim 2</u>: Predict the risk of radiation necrosis incidence for VMAT, PSPT and IMPT plans for the cohort of pediatric patients using existing risk models to determine if the relative risk is statistically significantly different between treatment modalities.

<u>Aim 3</u>: Perform sensitivity analysis to determine if the baseline risk is dependent on setup error, proton range uncertainties and selection of risk model.

Chapter 2   : Methods

2.1   Aim 1 – Design and Evaluation of Radiation Treatment Plans

2.1.1   Patient Sample

A patient database was constructed with 13 anonymized CT data sets from pediatric patients with varying age, sex and treatment sites. These patients were consecutively sampled from patients that were previously treated with proton CSI at the University of Texas at M.D. Anderson between 2007 and 2009. Inclusion criteria were that patients be between 2 and 16 years old at the time of treatment. Exclusion criteria were severe edema from the original CSI treatment and/or the insertion of a stint. Five of these patients were used for our ependymoma comparison and 8 for the astrocytoma (glioma) comparison. A list of these patients based on age, sex and disease type can be seen in Table 2.1.

Table 2.1 Patient index, age, sex and diagnosis used for the study

Patient index	Age at treatment	Sex	Assigned Diagnosis*
1	2	F	Glioma
2	4	M	Glioma
3	6	F	Glioma
4	8	F	Glioma
5	10	F	Glioma
6	4	M	Glioma
7	6	M	Glioma
8	8	M	Glioma
9	10	M	Ependymoma
10	12	F	Ependymoma
11	13	F	Ependymoma
12	16	F	Ependymoma
13	16	F	Ependymoma

*Note: Diagnoses were assigned were assigned for the purposes of this study and were different from the diagnoses listed in the medical records

2.1.2 Contouring of Target Volume and Healthy Tissue

Contouring was performed in Phillips Pinnacle treatment planning system. A clinical treatment volume (CTV) was created for each patient by the same board certified radiation oncologist to represent the glioma and ependymoma gross tumor volume (GTV) plus any subclinical disease that may exist. An additional 1 cm margin was then added to the CTV to define the planned treatment volume (PTV). This additional PTV margin accounts for patient setup error. A PTV reduction of no more than 0.5cm was allowed to account for organs at risk or boney anatomy.

Additional contours included a partial brain contour that was constructed by subtracting the PTV plus an additional 1 cm margin from the brain contour. This structure was used in plan optimization. Other contours used for treatment planning included the brainstem, optic chiasm, optic nerve, spinal cord, eyes, and lens of the eye. These structures were used for each patient across all planning modalities for consistency.

2.1.3 Treatment Plans

A prescription dose of 54 Gy in 1.8 Gy/fraction over 30 fractions was used for all patients. Plans were considered provisionally acceptable when the dose to 95% of the PTV ($D_{95\%}$) was 95% (51.3 Gy) of the prescription for glioma plans and 90% (48.6 Gy) for ependymoma plans. These dose objectives were maintained unless the constraint for the optic chiasm (50 Gy) or brainstem (54 Gy) was not met. Some other organs at risk and their dose tolerance limits can be seen in Table 2.2.

The relative biological effect (RBE) of Protons is greater than that of photons. The mean relative biological effectiveness (RBE) of protons between the energies of 60

MeV and 250 MeV is 1.1 as reported by ICRU report 78. This generic value of 1.1 is recommended by ICRU report 78 to account for the increase in RBE when reporting proton dose. This convention was used in our proton plans and dose reported in this research were assigned the unit Gray-RBE (Gy-RBE). Gy-RBE was also used to report photons dose. This convention for photons was used for simplicity of reporting units and equivalent to dose of photons in Gray (Gy) assuming an RBE of one compared to protons.

Table 2.2 Normal tissue radiation tolerance for pediatrics for various organs at risk (Haas-Kogan *et al.*, 2010; Hall and Giaccia, 2012).

Structure	Late Effect	Pediatric Threshold Dose
Spinal cord	Chronic progressive myelitis	45 Gy
Brain	Radiation necrosis Intellectual deficits	54 Gy 12-18 Gy
Lens of eye	Cataract formation	6 Gy
Retina	Radiation retinopathy	30-35 Gy
Optic nerve	Optic neuritis	50 Gy
Inner ear	Sensorineural hearing loss	40-50 Gy
Brainstem	Necrosis	54 Gy

2.1.3.1   Photon Plans

Volumetric Modulated Arc Therapy (VMAT) was selected for this study due to the increased dose conformity and the age of the patients that have to undergo radiation therapy. Although our patient demographic had some adolescent (12-16y), younger patients would likely require anesthesia during treatment for immobilization. VMAT offers a reduction in the treatment time need to deliver a highly conformal dose to the

treatment volume and therefore the time that the pediatric patient will have to spend under anesthesia (Otto, 2008).

The use of VMAT gives us the ability to vary the arc angle through which the patient gets treated. The selection of a partial arc vs. a full 360-degree arc was determined by the location of the PTV isocenter, coverage of the PTV and reduction of dose in the surrounding brain. For all patients, full arc and partial arc plans were created. If the tumor was non-centrally located within the brain, PTV coverage could typically be achieved with 2 partial arcs up to 225 degrees per arc. Additionally this setup would reduce the extra brain dose. If good PTV coverage could not be achieved then a full was selected for treatment.

Most of the glioma patients had non-centrally located tumors and were planned with 2 partial arcs. For gliomas located in the right cerebral hemisphere typical start and stop angles were 45 and 181 degrees, respectively, starting with a counter clockwise rotation followed by a clockwise rotation and where a gantry angle of zero refers to the gantry position at top center. For patient 7, who had a glioma located in the left cerebral hemisphere, the gantry rotated counter clock wise from 179 degrees to 320 degrees.

Ependymoma patients had treatment volumes that were centrally located and good PTV coverage could not be achieved with a partial arc. All of these patients were planned using a full arc rotating counter clock wise from 179 degrees to 181 degrees.

The selection of 6 MV beam energy for VMAT plans was based on several factors. Several studies have shown that there is little benefit to using higher beam energies (Pasler *et al.*, 2011). Additionally, with beam energies of 10 MV and greater,

photonuclear interactions lead to unwanted neutron contamination in the beam and additional dose to the patient (Attix, 2007). For this reason, 6MV was used in all cases.

For both partial and full arc treatments the partial brain contour was used to help optimize VMAT plans. In many ways this is the same as creating a "ring" structure surrounding the PTV to achieve a sharper dose falloff outside of the PTV and increase conformity within the PTV. An example of the partial brain structure can be seen in Figure 2.1.
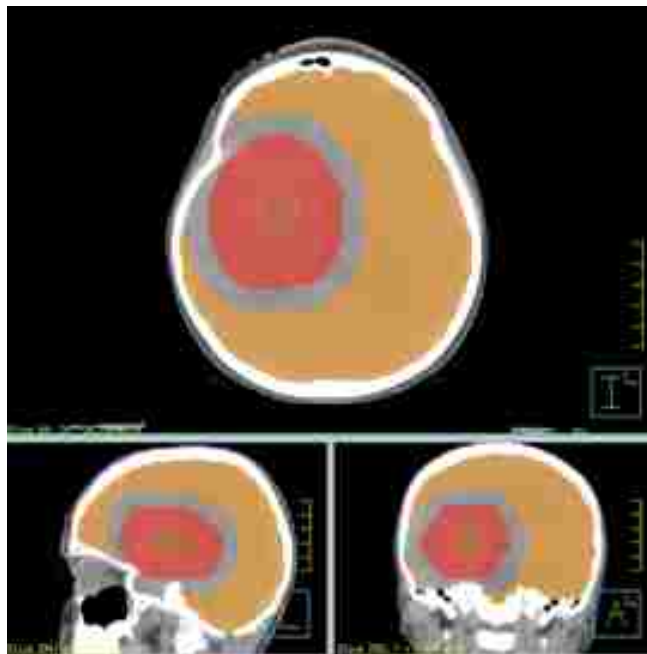
Figure 2.1. The partial brain contour, shown in orange colorwash, surrounds the PTV shown in red color wash with an additional 1 cm margin (shown as grey brain tissue). This contour was used for VMAT optimization to reduce the dose to the normal brain tissue surrounding the PTV and achieve a sharper dose fall off outside of the PTV.

The parameters for VMAT dose optimization can be seen in Table 2.3 These objectives were set at or below the dose threshold limits for organs at risk listed in Table 2.2. After an initial VMAT optimization was run the criteria were adjusted until an provisionally acceptable plan was produced.

The criteria for acceptability were based on the dose to the PTV as well as the organs at risk (OAR). These criteria differed for disease type and was set to $D_{95\%} = 95\%$ for the glioma PTV and $D_{95\%} = 90\%$ for the ependymoma PTV. Additionally the brainstem and optic chiasm where set as dose constraints so that the dose to these structures was limited even if the dose to the PTV suffered. Final acceptability of the plans was determined according to an assessment by a board certified radiation oncologist based on the standard-of-care evaluation methods and subjective judgment. The provision plans were modified, if needed, until final acceptance by the radiation oncologist. The workflow for VMAT planning can be seen in Figure 2.2.

Table 2.3 Initial optimization parameters for VMAT and IMPT plans. The objective represents a limit. Max Dose is a upper limit of dose that the planning system optimizes to stay below for the entire structure. Max DVH is an upper limit for a dose that the planning system optimizes to stay below for the specified percentage of the volume. The weighting is the preference given to the specified objective for optimization

Region of interest	Objective	Dose (Gy)	Volume (%)	Weighting
PTV	Max Dose	56.7	0	90
	Uniform Dose	54.0	100	90
Brain Stem	Max Dose	54.0	0	8
	Max DVH	25.0	25	3
Optic Chiasm	Max Dose	40.0	0	1
	Max DVH	30.0	50	1
Lt. Optic Nerve	Max Dose	28.0	0	1
	Max DVH	12.0	15	1
Rt. Optic Nerve	Max Dose	28.0	0	1
	Max DVH	12.0	15	1
Spinal Cord	Max Dose	3.0	0	1
Lt. Eye	Max Dose	18.0	0	1
Rt. Eye	Max Dose	18.0	0	1
Lt. cochlea	Max Dose	40.0	0	1
Rt. cochlea	Max Dose	40.0	0	1
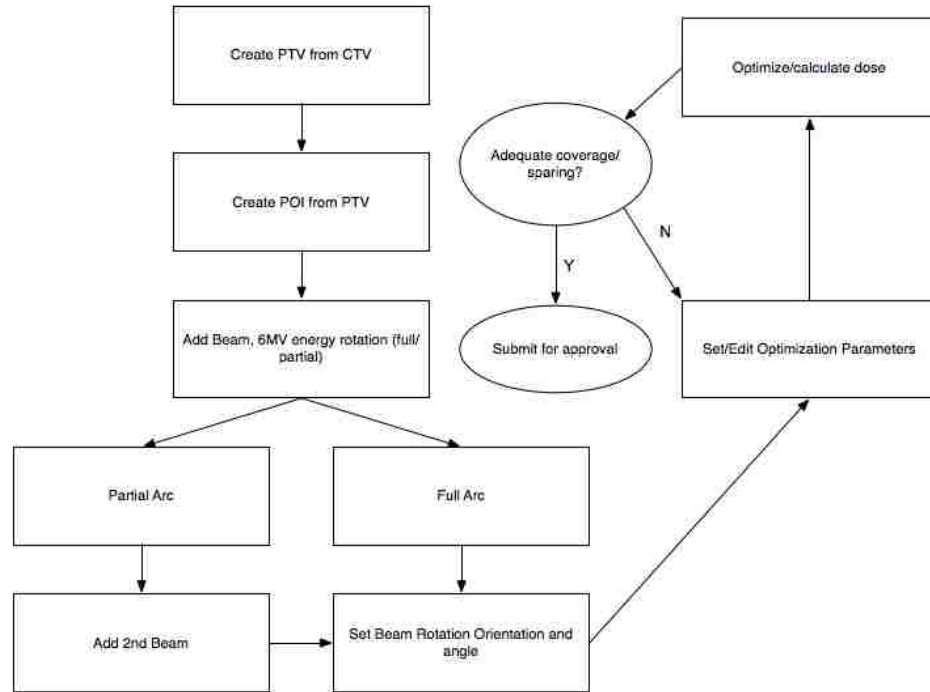
Figure 2.2. VMAT treatment planning workflow.

2.1.3.2 Proton Treatment Plans

Patients were planned using protons with the passively scattered technique and intensity modulated technique. Passively scattered proton therapy (PSPT) employs the use of a beam spreader and of a range compensator. The field is conformed laterally by a block made of brass and the distally using a compensator that is milled out of lucite to conform to the distal surface of the treatment volume. Intensity modulated proton therapy (IMPT) is a form of dynamic beam delivery using multiple beams angles to deliver a highly conformal dose to the PTV. Dynamic beam delivery incorporates the use of scanning magnets to deflect a pencil beam of protons and deliver a single spot of dose to a desire location within the PTV. This is repeated spot by spot in layers across the PTV until the desired uniform dose is delivered to the entire treatment volume.

2.1.3.2.1 Passively Scattered Proton Therapy (PSPT) Treatment Plans

Passively scattered proton therapy plans, in most cases, were planned using a
single field using the double scatter technique. The benefit of using a single field was to
reduce dose to surrounding normal brain tissue while still offering adequate PTV
coverage. In circumstances where PTV coverage was not adequate, more than one beam
was used to attain adequate coverage. Beam angle for PSPT varied from plan to plan and
were dependent on the location of the tumor as well as other factors such as normal
incidence with patient boney anatomy, reduction of heterogeneities within the beam line,
reduction of critical structures within the beam line and reduction of excess brain tissue
irradiatied.

After beam angles were set additional beam specific proximal margins (PM) and
distal margins (DM) had to be determined due to range uncertainties inherent in proton
beam therapy (Li, 2012). Equations (1) and (2) were used in accordance with previously
defined techniques by Moyers *et al.* (2001) for approximating the additional margins with
respect to the CTV.

$$\text{DM on CTV} = [(3.5\% \text{ x distal CTV depth}) + 3 \text{ mm}] \tag{1}$$

$$\text{PM on CTV} = [(3.5\% \text{ x (proximal CTV depth}) + 3 \text{ mm}] \tag{2}$$

where the 3.5% change is to account for conversion of the Hounsfield unit to proton
stopping power and the additional 3mm accounts for the inaccuracies in the proton
planning algorithm

For lateral margins the double scattering technique employs the use of a block or
collimator. This collimator is constructed from a piece of brass that is milled to match

the desired target shape. An example of this aperture can be seen in Figure 2.3. Equation

(3) was used to determine the initial additional aperture margin.

$$\text{Lateral Margin} = \text{PTV margin} + 95\%\text{-}50\% \text{ Penumbra} \tag{3}$$

where an additional margin is added to the PTV margin to account for the 95%-50%

beam penumbra. In most cases this additional margin was small (4 mm or less) and the

plans were checked for adequate lateral dose coverage

Figure 2.3 Proton collimator with custom milled aperture. (Varian Medical Systems)

A range compensator achieved distal coverage of the passive scattered proton

plans. The range compensator is typically made from Lucite and is milled to differential

depths depending on the distal shape of the PTV. An example of a range compensator

can be seen in Figure 2.4. The purpose of the range compensator is to reduce the proton

beam energy in regions where the compensator is thicker and less in regions where it is

thinner, thereby changing the range of the protons beam to conform to the distal edge of

the PTV. A smearing of 13-14 mm was used to account for patient misalignment and to

account for any motion during treatment. This value defaults to the compensator margin

and was not changed during planning. A border smoothing value of 1 cm was used for

planning. This default value is recommended to ensure that steep gradients below the

compensator edge are avoided in order to reduce large dose gradients at the field edge.

Figure 2.4. Lucite proton range compensator (Varian Medical Systems).
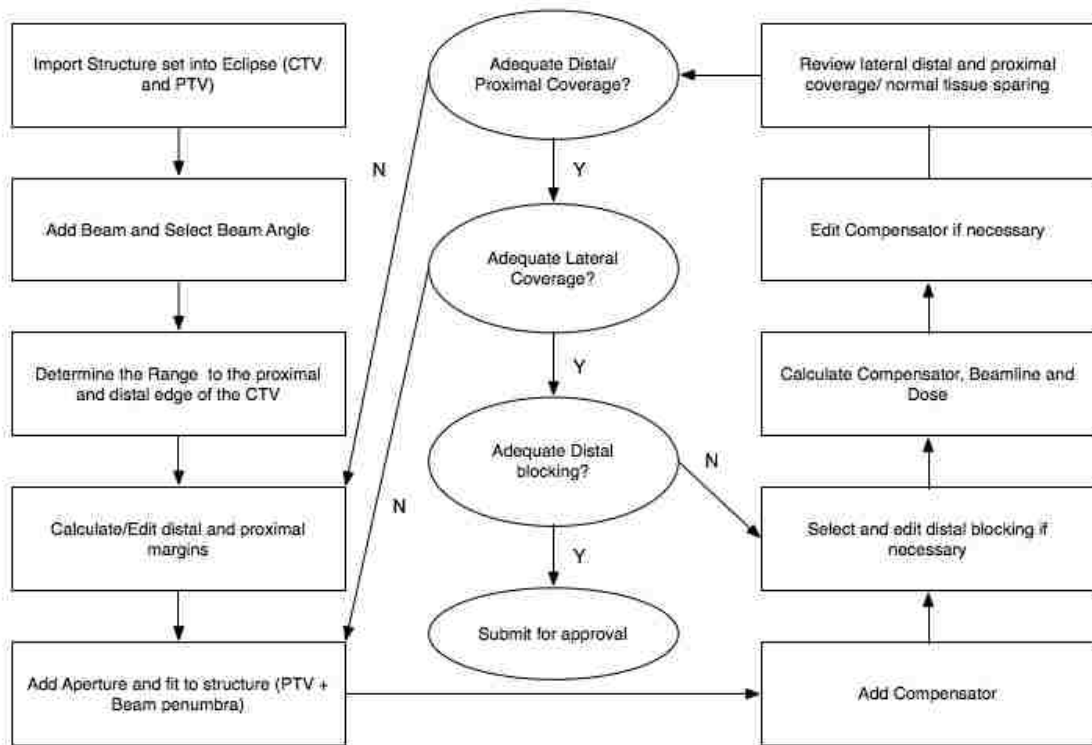
Figure 2.5. PSPT planning workflow.

After the beam line was configured with the collimator and compensator, the plan

dose was calculated. Additional edits were made to the compensator by adding or

removing material to try and attain adequate distal and lateral coverage of the PTV. In

certain situations distal blocking was added to reduce the dose to critical structures distal to the PTV. Distal blocking reduces the initial distal margin assigned to the plan and increases the compensator thickness in the designated region, thereby reducing the penetration range of the protons within the patient. As with the VMAT plans initial acceptance was based on the dose to the PTV as well as critical structures. Once PTV coverage and critical structure dose constraints were met, plans were submitted for final approval to a radiation oncologist. The planning workflow for double scattered proton plans can be seen in Figure 2.5

2.1.3.2.2   Intensity Modulated Proton Therapy (IMPT) Treatment Plans

Intensity modulated proton plans used the same PTV and CTV as the VMAT and passive scattered proton plans. For most patients a 3-beam IMPT plan was constructed to ensure adequate distal, proximal, and lateral coverage of the PTV. This 3 beams arrangement in general was composed of a right lateral beam, a left lateral beam and a posterior/anterior (PA) beam. However the angles of the beams were allowed to vary to some degree to ensure that the beam was en face, to reduce beam line heterogeneities and for critical structure avoidance (brainstem, optic chiasm, etc.)

Additional margins to account for proton range uncertainties for IMPT on a beam by beam basis cannot currently be achieved in the Varian Eclipse v11.0 treatment planning system. Additionally, there is no good technique in IMPT to account for these uncertainties on a beam by beam basis (Hoppe *et al.*, 2010). Therefore, either no additional distal and proximal margin is added or a uniform expansion of the PTV was necessary to account for additional distal and proximal margins for all beams. In this research, IMPT plans were assessed to determine the necessity for a uniform expansion to account for range uncertainty. PTV coverage was determined to be acceptable based on

our 3 beam arrangement and no additional margins were added to account for proton range uncertainty.

Initial optimization of IMPT plans was the same as VMAT. A list of the initial optimization parameters can be found in Table 2.3. After initial optimization was performed these parameters were adjusted to reduce the dose to critical avoidance structure without sacrificing plan acceptability. After plans were considered provisionally acceptable they were submitted to the radiation oncologist for final approval.
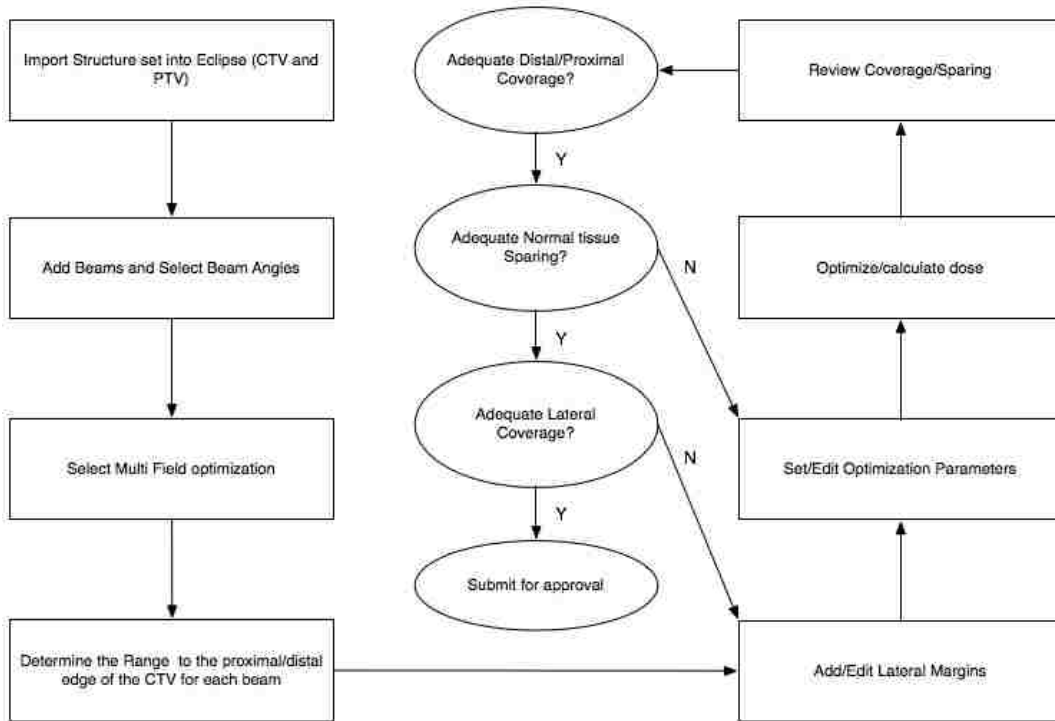
Figure 2.6. IMPT planning workflow.

2.1.4   Plan Evaluation

A post planning comparison was performed to assess the congruence between the

photon and proton plans. The following dose metrics were determined for each plan for

the purposes of comparing the plans.

1. Mean, maximum and minimum doses to the PTV.

2. Dose to 95% of the PTV (D_{95})

3. Conformity index

4. Dose homogeneity index

5. Mean and maximum doses to the brain

6. Volume of brain receiving 5, 10, 50, 52 and 56 Gy-RBE Dose

The minimum and maximum doses to the PTV were reported by the Eclipse

treatment planning system. These doses are point dose approximations and are

equivalent to the $D_{100\%}$ for D_{min} and $D_{0\%}$ for D_{max}.

The Mean dose and standard deviation of the mean was calculate using equations

(6) and (7)

$$D_{mean} = \Sigma_i D_i \times \frac{v_i}{V} \tag{6}$$

$$D_{SD} = \sqrt{\Sigma (D_i - D_{mean})^2 \times \frac{v_i}{V}} \tag{7}$$

where the mean dose D_{mean} is the sum of the the incremental dose from each dose

bin D_i multiplied by the volume from that bin v_i divided by the total volume of the

structure V. The incremental dose D_i and volume v_i were taken from the differential dose

volume histogram (DVH). The dose exported with the differential DVH were separated

by 0.1 Gy increments. This is equivalent to the mean dose given by the treatment

planning system and was found by Yoon *et al.* (2007) to be a more accurate measure of the homogeneity of the planned treatment volume.

Conformity of the dose in the PTV is evaluated using the conformity index (CI) or conformity number as described by Feuvret *et al.* (2006). This metric is a measure of how well the dose conforms to the PTV contour and is

$$CI = \frac{TV_{RI}}{TV} \times \frac{TV_{RI}}{V_{RI}} \tag{8}$$

where TV is the target volume (PTV), TV_{RI} is the target volume that is covered by the reference isodose, and V_{RI} is the volume of the reference isodose. In this work the reference isodose was 95% (51.3 Gy-RBE) of the prescription dose. Conformity index has a range from 0 to 1, where 1 is ideal. The Dose to 95% was also used to quantify the coverage of the PTV and can be extracted from the cumulative DVH in tabular form.

The dose homogeneity index is a measure of how homogeneous the dose is within the PTV. This metrics was described by Yoon *et al.* (2007) and is given by

$$HI = \frac{D_{2\%} - D_{98\%}}{D_p} \tag{9}$$

where $D_{2\%}$ is the dose to 2% of the PTV volume, $D_{98\%}$ is the dose to 98% of the PTV volume, and D_p is the prescribed dose. Homogeneity index has an optimal value of 0.

2.2 Aim 2 – Risk Evaluation

Plans were evaluated on radiation induced necrosis necrosis in the brain. The normal tissue complication probability (NTCP) was calculated for the whole brain using the Lyman Kutcher Burman (LKB) probit model (Burman, 1991). This model uses 4 parameters and is given by

$$NTCP = \frac{1}{\sqrt{2\pi}} \int_{-\infty}^{t} e^{-t^2/2} \, dt \tag{10}$$

$$t = \frac{D_{max} - TD_{50}(v)}{m \cdot TD_{50}(v)} \tag{11}$$

22

$$TD_{50}(v) = \frac{TD_{50}}{v_{eff}^n} \qquad (12)$$

where TD_{50} is the whole organ dose that would lead to 50% complication rate, m is the

slope in the linear region of the sigmoidal dose response curve, n is a volume effect

parameter and v_{eff} is the effective volume of the brain irradiated given by

$$v_{eff} = \sum_i v_i \left(\frac{d_i}{D_{max}}\right)^{1/n} \qquad (13)$$

where v_i is the fractional volume of sub volume i, d_i is the dose to sub volume i, and D_{max}

is the maximum dose to the volume of interest (VOI) (Kutcher and Burman, 1989). The

other parameters used for equations 10-12 can be found in Table 2.4

Table 2.4 Parameter used in brain necrosis NTCP calculation (Burman, 1991).

Parameter	Value	Description
m	0.15	Slope parameter
n	0.25	Volume-effect parameter
TD_{50}	60 Gy	Whole brain dose for an expected 50% complication at 5yrs

NTCP was evaluated for pairs of plans using the ratio of NTCP (rNTCP) given by

$$rNTCP = \frac{NTCP_{proton}}{NTCP_{VMAT}} \qquad (14)$$

where the NTCP calculated for protons plans was divided by the NTCP calculated for the

VMAT plans.

2.3 Aim 3 – Sensitivity Analysis

Calculation of the uncertainty in risk evaluation is a critical component in

determining whether the results are accurate. Many uncertainties are dependent on

planning uncertainty as well as effective delivery of the treatment plan. Setup uncertainty

is a large portion of the uncertainty in effective delivery of which both protons and

photons are susceptible. Additionally, proton plans are susceptible to range uncertainties from planning to delivery. Both setup uncertainty and range uncertainty was evaluated to determine the effect they have on the risk of necrosis using NTCP for 2 patients, 1 glioma (patient 5) and 1ependymoma (patient 12)

Other sources of uncertainty may include the risk model itself. For this reason other models were evaluated to determine the sensitivity of the ratio of risk between protons and photons based on the choice of models used.

2.3.1   Setup Uncertainty

To determine the NTCP dependence on proper plan delivery a maximum setup error of ± 1 cm in each dimension was simulated in the treatment planning system by moving the isocenter in each dimension individually to account for setup error at the time of treatment and patient movement. A common coordinate system was defined for both treatment planning system to ensure that the same shifts were made across systems. The common coordinate system can be seen in Table 2.5. Isocenter shifts were performed in Pinnacle v9.0 for VMAT plans and in Eclipse v11.0 for proton plans. For all sets of shifts it was important that only the dose was recalculated without changes in original plan optimization. For VMAT plans this entailed copying the original plan and after shifting each point individually by 1 cm recalculating the dose for each beam in the beam spreadsheet based on the original beam weightings with no other modifications. For proton plans the dose was recalculated after shifts without recalculating the original beamline for IMPT plans and the beamline and compensator for passive scatter protons. The differential DVH for each of these shifts was exported for NTCP calculation and compared to the nominal plan.

Table 2.5 The commom coordinate system for isocenter shifts between treatment planning systems. Shifts in the x direction indicate lateral shifts, y direction indicate anterior-posterior shifts and z direct indicate superior inferior shift. The isocenter shift is opposite the table shift.

Coordinate	Table shift	Isocenter shift
+x	patients right	patients left
-x	patients left	patients right
+y	anterior	posterior
-y	posterior	anterior
+z	inferior	superior
-z	superior	inferior

2.3.2 Range Uncertainty

Proton range uncertainty is largely caused by the conversion from Hounsfield units (HU) to relative linear proton stopping powers (Schaffner and Pedroni, 1998). HU's are determined at the time of imaging and are a measure of the linear attenuation of the material compared to water (Bushberg, 2002). Eclipse v11.0 has tools to evaluate the effect of changes in the ratio of HU to stopping power conversions known as calibration curve errors. Using this tool a $\pm$10% calibration curve error was simulated for the 2 patients.

The DVH's for simulated calibration curve errors cannot be exported in tabular format from the Eclipse treatment planning system. For this reason screen grabs were utilized in a program called plot digitizer v2.6.6. These screen shots were then digitized as accurately as possible. NTCP was then calculated for digitized $\pm$10% calibration curve error and compared to the NTCP obtained using the nominal DVH curve. The ratio of NTCP from the calibration curve errors was then determined using equation 14.

2.3.3 Risk Model Uncertainty

Normal tissue complication probability is a widely used model for describing several secondary effects in many organs. However, because of the inherent uncertainty

25

in predicting the risk of radiation necrosis, which is poorly understood, another uncertainty analysis was carried out. Alternative models were studied to determine if the relative predicted risk of necrosis is dependent on the choice of the model used to predict it. These models include several that have been widely used in second cancer prediction, such as the linear no-threshold model (LNT), linear threshold model (LT), linear plateau model (LP) and linear quadratic model (LQ), but that have not been applied to radiation necrosis.

All models were fit to the total whole brain dose of 60 Gy to induce 50% complication (TD50) fromBurman (1991). Additionally the linear threshold model passed through both the TD_{50} and TD_5 points, which are 60 Gy and 45 Gy, respectively. The linear plateau model was fit to TD_{50} at 98% of the plateau max. Equations 15-18 show the equations used for the initial fit

LNT	$P = D \cdot m$	(15)

LT	$P = D \cdot m - b$	(16)

LP	$P = \dfrac{\left(\frac{R}{D}\right)^0_T}{\alpha_T} \cdot \left(1 - e^{-\alpha_T D_i}\right)$	(17)

LQ	$P = \alpha D - \beta D^2$	(18)

where P is the probability of complication, D is the dose, m is a slope parameter, R is a risk parameter, α_T is a linear plateau fit parameter, α and β and the linear and quadratic fit parameters, respectively, for the linear quadratic equation. Table 2.6 shows the values of these fit parameters and the initial fit can be seen in Figure 2.7

Table 2.6 Alternative risk model fit parameters determined in this research.

	m	b	R	α_T	α	β
LNT	0.00833333	-	-	-	-	-
LT	0.03	1.3	-	-	-	-
LP	-	-	0.03325	0.0652	-	-
LQ	-	-	-	-	10.2	60
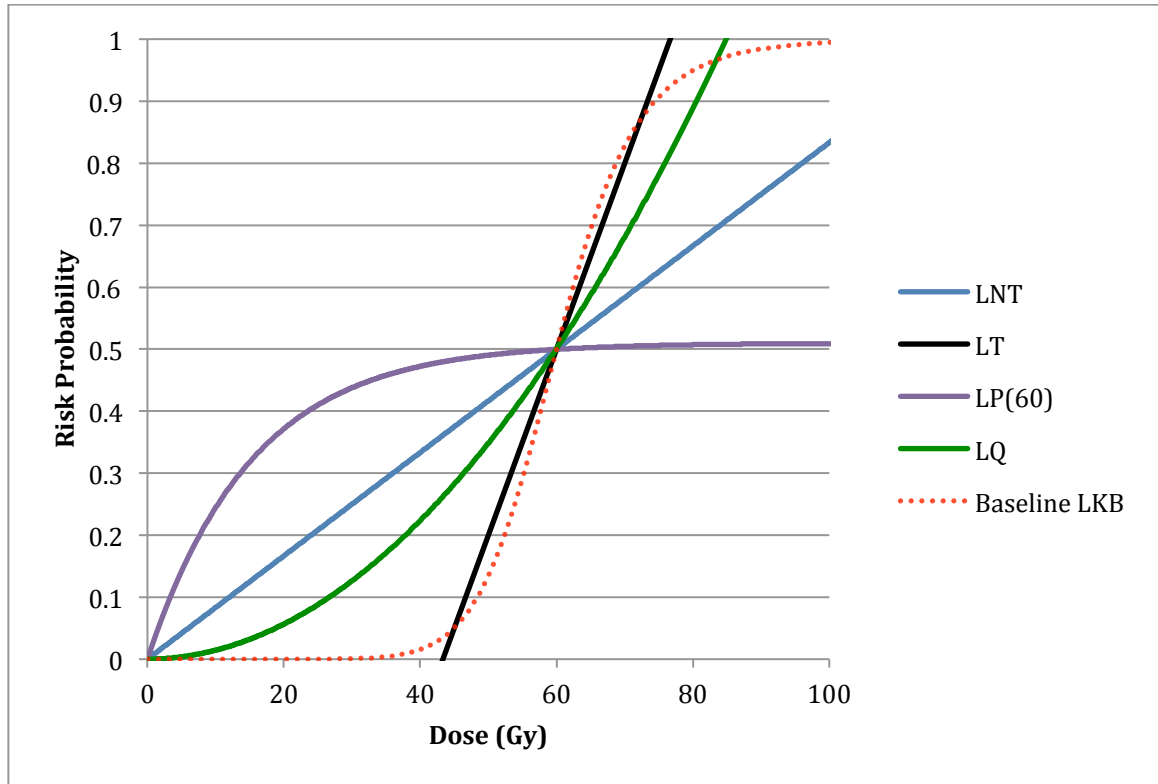
Figure 2.7. Alternative risk models used to test the sensitivity of rNTCP to the shape of the model used. LNT is the linear no-threshold model, LT is the linear threshold model, LP(60) is the linear plateau model fit to 60 Gy at 98% of the maximum, and LQ is the linear quadratic model.

TD$_5$ and TD$_{50}$ from Burman (1991) are based on the whole brain dose and since the current technique in this study only irradiates a fraction of the brain, the fractional volume for each 0.1 Gy dose bin was determined by dividing the volume irradiated in each dose bin as determined by the differential DVH by the total volume of the brain. This can be seen in the following equations

LNT $$Risk = \sum_i \frac{V_i}{V_T} \cdot D_i \cdot m \tag{19}$$

LT $$Risk = \sum_i \frac{V_i}{V_T} \cdot D_i \cdot m - b \tag{20}$$

LP $$Risk = \sum_i \frac{V_i}{V_T} \cdot \frac{\left(\frac{R}{D}\right)_T^0}{\alpha_T} \cdot (1 - e^{-\alpha_T D_i}) \tag{21}$$

LQ $$Risk = \sum_i \frac{V_i}{V_T} \cdot (\alpha D_i - \beta D_i^2) \tag{22}$$

where the fractional bin volumes were multiplied by the probability of risk for each dose bin and then summed over all bins. This has been done similarly by Rechner *et al.* (2012) to determine the overall risk.

The ratio of risk between protons to photons will be determined using the following equation

$$rRisk = \frac{Risk_{proton}}{Risk_{VMAT}} \tag{23}$$

where the risk from protons was divided by the risk from VMAT. The results were then compared to the baseline ratio of risk calculated from the LKB model.

Chapter 3   : Results

Glioma and ependymoma plans had differences in treatment locations and coverage criteria. Therefore a single patient from each group was selected for complete evaluation of isodose distribution and DVH comparison. Other metrics will be evaluated across all patients. Results will be presented for patients 5 and 12 first and then a comprehensive assessment will be made across other patients for the dosimetric and radiobiological results for the PTV and brain.

Isodose distributions for patients 5 and 12 are presented for a single transverse CT slice through plan isocenter. In all images the PTV is shown in red color wash and isodose lines representing certain percentage dose levels are presented following the color coding system in Table 3.1.

Table 3.1 Isodose and region of interest (ROI) display color scheme for isodose figures.

Isodose or ROI	Color
59.4 Gy-RBE	Yellow
56.7 Gy-RBE	Green
54 Gy-RBE	Blue
51.3 Gy-RBE	Cyan
48.6 Gy-RBE	Orange
30-Gy-RBE	Forest Green
20 Gy-RBE	Purple
10 Gy-RBE	Pink
5 Gy-RBE	Red
PTV	Red (color wash)
Brain	Magenta
Brain Stem	Green (color wash)
Optic Chiasm	Cyan (color wash)

DVH figures for selected patients 5 and 12 are shown in this section. All other

patient DVH data are presented in Appendix B: Patient DVH. All DVH figures include

PTV, brain, brainstem, and optic chiasm for VMAT, passively scattered proton therapy

(PSPT), and IMPT plans. The color-coding for all DVH ROIs is listed in Table 3.1.

3.1   Patient 5

Patient 5 was a 9-year-old female with a glioma designated in the right cerebral

hemisphere. In patient 5, as in all other patients, the tumor was considered totally

resected or sub-totally resected before the radiation therapy.

3.1.1   Isodose distribution comparison

Isodose distributions for VMAT, PSPT, and IMPT plans are plotted in Figure

3.1(a-c). All plans are shown for a transverse CT slice at plan isocenter indicated by the

yellow line in Figure 3.1(d).

All plans have a max dose less than 105% of the prescription dose (56.7 Gy-RBE)

to the PTV. In the selected slice the coverage for the VMAT plan looks considerably

worse. Complete coverage of the PTV is to the 90% (48.6 Gy-RBE) isodose line

compared to the 95% (51.3 Gy-RBE) for PSPT and IMPT plans. The homogeneity of the

proton plans at the 100% (54 Gy-RBE) isodose line appear to be worse than the VMAT

plan.

The low dose region is largely different between the VMAT and proton plans.

The 5-30 Gy-RBE isodose lines encompass a much larger volume of normal tissue in the

VMAT plans as compared to both proton plans. The IMPT plan shown in Figure 3.1c

has a greater extension of the 5-20 Gy-RBE isodose lines into the normal brain tissue

Isodose	Color
59.4 Gy-RBE	
56.7 Gy-RBE	
54 Gy-RBE	
51.3 Gy-RBE	
48.6 Gy-RBE	
30 Gy-RBE	
20 Gy-RBE	
10 Gy-RBE	
5 Gy-RBE	
ROI	Color
PTV	
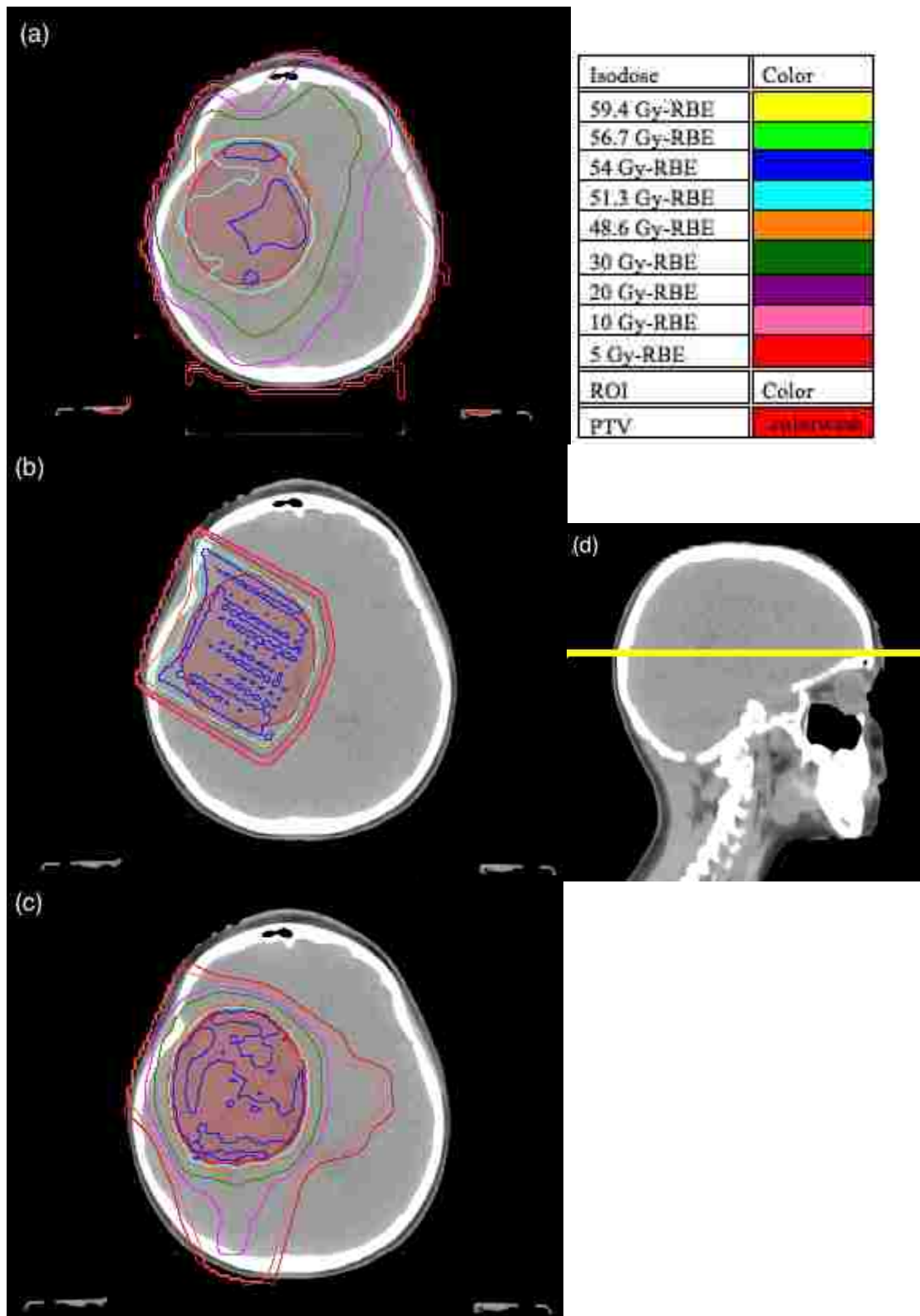
Figure 3.1. Patient 5 isodose distribution at isocenter CT slice location for (a) VMAT, (b) PSPT, and (c) IMPT. Axial CT slice location (d) is represented by the yellow line.

compared to the PSPT plan shown in Figure 3.1b. This is due to the increase in photon

exit dose for VMAT plans and the number of beams used to create the IMPT plans,

respectively. The IMPT plan for patient 5 was constructed in a 3-beam arrangement and

the dose extension into the normal brain tissue is along those beam angles.

3.1.2   DVH Comparison

Figure 3.2 plots the DVH for VMAT, PSPT, and IMPT plans for patient 5. The

shoulder of the PTV is typically used to determine plan coverage. This is the region

where the PTV DVH curve drops away from the 100% line. For patient 5 the IMPT plan

has the greatest coverage with the narrowest shoulder and steeper fall off than the other 2

plans. The PTV for the PSPT plan has the worst coverage. The DVH line drops away

from the 100% early and has a slow gradual reduction in the volume covered up to the

prescription dose where it falls sharply. The VMAT plan also drops away from the 100%

volume line relatively early and falls off much less sharply at the prescription.
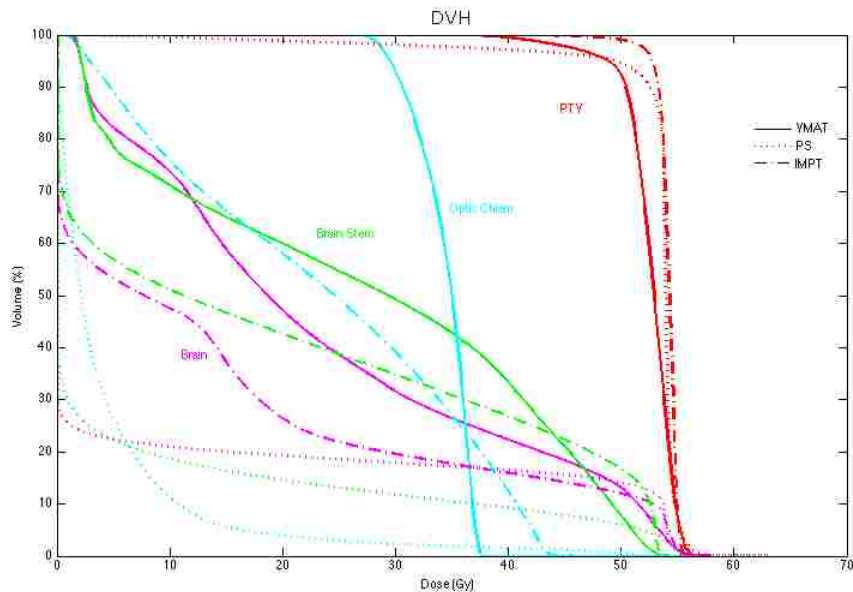
Figure 3.2. The dose volume histograms (DVH) for patient 5. VMAT plans are
represented with the solid lines, PSPT with the dotted lines and IMPT with the dash-dot
lines. Different regions of interest are represented with different colored lines.

Compared to VMAT, proton therapy consistently reduced the dose to organs at risk. This trend can also be seen in Figure 3.2 for patient 5. For the brainstem, IMPT and PSPT plans have a high dose tail compared to VMAT. Similar results are seen with the optic chiasm between plans.

3.1.3   PTV

PTV results for patient 5 are shown in Table 3.2. This patient had a glioma that was situated low in cerebral hemisphere with brainstem involvement. In almost every dose metric the IMPT plan showed better results. The reduction in the PTV mean and minimum dose for the VMAT and PSPT is likely due to the dose constraints place on the brainstem and as a result the dose to the PTV was sacrificed. This can be seen in the failure of the VMAT and PSPT plans to reach the planning objective of $D_{95\%}$= 51.3 Gy-RBE or 95% of the prescription dose. For this reason the conformity and homogeneity of both the VMAT and PS proton plans also suffered but were similar to each other.

Table 3.2 The mean, maximum, minimum conformity index (CI), homogeneity index (HI) and dose to 95% ($D_{95\%}$) of the PTV for patient 5.

Treatment Plans	D_{mean} (Gy-RBE)	D_{max} (Gy-RBE)	D_{min} (Gy-RBE)	$D_{95\%}$ (Gy-RBE)	CI	HI
VMAT	52.5	57.5	31.7	48.8	0.60	0.21
PSPT	52.9	63.2	0.5	49.5	0.57	0.46
IMPT	54.1	57.2	39.2	52.8	0.84	0.07

3.1.4   Brain

Dosimetric results for patient 5 brain ROI are shown in Table 3.3 and Table 3.4. Compared to the VMAT plan, the PSPT plan resulted an increase in the maximum dose and a decrease in the mean dose to the brain. The IMPT plan also resulted in a reduction of the mean brain dose compared to the VMAT plan, with a maximum dose that was similar to the VMAT plan.

Table 3.3 The mean and maximum doses to the brain for patient 5.

Patient 5	D_{max} (Gy-RBE)	D_{mean} (Gy-RBE)
VMAT	57.5	23.2
PSPT	63.2	10.0
IMPT	58.0	15.0

The PSPT plan shows smaller volume receiving low dose compared to VMAT or IMPT plan, as seen by the $V_{5Gy\text{-}RBE}$ and $V_{10Gy\text{-}RBE}$ of 22% and 21%, respectively (Table 3.4). The volume receiving high dose was similar across VMAT, PSPT, and IMPT plans and the calculated NTCP was similar with values of 0.14%, 0.10%, and 0.08% risk of radiation necrosis for VMAT, PSPT and IMPT, respectively.

Table 3.4 The volume of the brain receiving 5, 10 50, 52, and 56 Gy-RBE and normal tissue complication probability (NTCP) of brain necrosis for patient 5.

Treatment plans	$V_{5Gy\text{-}RBE}$ (%)	$V_{10Gy\text{-}RBE}$ (%)	$V_{50Gy\text{-}RBE}$ (%)	$V_{52Gy\text{-}RBE}$ (%)	$V_{56Gy\text{-}RBE}$ (%)	NTCP(%)
VMAT	82.2	73.7	13.1	8.6	0.2	0.14
PSPT	22.4	21.0	14.1	13.0	0.3	0.10
IMPT	53.3	47.5	12.0	10.8	0.0	0.08

3.2 Patient 12

Patient 12 was a 16-year-old female with an ependymoma designated infratentorial in the posterior fossa which can be seen in Figure 3.3. All ependymomas were considered sub-totally resected which generally calls for radiation therapy treatment.

3.2.1 Isodose distribution comparison

Figure 3.3 displays the isodose lines for patient 12 taken from a CT through the plan isocenter. The location of the CT slice within the patient can be seen by the yellow line in Figure 3.3(d).

34

Isodose	Color
59.4 Gy-RBE	(yellow)
56.7 Gy-RBE	(green)
54 Gy-RBE	(blue)
51.3 Gy-RBE	(cyan)
48.6 Gy-RBE	(orange)
30 Gy-RBE	(dark green)
20 Gy-RBE	(purple)
10 Gy-RBE	(pink)
5 Gy-RBE	(red)
ROI	Color
PTV	colorwash
Brain Stem	colorwash
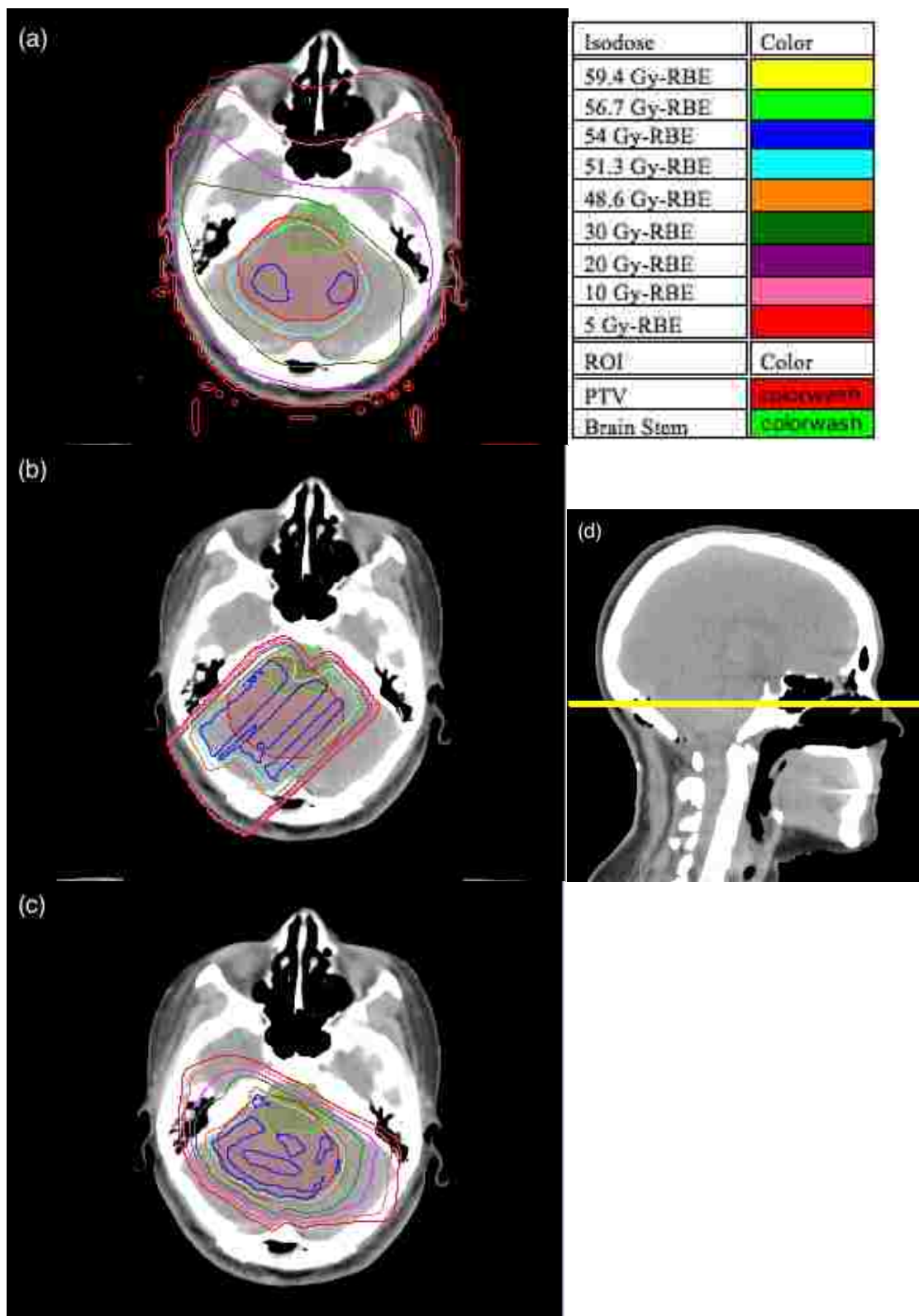
Figure 3.3. Patient 12 isodose distributions for VMAT (a), PSPT (b) and IMPT (c). CT slice location is through isocenter and is designated by a yellow line in figure d.

35

The VMAT plan (Figure 3.3(a)) shows fairly good coverage to the 95% (51.3 Gy-RBE) isodose line, which covers all but small region of the PTV anteriorly. However the VMAT plan shows little coverage to the 100% (54 Gy-RBE) isodose line. The PSPT plan had good homogeneity to the 95% (51.3 Gy-RBE) isodose line with only incomplete coverage where distal blocking is used. However the coverage 100% (54 Gy-RBE) was poor. The IMPT plan had similarities to the PSPT and VMAT plans. Coverage of the 100% (54 Gy-RBE) isodose line is was poor but there is excellent coverage with the 95% (51.3 Gy-RBE) line.

The VMAT plan resulted in an greater extension of the low dose region into the normal brain tissue compared to either proton plans with the 5-30 Gy isodose lines extending much further from the PTV. The PSPT plan resulted in much less low dose region to the brain than either VMAT or IMPT, likely due to fewer number of beams and beam angle selection. The IMPT plan resulted in a greater extension of the 5-30 Gy-RBE isodose lines into surrounding brain tissue than the PSPT but a reduction compared to the VMAT plan.

3.2.2 DVH comparison

Comparison of the DVH between the plans for patient 12 can be seen in Figure 3.4. The PTV for the VMAT and IMPT plans are very similar with only a slightly broader shoulder for the IMPT plan and a slightly larger volume receiving a higher dose as seen in the tail of the PTV curve. The PSPT (dotted line) curves has a much larger shoulder that dips away from the 100% volume at around 10 Gy-RBE and slowly falls until it drops sharply just before the prescription dose of 54 Gy-RBE. This characteristic

is due in part to the overlap of the PTV with the brainstem and the use of distal blocking

to reduce the dose to the brainstem to the level of the constraint that was set upon it.
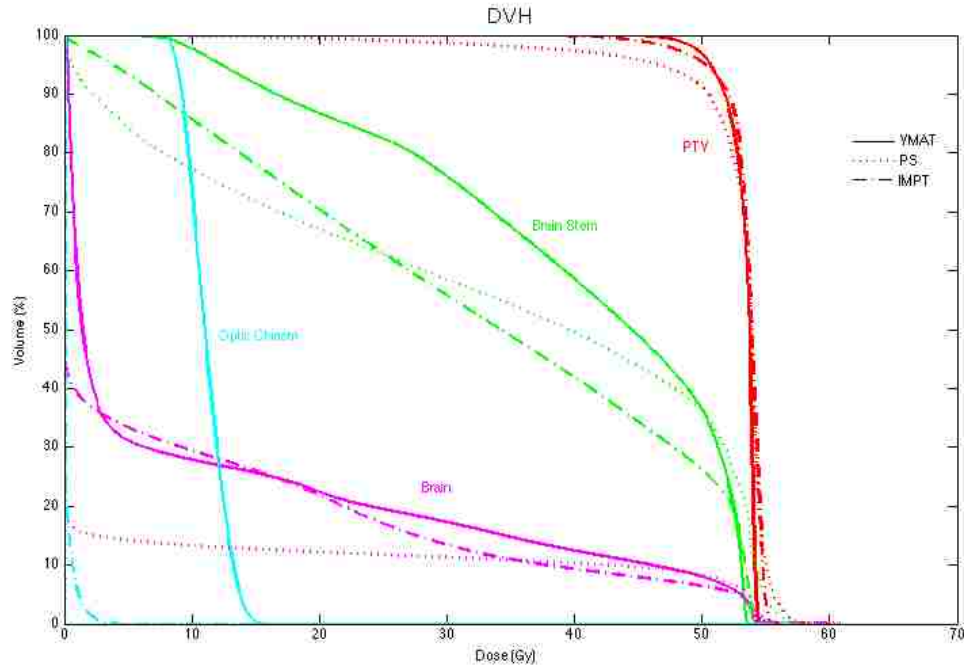
Figure 3.4. The dose volume histogram (DVH) for patient 12. VMAT plans are represented with the solid lines, PSPT with the dotted lines and IMPT with the dash-dot lines. Different regions of interest are represented with different colored lines.

Both proton plans showed a reduction in the volume of the brainstem receiving

dose compared to VMAT, except in the high dose region for the PSPT plan. The PSPT

plan shows a reduction in the total brain dose compared to VMAT, but VMAT and IMPT

plans were very similar. Both proton plans also resulted in much lower dose to the optic

chiasm compared to VMAT.

3.2.3   PTV

The PTV dose metrics for patient 12 are listed in Table 3.5. The mean dose for all

plans was very similar with an average of 53.2 $\pm$ 0.4 Gy-RBE for all plans. However the

37

minimum dose for the proton plans was much lower which is revealed by an inferior homogeneity index than that for the VMAT plan. Additionally the $D_{95\%}$ for the PSPT plan fell below 90% (48.6 Gy-RBE) of the prescription dose, which was our criterion for acceptance of our ependymoma plans. Again, this is due to the overlap of the PTV with the brainstem and the constraint that was placed on the brainstem. Conformity index of the PTV was highest for IMPT (0.76), intermediated for VMAT plans (0.63), and lowest for PSPT (0.49).

Table 3.5 The mean, maximum, minimum conformity index (CI), homogeneity index(HI) and dose to 95% ($D_{95\%}$) of the PTV for patient 12.

Treatment Plans	D_{mean} (Gy-RBE)	D_{max} (Gy-RBE)	D_{min} (Gy-RBE)	$D_{95\%}$ (Gy-RBE)	CI	HI
VMAT	53.3	54.7	42.8	50.6	0.63	0.09
PSPT	52.7	60.0	3.5	46.5	0.49	0.39
IMPT	53.5	58.2	32.8	50.2	0.76	0.14

3.2.4   Brain

Table 3.6 and 3.7 list the predicted dosimetric and radiobiological results in the brain for patient 12. The maximum dose to the brain for patient 12 was higher for both the PSPT and IMPT compared to the VMAT plan. Additionally the mean doses for both the PSPT and IMPT plans were slightly lower than that for the VMAT plan.

Table 3.6 The mean and maximum doses to the brain for patient 12.

Patient 12	D_{max} (Gy-RBE)	D_{mean} (Gy-RBE)
VMAT	54.7	11.1
PSPT	60.3	6.2
IMPT	60.9	9.9

Table 3.7 The volume of the brain receiving 5, 10 50, 52, and 56 Gy-RBE and normal tissue complication probability (NTCP) for patient 12.

Treatment Plans	$V_{5Gy-RBE}$ (%)	$V_{10Gy-RBE}$ (%)	$V_{50Gy-RBE}$ (%)	$V_{52Gy-RBE}$ (%)	$V_{56Gy-RBE}$ (%)	NTCP(%)
VMAT	31.2	27.9	8.0	6.4	0.0	0.027
PSPT	14.2	13.3	8.3	7.1	0.3	0.022
IMPT	33.4	29.4	6.4	5.6	0.0	0.015

The volume of the brain irradiated between 5 and 56 Gy-RBE is relatively similar between VMAT and IMPT as seen in Table 3.7. The volume of brain irradiated to 5 and 10 Gy-RBE for the PSPT plan was less than half the value of the VMAT plan, however the PSPT plan had a similar volume irradiated at the higher dose point between 50-56 Gy-RBE as the VMAT and IMPT plans. Again the NTCP values were similar between plans with a slight reduction for the IMPT plan compared to the VMAT plan.

3.3   Overview of all patients

Results for all patients are presented in the following section. All metrics were compared for significance using the Student's t-test and Wilcoxon signed rank test (WSR).

3.3.1   PTV

Table 3.8 lists the mean, maximum and minimum doses to the PTV for the entire pediatric cohort (patients 1-13). The average mean dose to the PTV was 53.8 ± 0.6 Gy-RBE for both VMAT and IMPT plans and showed no significant difference for either the Student's t-test or the Wilcoxon signed rank test, but the PSPT plans had a significantly lower mean dose to the PTV (53.3 ± 0.6 Gy-RBE) than VMAT or IMPT plans. The maximum dose to the PTV for all patients is displayed in Figure 3.5 and was significantly different from VMAT for both IMPT and PSPT. Both PSPT and IMPT resulted in a

higher average maximum dose, with values of 58.3 $\pm$ 2.5 and 57.4 $\pm$ 1.0 Gy-RBE,

respectively, compared to VMAT which had an average maximum dose of 55.8 $\pm$ 1.0

Gy-RBE. The minimum dose to the PTV was significantly lower for PSPT and IMPT

plans with average minimum values of 23.0 $\pm$ 21.1, 36.5 $\pm$ 10.4, respectively, compared

to VMAT which had an average minimum dose of 45.3 $\pm$ 5.5 Gy-RBE.

Table 3.8 The mean, maximum and minimum dose to the PTV for all patients. Descriptive statistics include the mean value with standard deviation (SD), and the p-value for the student t-test and Wilcoxon signed rank (WSR) test.

Patient index	D_{mean} (Gy-RBE)			D_{max} (Gy-RBE)			D_{min} (Gy-RBE)		
	VMAT	PSPT	IMPT	VMAT	PSPT	IMPT	VMAT	PSPT	IMPT
1	54.2	53.9	54.2	55.3	57.5	55.8	50.9	47.2	47.4
2	54.0	53.9	53.9	55.0	57.8	58.9	51.5	48.3	46.1
3	54.5	53.1	53.5	56.2	57.6	58.5	46.4	30.9	35.1
4	54.2	53.8	54.0	57.7	59.6	56.8	39.7	22.5	33.9
5	52.5	52.9	54.1	57.5	63.2	57.2	31.7	0.5	39.2
6	54.0	53.7	54.2	55.3	55.8	56.3	52.2	45.3	47.2
7	54.2	53.9	54.1	55.5	55.6	56.6	48.8	46.3	43.7
8	53.9	53.7	54.3	56.0	56.4	58.7	46.7	43.9	45.7
9	53.3	53.1	53.8	55.2	57.4	57.8	44.8	1.0	36.3
10	54.5	52.1	52.0	57.0	56.8	57.4	44.1	7.6	11.1
11	53.7	53.3	53.8	54.6	57.6	58.3	44.1	1.4	29.5
12	53.3	52.7	53.5	54.7	60.0	58.2	42.8	3.5	32.8
13	53.6	52.8	53.6	55.5	63.1	56.2	44.7	0.5	25.8
Mean	53.8	53.3	53.8	55.8	58.3	57.4	45.3	23.0	36.5
SD	0.6	0.6	0.6	1.0	2.5	1.0	5.5	21.1	10.4
p-value	-	VMAT-PSPT	VMAT-IMPT	-	VMAT-PSPT	VMAT-IMPT	-	VMAT-PSPT	VMAT-IMPT
t-test	-	0.02	0.8	-	0.003	0.003	-	0.0007	0.007
WSR	-	0.01	0.8	-	0.002	0.005	-	0.002	0.008
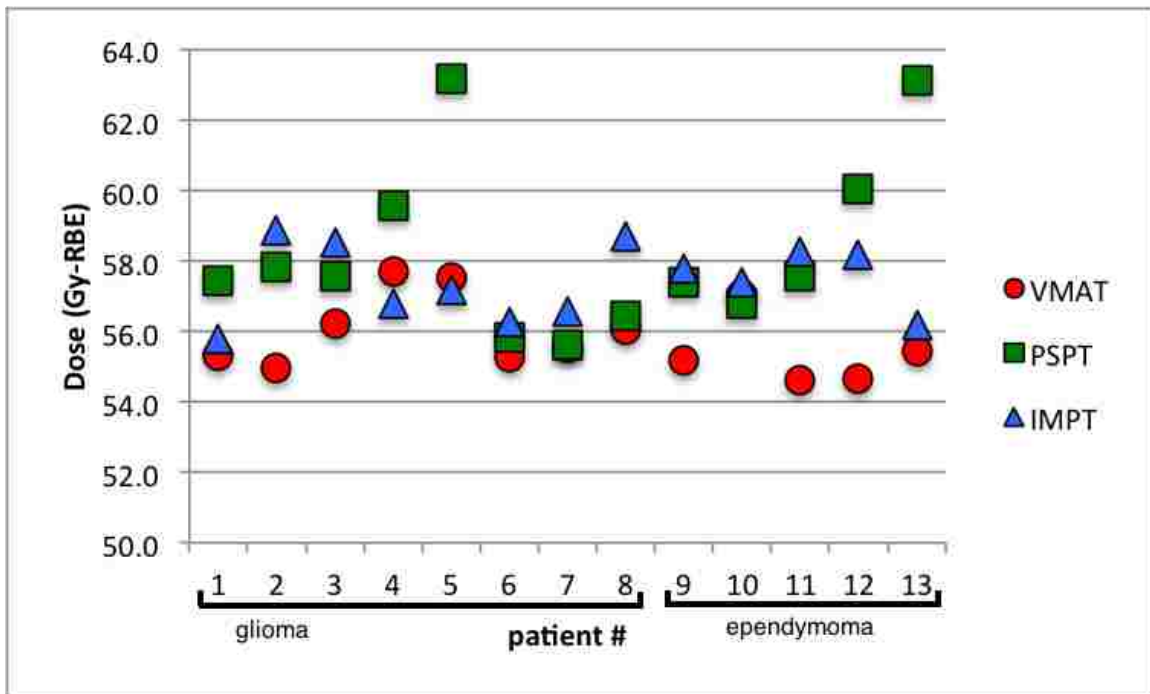
Figure 3.5 The maximum dose to the PTV for all patients and treatment plans.

Table 3.9 summarizes the results for the conformity index (CI), homogeneity index (HI) and dose to 95% of the PTV ($D_{95\%}$) and these results are also displayed in Figure 3.6 through 3.8 for all patients. PSPT plans showed no significant difference in the conformity compared to VMAT with average CI values of 0.58 ± 0.07 and 0.62 ± 0.08, respectively. The IMPT plans resulted in significantly better conformity than the VMAT plans with an average CI value of 0.83 ± 0.06 versus 0.62 ± 0.08 for VMAT.

The homogeneity of the dose to the PTV was determined with the homogeneity index. With an optimal value of zero both the VMAT and IMPT plans showed good homogeneity with average HI values of 0.07 ± 0.05 and 0.12 ± 0.12. On the other hand, PSPT plans had significantly worse homogeneity than the VMAT plans with an average HI of 0.23 ± 0.19.

41

The dose to 95% of the volume ($D_{95\%}$) was also used as an indicator of PTV dose coverage. PSPT plans resulted in a significantly lower average $D_{95\%}$ than the VMAT plans and 5 of the 13 plans did not meet the criteria for acceptable coverage. IMPT and VMAT average $D_{95\%}$ values were not significantly different from one another and only one patient from each modality failed to meet the coverage criteria (patient 10 and 5, respectively).

Table 3.9 Conformity index (CI), homogeneity index (HI), and dose to 95% of the PTV ($D_{95\%}$) for all patients. Descriptive statistics include the mean value with standard deviation (SD), and the p-value for the student t-test and Wilcoxon signed rank (WSR) test.

Patient index	CI			HI			$D_{95\%}$ (Gy-RBE)		
	VMAT	PSPT	IMPT	VMAT	PSPT	IMPT	VMAT	PSPT	IMPT
1	0.57	0.59	0.84	0.02	0.08	0.05	53.8	52.3	53.1
2	0.68	0.59	0.86	0.02	0.05	0.07	53.4	52.8	52.9
3	0.74	0.63	0.77	0.06	0.16	0.08	53.2	49.4	52.1
4	0.64	0.60	0.88	0.11	0.11	0.08	52.5	51.9	52.6
5	0.60	0.57	0.84	0.21	0.46	0.07	48.8	49.5	52.8
6	0.55	0.61	0.87	0.03	0.06	0.05	53.5	52.6	53.2
7	0.62	0.62	0.89	0.02	0.06	0.07	53.7	52.6	52.6
8	0.73	0.67	0.92	0.03	0.06	0.05	53.3	52.8	53.2
9	0.62	0.49	0.83	0.10	0.29	0.12	50.6	50.6	51.1
10	0.44	0.63	0.73	0.11	0.40	0.50	52.5	43.9	40.7
11	0.60	0.58	0.84	0.05	0.28	0.15	52.8	50.8	51.4
12	0.63	0.49	0.76	0.09	0.39	0.14	50.6	46.5	50.2
13	0.64	0.43	0.80	0.08	0.61	0.16	51.8	47.5	50.9
Mean	0.62	0.58	0.83	0.07	0.23	0.12	52.35	50.25	51.29
SD	0.08	0.07	0.06	0.05	0.19	0.12	1.50	2.82	3.33
p-value	-	VMAT-PSPT	VMAT-IMPT	-	VMAT-PSPT	VMAT-IMPT	-	VMAT-PSPT	VMAT-IMPT
t-test	-	0.2	0.0000004	-	0.003	0.1	-	0.01	0.3
WSR	-	0.1	0.002	-	0.002	0.08	-	0.005	0.07
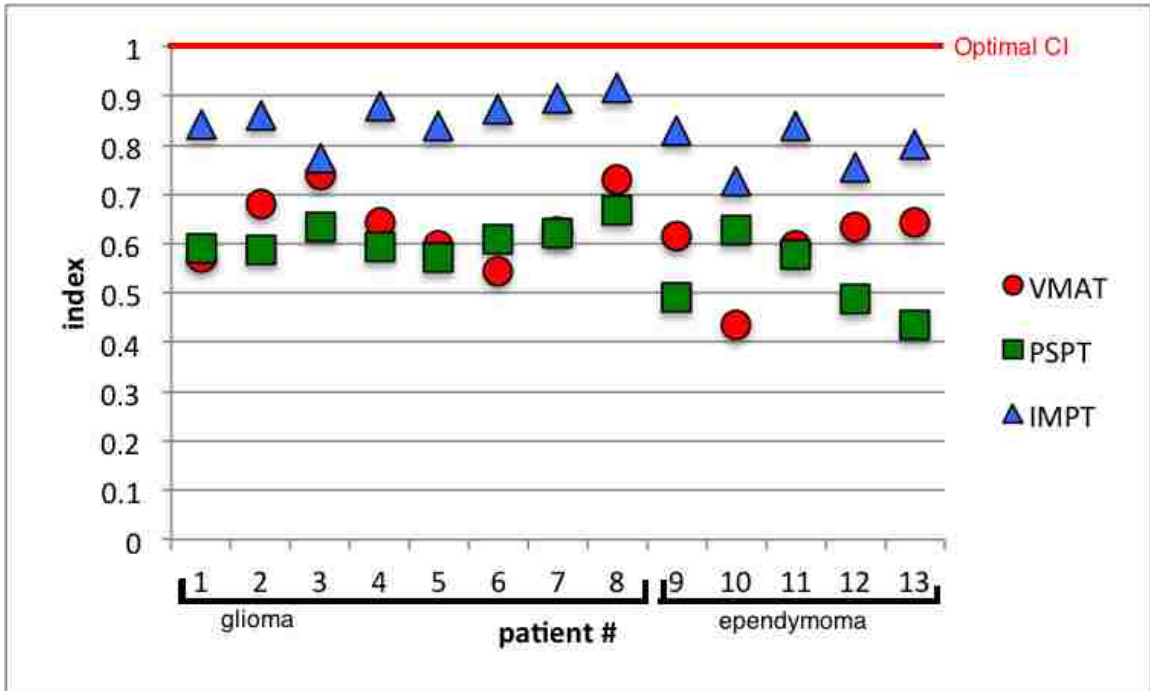
Figure 3.6 The conformity of the dose to the PTV represented by the conformity index for VMAT, PSPT, and IMPT for all patients.
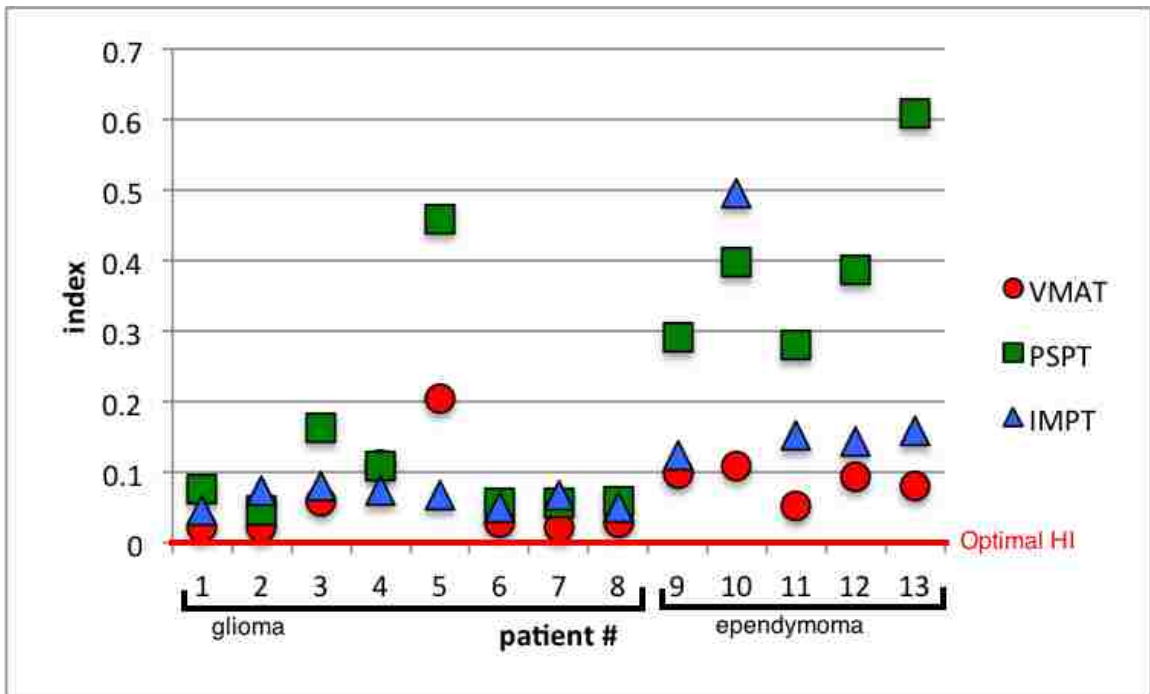
Figure 3.7 The homogeneity of the dose to the PTV represented by the homogeneity index for VMAT, PSPT, and IMPT for all patients.
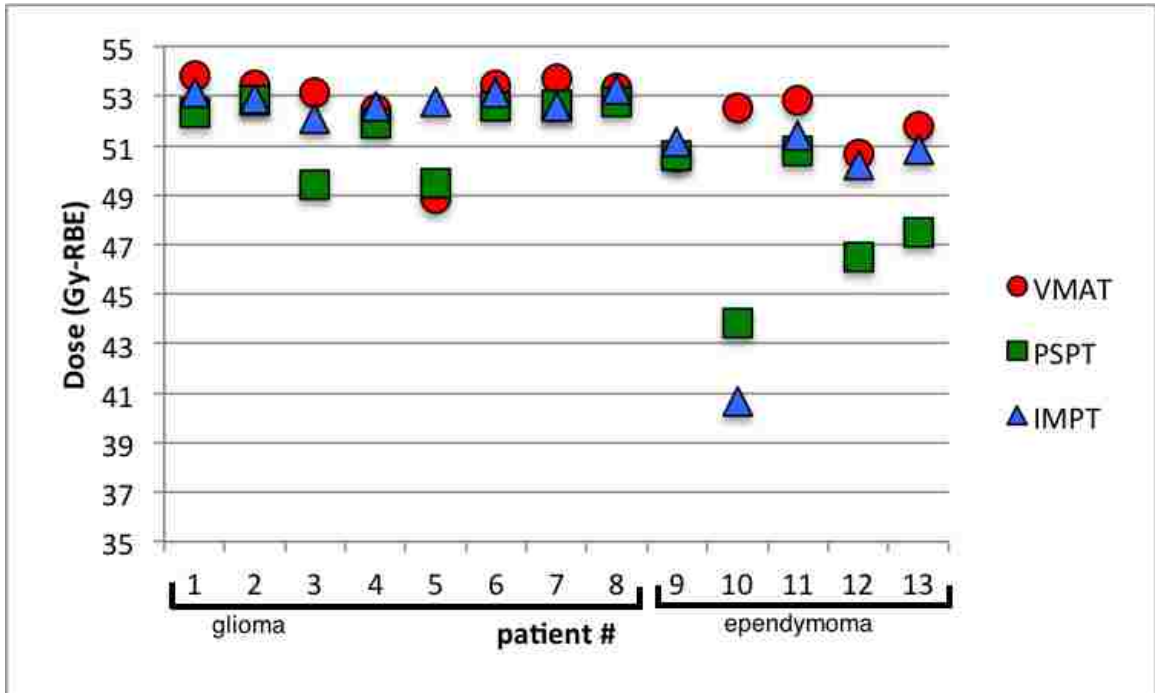
Figure 3.8 The dose to 95% of the PTV ($D_{95\%}$) for VMAT, PSPT, and IMPT for all patients.

3.3.2 Brain

Table 3.10 lists the mean and max doses to the brain for all patients. The maximum dose to the brain for all patients is displayed in Figure 3.9. Both IMPT and PSPT plans resulted in a significantly higher maximum dose to the brain than the VMAT plans with average maximum values of 57.6 ± 1.44, 58.5 ± 2.51, and 55.8 ± 1.08 Gy-RBE, respectively. The mean dose to the brain was significantly lower for both the PSPT and IMPT plans compared to VMAT with average mean values of 7.9 ± 1.1, 10.3 ± 4.0, and 17.5 ± 5.6 Gy-RBE, respectively.

44

Table 3.10 The maximum and mean doses to the brain for all patients. Descriptive statistics include the mean value with standard deviation (SD), and the p-value for the student t-test and Wilcoxon signed rank (WSR) test.

Patient index	D_{max} (Gy-RBE)			D_{mean} (Gy-RBE)		
	VMAT	PSPT	IMPT	VMAT	PSPT	IMPT
1	55.3	57.9	55.8	21.2	9.3	12.9
2	55.0	57.8	58.9	17.2	6.3	8.1
3	56.2	57.6	58.5	9.4	4.9	5.7
4	58.0	60.2	56.8	27.4	12.9	16.5
5	57.5	63.2	58.0	23.2	10.0	15.0
6	55.4	55.8	55.8	17.7	5.4	5.4
7	55.5	55.6	56.6	14.3	4.7	6.9
8	55.3	56.6	58.7	24.3	12.1	16.2
9	55.2	57.5	57.5	11.0	6.2	6.3
10	57.0	56.8	57.4	13.8	6.2	8.5
11	54.6	57.6	58.3	16.2	7.7	9.3
12	54.7	60.3	60.9	11.1	6.2	9.9
13	55.5	63.2	56.3	20.5	10.9	12.8
Average	55.8	58.5	57.6	17.5	7.9	10.3
SD	1.08	2.51	1.44	5.59	2.80	3.99
p-value	-	VMAT-PSPT	VMAT-IMPT	-	VMAT-PSPT	VMAT-IMPT
t-test	-	0.002	0.01	-	0.0000003	0.000001
WSR	-	0.005	0.007	-	0.001	0.001
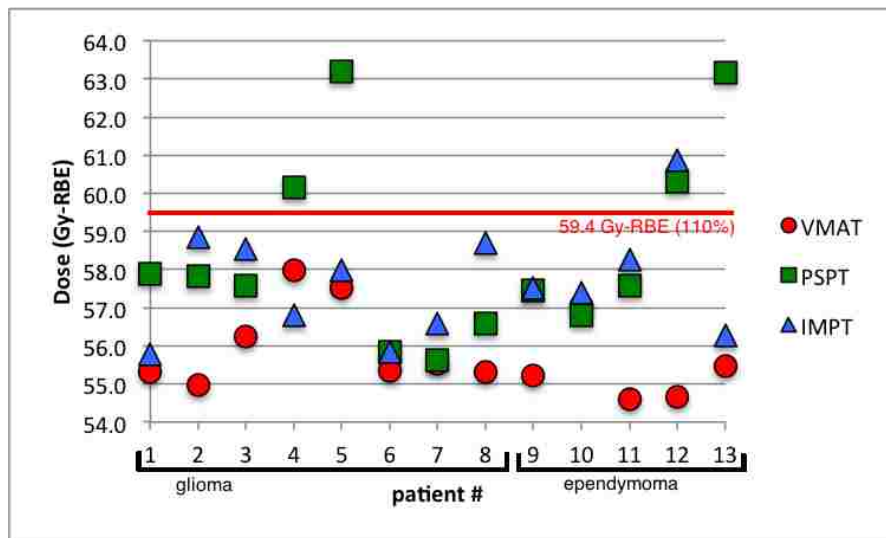
Figure 3.9 The maximum dose to the brain for VMAT, PSPT, and IMPT for all patients.

45

The percentage volume of the brain receiving 5, 10, 50, 52, and 56 Gy-RBE is listed in Table 3.11 and 3.12. These result show that both the PSPT and IMPT plans resulted in a significant reduction in the volume of the brain that was irradiated to the 5 and 10 Gy-RBE dose levels compared to VMAT. VMAT plans resulted in a low dose bath of 10 Gy-RBE to nearly 50% of the brain. PSPT and IMPT reduced the volume receiving 10 Gy-RBE to nearly half of that from VMAT. Additionally, the IMPT plans resulted in a reduction of the brain volume receiving 50 Gy-RBE compared to VMAT. There was no statistically significant difference between any of the plans at the 52 and 56 Gy-RBE dose based on the Wilcoxon signed rank test.

Table 3.11 The percentage volume of the brain receiving 5 and 10 Gy-RBE for all patients. Descriptive statistics include the mean value with standard deviation (SD), and the p-value for the student t-test and Wilcoxon signed rank (WSR) test.

Patient index	$V_{5Gy\text{-}RBE}$ (%)			$V_{10Gy\text{-}RBE}$ (%)		
	VMAT	PSPT	IMPT	VMAT	PSPT	IMPT
1	72.7	22.0	47.3	51.4	20.2	41.1
2	69.3	14.4	26.1	54.0	13.5	23.1
3	40.8	17.0	25.7	29.5	15.5	20.7
4	85.8	29.0	56.8	78.3	27.2	50.6
5	82.2	22.4	53.3	73.7	21.0	47.5
6	62.7	12.5	35.6	45.4	11.6	30.2
7	60.9	11.0	22.9	47.1	10.2	20.3
8	84.0	26.8	54.2	62.4	25.3	49.2
9	31.6	14.3	19.2	28.3	13.4	17.1
10	40.4	18.1	34.0	34.2	16.7	28.9
11	49.6	17.6	28.2	40.6	16.4	25.0
12	31.2	14.2	33.4	27.9	13.3	29.4
13	65.0	25.4	49.7	56.6	23.7	43.1
Average	59.71	18.84	37.41	48.42	17.54	32.78
SD	19.40	5.79	13.16	16.57	5.46	11.96
p-value		VMAT-PSPT	VMAT-IMPT		VMAT-PSPT	VMAT-IMPT
t-test		0.000001	0.00004		0.000002	0.0001
WSR		0.001	0.02		0.001	0.02

Table 3.12 The percentage volume of the brain receiving 50, 52, and 56 Gy-RBE for all patients. Descriptive statistics include the mean value with standard deviation (SD), and the p-value for the student t-test and Wilcoxon signed rank (WSR) test.

Patient index	$V_{50Gy-RBE}$ (%)			$V_{52Gy-RBE}$ (%)			$V_{56Gy-RBE}$ (%)		
	VMAT	PSPT	IMPT	VMAT	PSPT	IMPT	VMAT	PSPT	IMPT
1	16.1	12.3	9.9	13.6	11.2	9.0	0.0	0.1	0.0
2	9.3	9.0	7.0	8.0	8.3	6.3	0.0	0.0	0.1
3	3.2	2.8	2.9	2.6	2.4	2.7	0.0	0.0	0.0
4	19.6	18.4	13.9	16.6	17.0	12.6	0.4	0.1	0.0
5	13.1	14.1	12.0	8.6	13.0	10.8	0.2	0.3	0.0
6	9.7	7.6	5.7	8.1	6.9	5.1	0.0	0.0	0.0
7	7.9	6.4	5.3	6.8	5.9	4.8	0.0	0.0	0.0
8	19.7	17.9	15.2	17.2	16.9	14.1	0.0	0.0	0.0
9	7.3	8.1	5.6	5.7	7.1	5.0	0.0	0.1	0.0
10	10.5	5.6	5.3	8.9	4.8	4.4	0.4	0.0	0.0
11	13.6	10.8	8.9	11.6	10.0	8.1	0.0	0.1	0.1
12	8.0	8.3	6.4	6.4	7.1	5.6	0.0	0.3	0.0
13	12.0	13.4	8.7	9.6	11.7	7.7	0.0	0.7	0.0
Average	11.54	10.36	8.23	9.52	9.39	7.40	0.08	0.13	0.02
SD	4.84	4.70	3.68	4.23	4.44	3.42	0.15	0.20	0.03
p-value		VMAT-PSPT	VMAT-IMPT		VMAT-PSPT	VMAT-IMPT		VMAT-PSPT	VMAT-IMPT
t-test		0.05	0.00003		0.8	0.002		0.5	0.2
WSR		0.6	0.001		0.8	0.08		0.4	0.01

The calculated risk of necrosis and ratio of risk are summarized by the NTCP and rNTCP values seen in Table 3.13. Both PSPT and IMPT resulted in a significant reduction in the NTCP compared to VMAT with average values of 0.065 ± 0.07 %, 0.042 ± 0.05 %, and 0.074 ± 0.05 %, respectively. This reduction can be seen in the ratio of normal tissue complication probability (rNTCP) with average values of 0.51 ± 0.3 for PSPT compared to VMAT and 0.32 ± 0.1 for IMPT compared to VMAT. The values of rNTCP for all PSPT and IMPT can be seen in Figure 3.10 and 3.11, respectively, for all patients compared to the average values. rNTCP values were compared to 1 using the

Wilcoxon signed rank test and were found to be significantly lower than 1, indicating that

both proton modalities should confer a reduction in the risk of necrosis.

Table 3.13 The normal tissue complication probability (NTCP) and ratio of normal tissue complication probability between plans for all patients. Descriptive statistics include the mean value with standard deviation (SD), and the p-value for the student t-test and Wilcoxon signed rank (WSR) test.

Patient index	NTCP(%)			rNTCP	
	VMAT	PSPT	IMPT	PSPT/VMAT	IMPT/VMAT
1	0.247	0.068	0.046	0.28	0.19
2	0.045	0.025	0.016	0.55	0.36
3	0.0035	0.0014	0.0014	0.39	0.39
4	0.45	0.23	0.13	0.50	0.28
5	0.1433	0.1031	0.0821	0.72	0.57
6	0.0694	0.0150	0.0097	0.22	0.14
7	0.0276	0.0095	0.0075	0.35	0.27
8	0.38	0.19	0.15	0.49	0.41
9	0.0230	0.0216	0.0090	0.94	0.39
10	0.0736	0.0076	0.0078	0.10	0.11
11	0.117	0.047	0.034	0.40	0.29
12	0.027	0.022	0.015	0.80	0.54
13	0.130	0.111	0.034	0.85	0.26
Mean	0.074	0.065	0.042	0.51	0.32
SD	0.05	0.07	0.05	0.3	0.1
p-value		VMAT-PSPT	VMAT-IMPT	VMAT-PSPT	VMAT-IMPT
t-test		0.01	0.01		
WSR				0.002	0.002
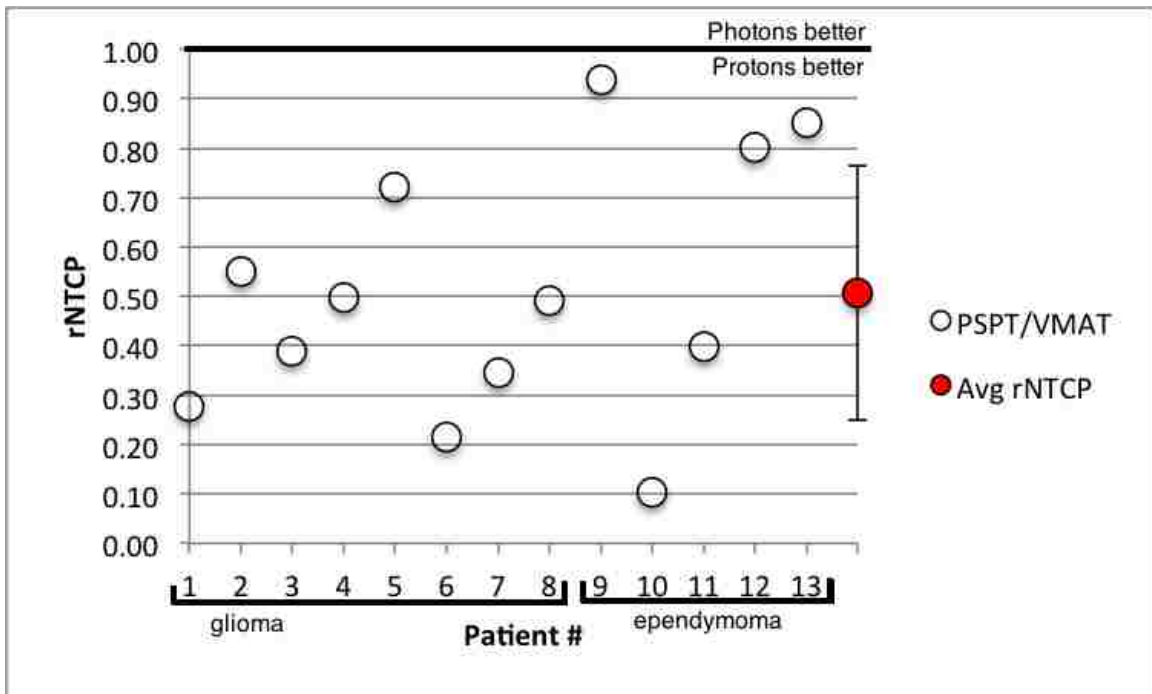
Figure 3.10 The ratio of risk (rNTCP) for PSPT plans compared to VMAT for all patients and compared with the average value of rNTCP represented by the red circle with standard deviation error bars.
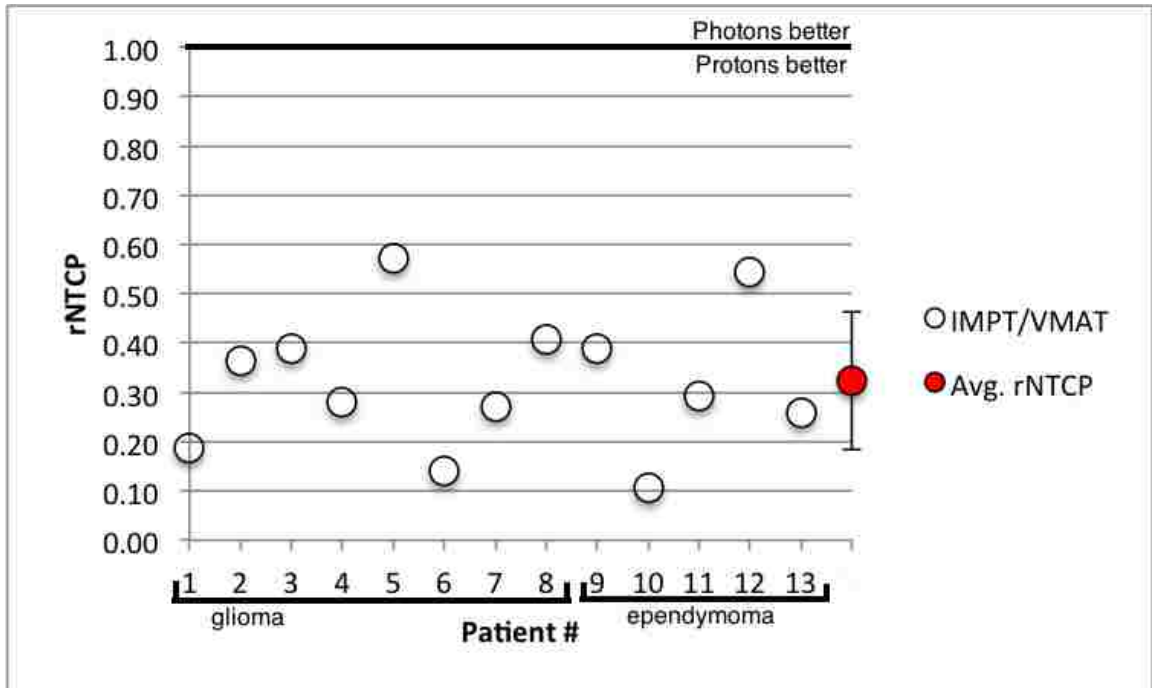
Figure 3.11 The ratio of risk (rNTCP) for IMPT plans compared to VMAT for all patients and compared with the average value of rNTCP represented by the red circle with standard deviation error bars.

3.4   Sensitivity Analysis

Isocenter shifts and range uncertainty estimates were calculated for patient 5 and 12 to determine the effects of setup error and changes in the CT number, respectively. Risk model analysis was performed for the entire pediatric cohort (patients 1-13) to determine the sensitivity of predicted risk on the choice of risk model used.

3.4.1   Isocenter shifts

The dose volume histograms (DVHs) for patient 5 and 12 isocenter shifts are shown in Appendix C (Figure C.1 through C.18) for VMAT, PSPT and IMPT plans. Additionally the results are summarized in Table C.1 through Table C.18. For both patients 5 and 12 the mean and minimum dose to the PTV and the dose to 95% of the PTV decreased with most isocenter shifts. The maximum dose to the PTV changed little for any of the isocenter shifts compared to the nominal plan. In the brain there was also little change in the mean and maximum doses except in the case of IMPT plans. The maximum dose to the brain for IMPT showed an increase with most isocenter shifts and the increase was up to 10 Gy. The volumes of the brain receiving high and low doses (V_{5Gy}, V_{10Gy}, V_{50Gy}, V_{52Gy}, and V_{56Gy}) also changed little for most of the isocenter shifts compared to the nominal plan.

The small changes in the brain irradiation resulted in minor variations in NTCP and rNTCP. rNTCP results for patients 5 and 12 are summarized in Table 3.14 and 3.15 and displayed in Figure 3.12 and 3.13, respectively. From the figures it is clear that there is little change in rNTCP for either patient with isocenter shifts compared to the nominal plan. For patient 5 the greatest change in rNTCP was 0.12 from a right lateral shift (x-1 cm) in the PSPT plan and 0.18 from a superior shift (z+1 cm) in the IMPT plan. The

greatest changes in rNTCP for patient 12 for PSPT and IMPT plans resulted from a

superior shift (z+1 cm) and left lateral shift (z+1 cm) and were 0.11 and 0.08,

respectively.

Table 3.14 The ratio of normal tissue complication probability (rNTCP) for isocenter
shifts in patient 5.

rNTCP	PSPT/VMAT	IMPT/VMAT
nominal	0.72	0.57
x+1 (left lateral)	0.67	0.52
x-1 (right lateral	0.84	0.51
y+1 (posterior)	0.70	0.57
y-1 (anterior)	0.79	0.55
z+1 (superior	0.75	0.75
z-1 (inferior)	0.69	0.47

Table 3.15 The ratio of normal tissue complication probability (rNTCP) for isocenter
shifts in patient 12.

rNTCP	PSPT/VMAT	IMPT/VMAT
nominal	0.80	0.54
x+1 (left lateral)	0.76	0.46
x-1 (right lateral	0.71	0.49
y+1 (posterior)	0.73	0.55
y-1 (anterior)	0.85	0.51
z+1 (superior	0.91	0.61
z-1 (inferior)	0.76	0.62
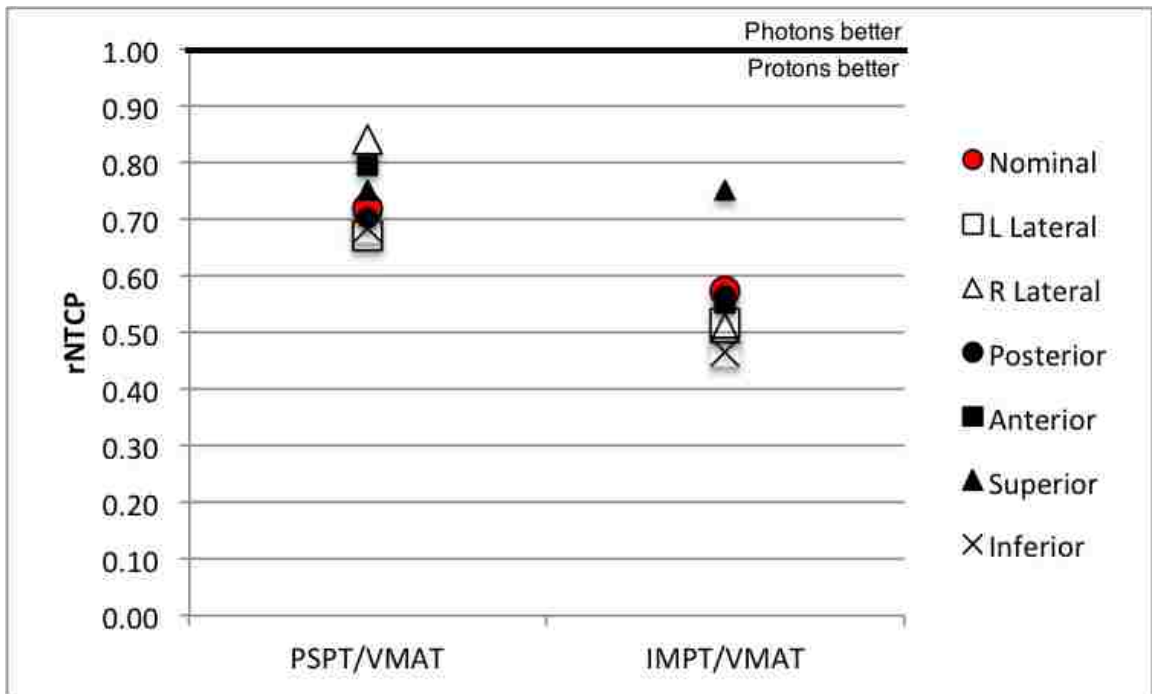
Figure 3.12 The change in rNTCP with isocenter shifts for patient 5.
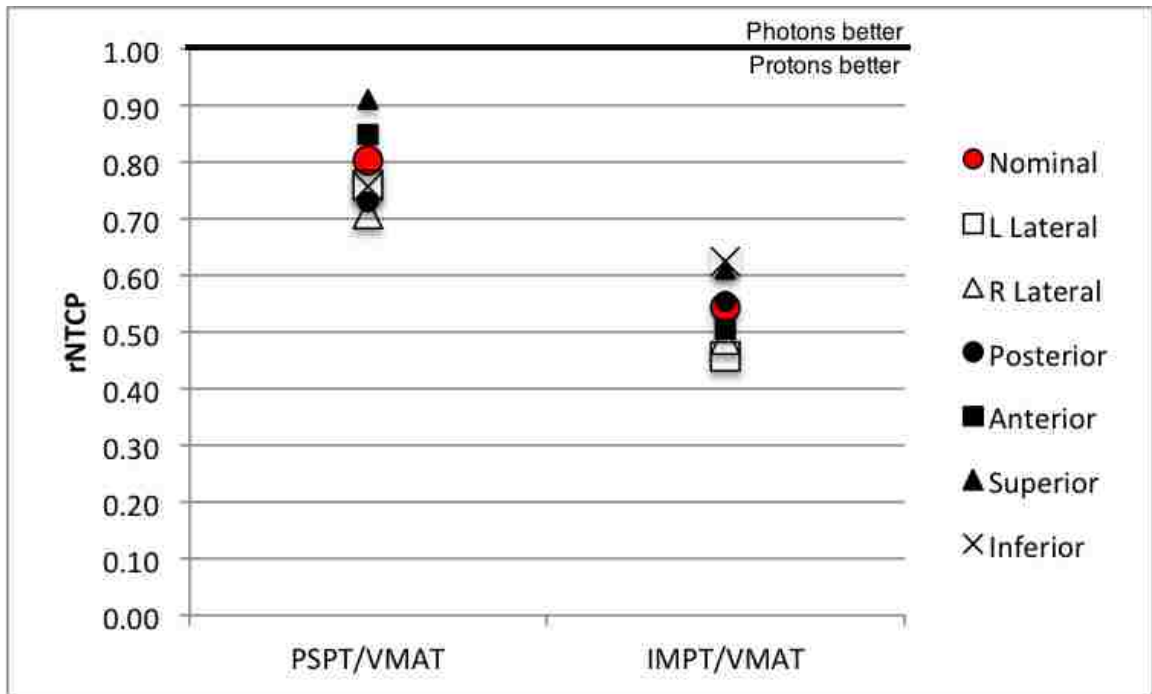
Figure 3.13 The change in rNTCP with isocenter shifts for patient 12.

3.4.2   Range Uncertainty Analysis

PSPT and IMPT DVHs with CT calibration curve errors for patient 5 and 12 are

shown in Figure 3.14 through 3.17. The changes in calibration curve affect the

conversion of Hounsfield units to proton stopping powers, ultimately resulting in a

change in proton range. An increase of the calibration curve by 10% decreased proton

range with a reduction of the doses for all structures compared to the nominal plan. A

decrease in the calibration curve of 10% had the opposite effect with an increase in the

proton range and increase of distal doses. The brain differential DVH curve was used for

NTCP calculation.
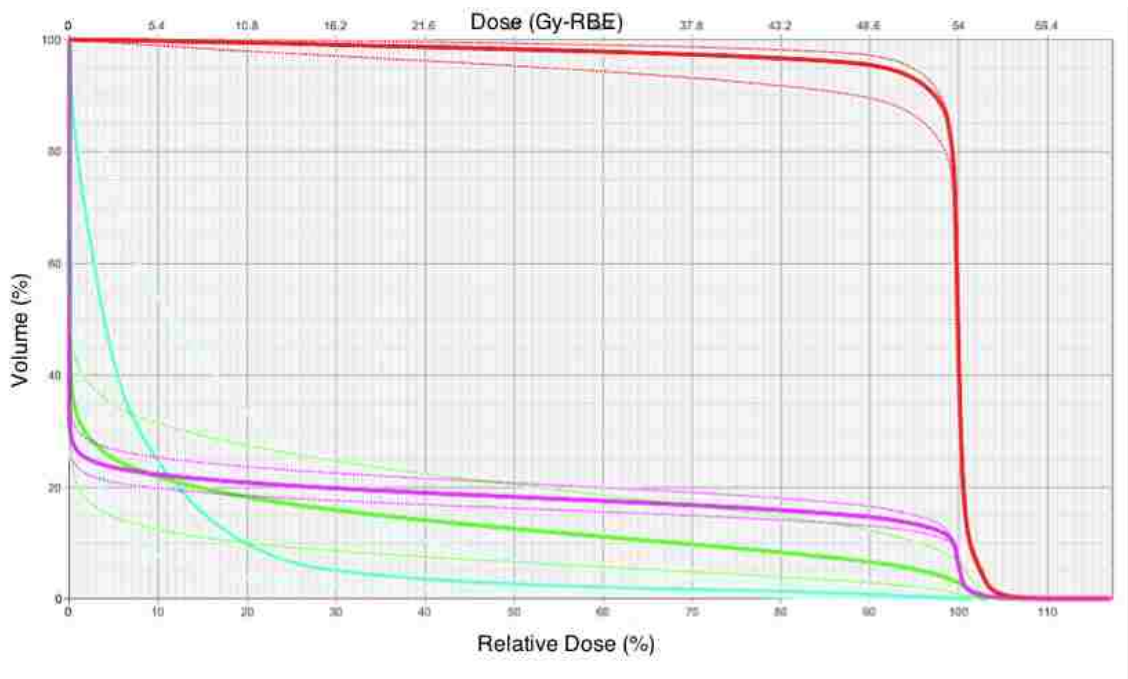
Figure 3.14 Screen shot of a plus and minus 10% calibration curve error for patient 5
PSPT DVH curve. Dotted lines represent the calibration error curve and the solid lines
are the nominal plan curves.
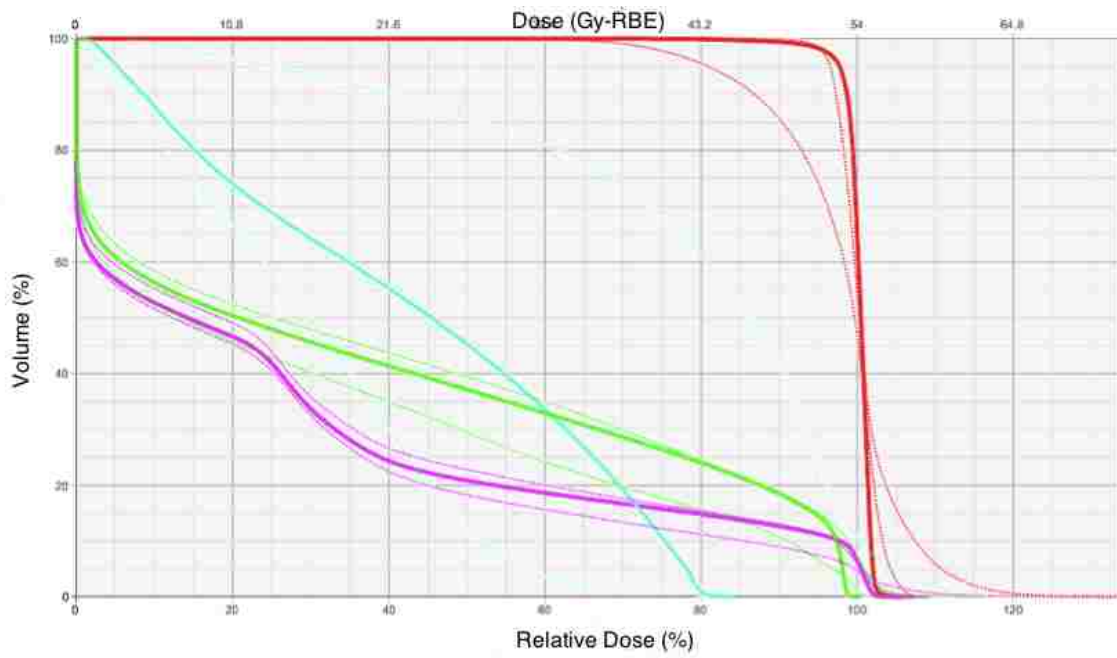
Figure 3.15 Screen shot of a plus and minus 10% calibration curve error for patient 5 IMPT DVH curve. Dotted lines represent the calibration error curve and the solid lines are the nominal plan curves.
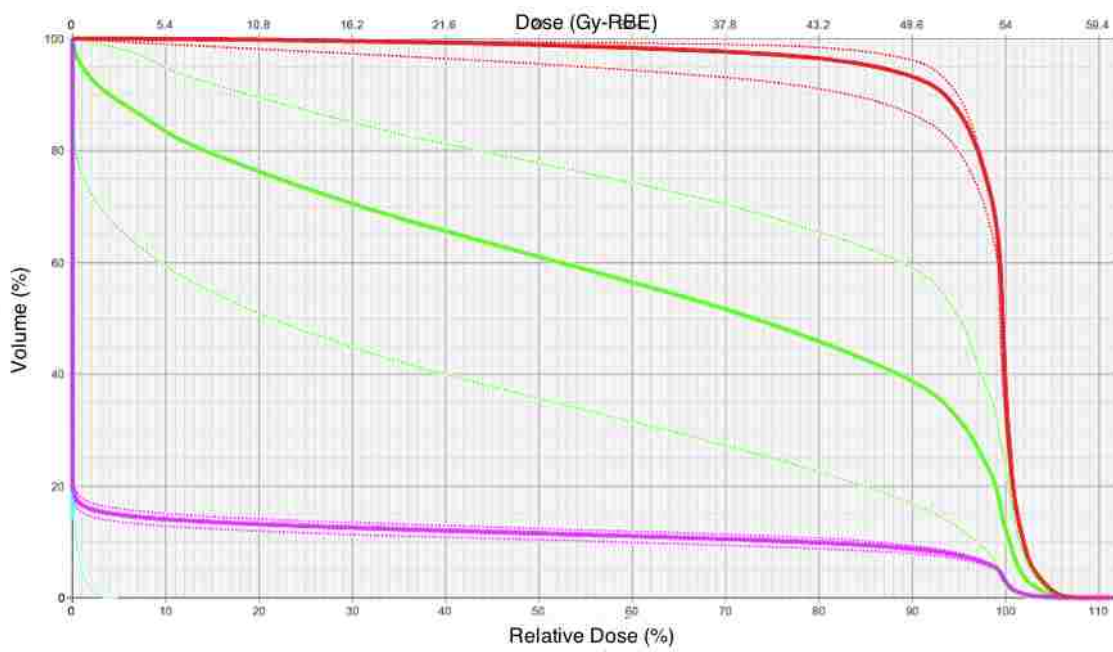
Figure 3.16 Screen shot of a plus and minus 10% calibration curve error for patient 12 PSPT DVH curve. Dotted lines represent the calibration error curve and the solid lines are the nominal plan curves.
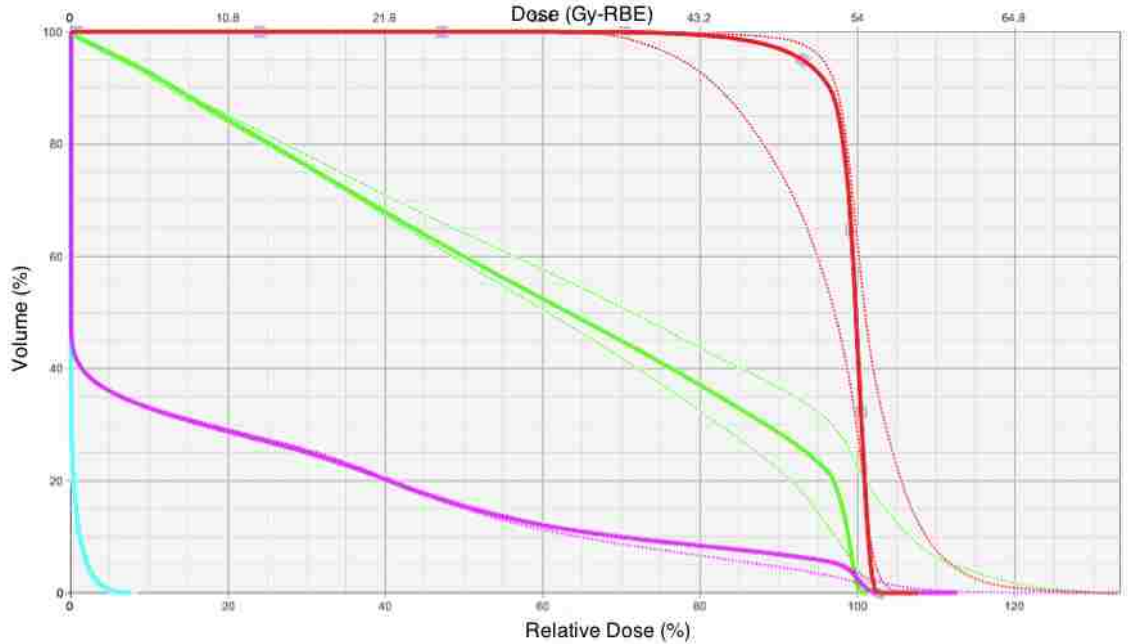
Figure 3.17 Screen shot of a plus and minus 10% calibration curve error for patient 12 IMPT DVH curve. Dotted lines represent the calibration error curve and the solid lines are the nominal plan curves.

NTCP and rNTCP results for patients 5 and 12 are summarized in Table 3.16 through 3.19 and displayed in Figure 3.18 and Figure 3.19. In both patients an increase in the calibration curve by 10% resulted in a reduction of NTCP for both PSPT and IMPT plans. A reduction of the calibration curve by 10% has the opposite effect and increased NTCP to levels near those of the VMAT plans.

Table 3.16 Effects of calibration curve error on NTCP for proton plans compared to the nominal in patient 5

	$NTCP_{VMAT}$	$NTCP_{PSPT}$	$NTCP_{IMPT}$
Nominal	0.14	0.10	0.08
+10%	-	0.08	0.03
-10%	-	0.14	0.12

Table 3.17 The ratio of NTCP (rNTCP) for calibration curve errors in patient 5.

rNTCP	PSPT/VMAT	IMPT/VMAT
Nominal	0.72	0.57
10%	0.57	0.20
-10%	0.99	0.84

Table 3.18 Effects of calibration curve error on NTCP for proton plans compared to the nominal for all plans for patient 12

	NTCP$_{VMAT}$	NTCP$_{PSPT}$	NTCP$_{IMPT}$
Nominal	0.027	0.022	0.015
10%	-	0.017	0.007
-10%	-	0.026	0.023

Table 3.19 Ratio of NTCP for calibration curve errors in patient 12.

rNTCP	PSPT/VMAT	IMPT/VMAT
Nominal	0.80	0.54
10%	0.61	0.25
-10%	0.95	0.84
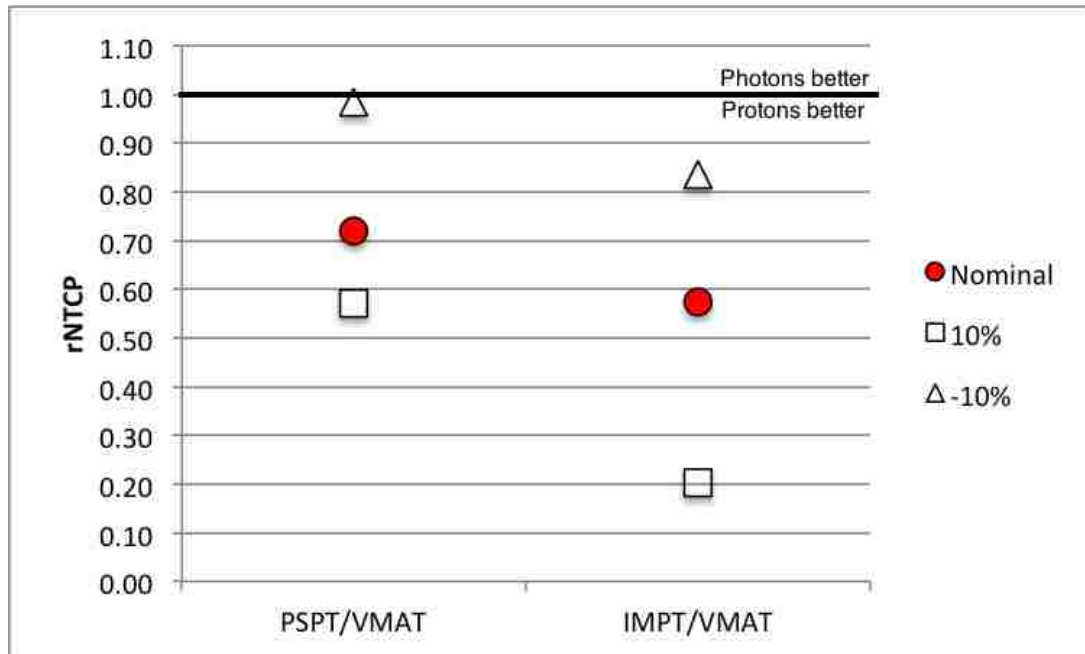
Figure 3.18 The ratio of normal tissue complication probability (rNTCP) for patient 5 with $\pm$10% calibration curve errors compared to the nominal rNTCP.
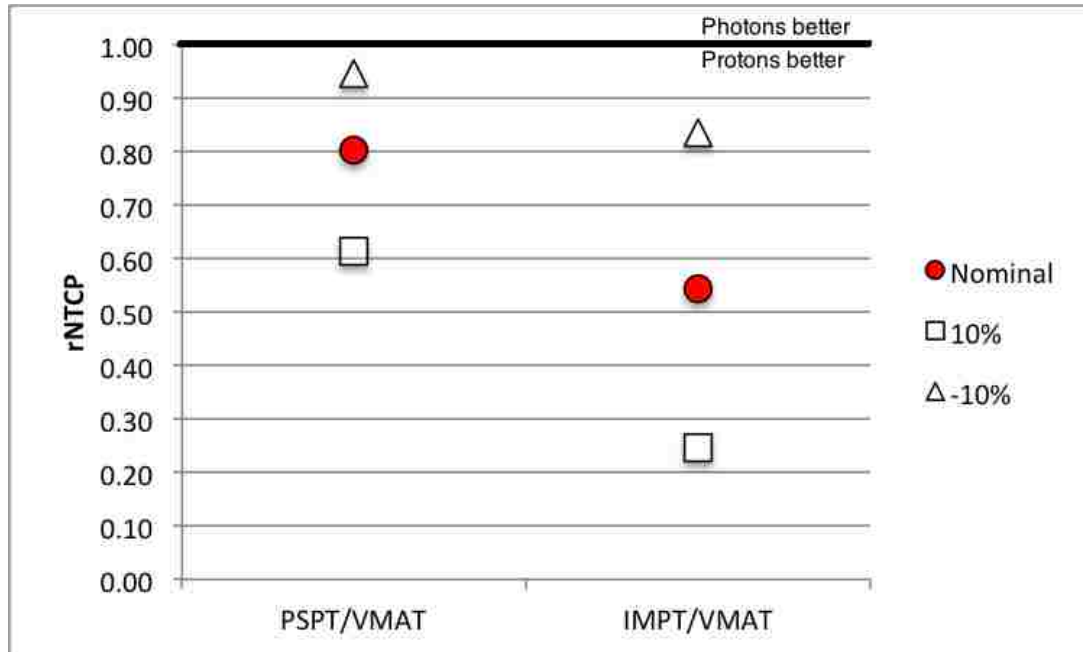
Figure 3.19 The ratio of normal tissue complication probability for patient 12 with ±10% calibration curve errors compared to the nominal rNTCP.

3.4.3   Risk Model Analysis

Table 3.20 and 3.21 summarize the results of the predicted risk of necrosis at 5 years post treatment calculated with the linear non threshold (LNT), linear threshold (LT), linear quadratic (LQ), and linear plateau (LP) models compared with the baseline risk calculated using the Lyman Kutcher Burman (LKB) model. All alternative risk models resulted in a higher percentage risk than the baseline LKB model. However, most of the models still showed a significant decrease in the risk for proton plans compared to VMAT plans. Only the linear threshold model for the PSPT plans resulted in risks that were not significantly different from the VMAT plans with an average value of 2.5 ± 1.2 % (PSPT) compared to 2.7 ± 1.2 % (VMAT).

Table 3.20 Calculated risk of necrosis using the linear non threshold (LNT) model and linear threshold (LT) model compared to the baseline risk calculated with the Lyman Kutcher Burman model for all patients. Descriptive statistics include the mean value with standard deviation (SD), and the p-value for the student t-test and Wilcoxon signed rank (WSR) test.

Patient index	LNT(%)			LT(%)			Baseline LKB(%)		
	VMAT	PSPT	IMPT	VMAT	PSPT	IMPT	VMAT	PS	IMPT
1	15.2	7.1	9.1	3.9	3.0	2.5	0.247	0.068	0.046
2	11.7	4.9	5.8	2.2	2.1	1.8	0.045	0.025	0.016
3	6.2	3.4	3.8	0.8	0.7	0.7	0.004	0.001	0.001
4	19.6	10.0	11.8	4.8	4.6	3.5	0.455	0.227	0.127
5	16.2	7.7	10.6	2.9	3.5	3.0	0.143	0.103	0.082
6	12.4	4.2	6.0	2.3	1.8	1.4	0.069	0.015	0.010
7	9.6	3.6	4.9	1.9	1.5	1.3	0.028	0.010	0.007
8	17.4	9.4	11.6	4.6	4.3	3.9	0.380	0.187	0.155
9	7.8	4.8	4.6	1.6	2.0	1.4	0.023	0.022	0.009
10	9.9	4.5	5.9	2.7	1.3	1.2	0.074	0.008	0.008
11	11.7	6.0	6.8	3.1	2.7	2.3	0.117	0.047	0.034
12	7.9	4.8	6.9	1.8	2.0	1.5	0.027	0.022	0.015
13	14.5	8.4	8.9	2.8	3.4	2.1	0.130	0.111	0.034
Average	12.3	6.1	7.4	2.7	2.5	2.1	0.13	0.07	0.04
SD	4.1	2.2	2.7	1.2	1.2	1.0	0.14	0.07	0.05
p-value	-	VMAT-PSPT	VMAT-IMPT	-	VMAT-PSPT	VMAT-IMPT	-	VMAT-PSPT	VMAT-IMPT
t-test	-	<<0.05	<<0.05	-	0.2	0.0005	-	0.008	0.006
WSR	-	0.001	0.001	-	0.2	0.02	-	0.001	0.001

Table 3.21 Calculated risk of necrosis using the linear quadratic (LQ) and linear plateau (LP) model compared to baseline risk calculated using the Lyman Kutcher Burman model for all patients. Descriptive statistics include the mean value with standard deviation (SD), and the p-value for the student t-test and Wilcoxon signed rank (WSR) test.

Patient index	LQ(%)			LP(%)			Baseline LKB(%)		
	VMAT	PSPT	IMPT	VMAT	PSPT	IMPT	VMAT	PSPT	IMPT
1	9.7	5.5	5.4	25.2	9.6	16.0	0.25	0.07	0.05
2	6.1	3.8	3.7	22.5	6.5	9.6	0.04	0.02	0.02
3	2.9	1.9	1.9	12.9	6.2	7.9	0.004	0.001	0.001
4	12.3	7.9	7.4	32.4	13.0	19.9	0.45	0.23	0.13
5	9.1	6.1	6.5	29.0	10.0	18.3	0.14	0.10	0.08
6	7.1	3.3	3.3	22.1	5.6	11.3	0.07	0.01	0.01
7	5.0	2.8	3.0	18.9	4.9	8.4	0.03	0.01	0.01
8	11.1	7.4	7.6	28.7	12.1	19.1	0.38	0.19	0.15
9	4.7	3.7	3.0	13.3	6.4	7.3	0.0230	0.0216	0.0090
10	6.3	3.0	3.2	16.3	7.2	10.9	0.0736	0.0076	0.0078
11	7.5	4.7	4.6	19.1	7.8	10.7	0.117	0.047	0.034
12	4.8	3.7	4.1	13.3	6.4	12.1	0.027	0.022	0.015
13	8.7	6.4	5.1	24.8	11.2	16.2	0.130	0.111	0.034
Average	7.3	4.6	4.5	21.4	8.2	12.9	0.13	0.07	0.04
SD	2.7	1.9	1.8	6.4	2.7	4.4	0.14	0.07	0.05
p-value	-	VMAT-PSPT	VMAT-IMPT	-	VMAT-PSPT	VMAT-IMPT	-	VMAT-PSPT	VMAT-IMPT
t-test	-	0.000002	0.000002	-	0.0000002	0.0000009	-	0.008	0.006
WSR	-	0.001	0.001	-	0.001	0.001	-	0.001	0.001

The ratio of risk from alternative risk model calculations can bee seen in Table

3.22 and 3.23 compared to the baseline ratio of risk calculated using the LKB model.

These results are also displayed in Figure 3.20 and 3.21 for PSPT and IMPT,

respectively. For all models the ratio was calculated and compared to 1 using the

Wilcoxon signed rank test. For almost all of the alternative risk models the calculated the

ratios of risk were significantly less than 1. Again the exception was the PSPT plans

calculated using the LT model: the average ratio of risk for these plans was 0.9 ± 0.2 and

4 of the 13 plans had a ratio above 1. The ratio of risk was not significantly less than one for these plans. There was also a single IMPT plan calculated using the LT model that had a ratio of risk above 1, but the average ratio of risk were still found to be significantly less than one.

Table 3.22 Ratio of risk calculated with the linear non threshold (LNT) and linear threshold (LT) models compared to the baseline ratio of risk calculated with the LKB model for all patients. Descriptive statistics include the mean value with standard deviation (SD), and the p-value for the Wilcoxon signed rank (WSR) test.

Patient index	rLNT		rLT		rRisk baseline	
	PSPT /VMAT	IMPT /VMAT	PSPT /VMAT	IMPT /VMAT	PSPT /VMAT	IMPT /VMAT
1	0.47	0.60	0.77	0.64	0.28	0.19
2	0.42	0.50	0.98	0.81	0.55	0.36
3	0.55	0.61	0.82	0.83	0.39	0.39
4	0.51	0.60	0.94	0.72	0.50	0.28
5	0.48	0.66	1.22	1.05	0.72	0.57
6	0.34	0.48	0.79	0.63	0.22	0.14
7	0.38	0.51	0.81	0.69	0.35	0.27
8	0.54	0.67	0.93	0.85	0.49	0.41
9	0.62	0.59	1.21	0.85	0.94	0.39
10	0.46	0.59	0.48	0.45	0.10	0.11
11	0.51	0.59	0.87	0.73	0.40	0.29
12	0.61	0.88	1.12	0.87	0.80	0.54
13	0.58	0.62	1.23	0.78	0.85	0.26
Average	0.5	0.6	0.9	0.8	0.5	0.3
SD	0.1	0.1	0.2	0.1	0.3	0.1
WSR	0.001	0.002	0.1	0.02	0.002	0.002

Table 3.23 Ratio of risk calculated with the linear quadratic (LQ) and linear plateau (LP) models compared to the baseline ratio of risk calculated with the LKB model for all patients. Descriptive statistics include the mean value with standard deviation (SD), and the p-value for the Wilcoxon signed rank (WSR) test.

Patient index	rLQ		rLP		rRisk baseline	
	PSPT /VMAT	IMPT /VMAT	PSPT /VMAT	IMPT /VMAT	PSPT /VMAT	IMPT /VMAT
1	0.56	0.56	0.38	0.63	0.28	0.19
2	0.62	0.60	0.29	0.43	0.55	0.36
3	0.64	0.64	0.48	0.61	0.39	0.39
4	0.64	0.61	0.40	0.61	0.50	0.28
5	0.66	0.71	0.35	0.63	0.72	0.57
6	0.46	0.47	0.25	0.51	0.22	0.14
7	0.55	0.59	0.26	0.44	0.35	0.27
8	0.67	0.68	0.42	0.67	0.49	0.41
9	0.79	0.64	0.48	0.55	0.94	0.39
10	0.47	0.51	0.44	0.67	0.10	0.11
11	0.63	0.62	0.41	0.56	0.40	0.29
12	0.77	0.84	0.48	0.91	0.80	0.54
13	0.74	0.59	0.45	0.66	0.85	0.26
Average	0.6	0.6	0.4	0.6	0.5	0.3
SD	0.1	0.1	0.1	0.1	0.3	0.1
WSR	0.001	0.001	0.001	0.001	0.002	0.002
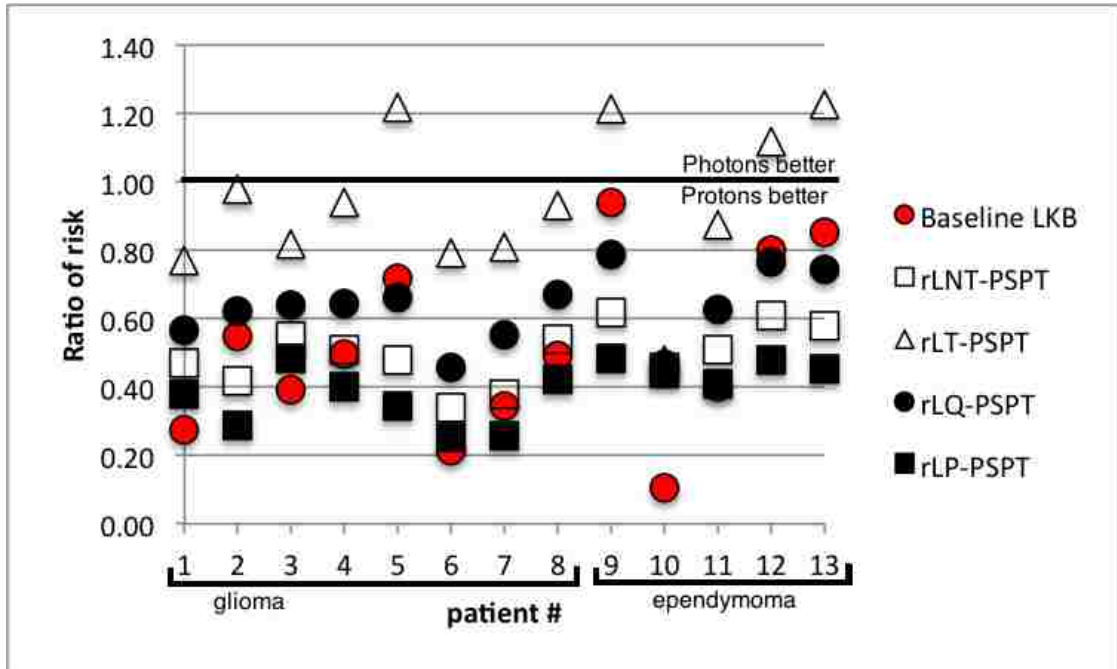
Figure 3.20 The ratio of risk of necrosis for PSPT plans compared to VMAT calculated with the linear no threshold (LNT), linear threshold (LT), linear quadratic (LQ), and linear plateau (LP) models compared to the baseline ratio of risk (red circles) calculated with the Lyman Kutcher Burman (LKB) model.
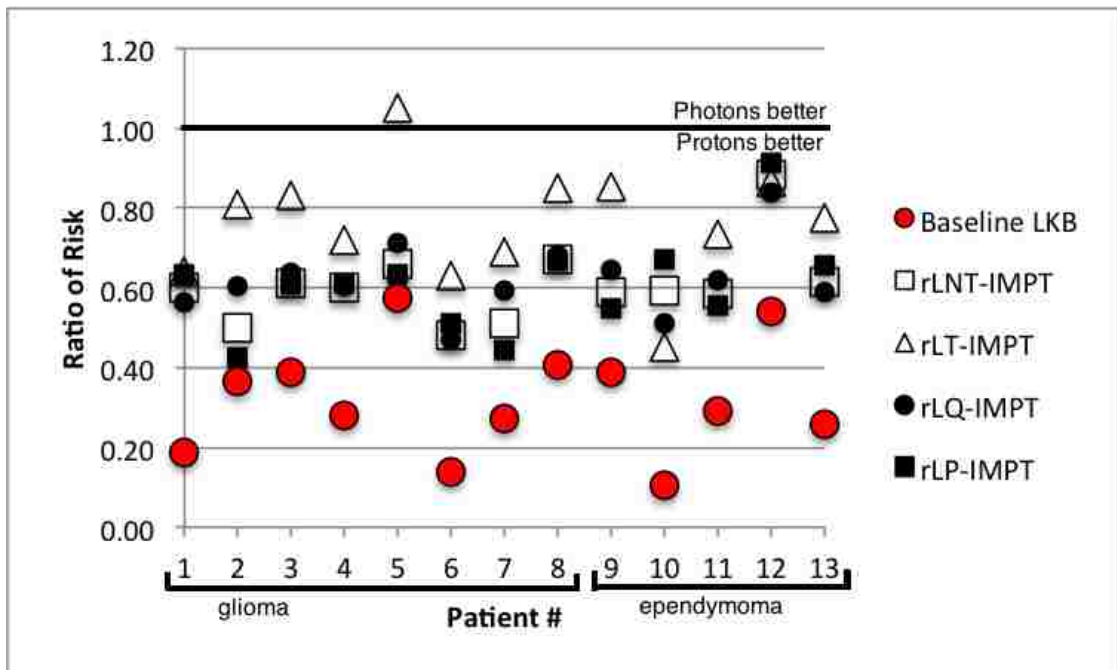
Figure 3.21 The ratio of risk of necrosis for IMPT plans compared to VMAT calculated with the linear non threshold (LNT), linear threshold (LT), linear quadratic (LQ), and linear plateau (LP) models compared to the baseline ratio of risk (red circles) calculated with the Lyman Kutcher Burman (LKB) model.

Chapter 4   Discussion

The objectives of this study were to calculate the predicted risk of radiation induced necrosis based on treatment plans for a cohort of pediatric patients using existing dose-risk models and to estimate the uncertainties in the calculated risk based on setup errors, proton range errors, and choice of risk model. The results show that both passively scattered proton therapy (PSPT) and intensity modulated proton therapy (IMPT) give a lower predicted risk of radiation induced necrosis than photon plans constructed using volumetric modulated arc therapy (VMAT). Sensitivity analysis reinforces the findings that protons confer a lower risk of radiation-induced necrosis.

4.1   Outcomes of specific aim one

Specific aim one was to evaluate and compare VMAT, PSPT and IMPT plans on the basis of dosimetric endpoints for the PTV and whole brain. For glioma patients (1-8) the planning goal was 95% of the prescription dose to be given to 95% of the volume. Most plans met this goal for all modalities of treatment plans with only 1 of the VMAT plans and 2 of the passive scatter plans falling below this value. Some studies have also found similar coverage between proton and with IMRT photon plans while others have shown better coverage for protons when compared against photon conformal radiation therapy (Bolsi *et al.*, 2003; Merchant *et al.*, 2008; Baumert *et al.*, 2004).

Ependymoma plans resulted in worse coverage than the glioma plans. Three of the PSPT plans and one of the IMPT plans fell below the planning goal of 90% of the prescription dose to 95% of the volume. However these plans were still clinically acceptable. It is important to note that with the location of the treatment volume there was some overlap in the brainstem. For this reason the PTV planning goal was sacrificed

63

in most cases since the constraint on the dose to the brainstem was considered as the paramount objective.

The minimum, maximum and mean dose metrics for the PTV were compared. The results typically showed a higher overall maximum dose for proton plans compared to VMAT, and a lower minimum dose. The mean dose showed no significant difference between PSPT, VMAT, or IMPT plans.

Passively scattered proton therapy (PSPT) plans tended to be much less homogeneous than either VMAT while IMPT plans showed no difference from VMAT in the PTV dose homogeneity. Contrary to our study Bolsi *et al.* (2003) found that passively scattered proton had better homogeneity than photons. However their comparison was with 3D conformal radiation therapy and not with VMAT, which typically has better conformity. Howell *et al.* (2012) also found that photon plans were found to have greater dose heterogeneity than passively scattered proton therapy (PSPT) for medulloblastoma Again, their study was not comparing PSPT to VMAT and additionally they used $D_{5\%}$ and $D_{95\%}$ for homogeneity calculation compared with $D_{2\%}$ and $D_{98\%}$ used in our study. Kozak *et al.* (2009) did compare protons to intensity modulated radiation therapy (IMRT) which has a similar dose delivery to VMAT and found that homogeneity was comparable between modalities.

The results of conformity showed that while PSPT and VMAT were similar, IMPT resulted in increase dose conformity to the PTV. Merchant *et al.* (2008) also found better conformity over photon therapy when using an active scanning technique for a variety of different brain cancer treatments. However the specific photon modality that was used for treatment was not specified in that study. Baumert *et al.* (2001) also found

increase conformity for IMPT and PSPT for irregularly shaped tumors compared to intensity modulated stereotactic radiotherapy but conformity was comparable between modalities for large concentric treatment volumes.

The dose metrics for the whole brain showed a reduction in the mean dose but an increased maximum dose for protons compared to VMAT. The reduction of the mean dose was expected since the protons have been shown to reduce the volume of surrounding tissue irradiated compared to photon therapies, thereby reducing the mean dose. Kozak *et al.* (2009) also found this reduction in the mean dose to surrounding normal tissues. The increase in the maximum dose is likely due to tissue heterogeneities (Urie *et al.*, 1984). Baumert *et al.* (2004) and Kozak *et al.* (2009)also found an increase in the maximum dose from protons compared to photon therapies.

The VMAT plans had much larger volumes of the brain that were irradiated to a low doses of 5 and 10 Gy RBE than the proton plans. Other studies have found similar results of normal tissue sparing for brain treatments (Fuss *et al.*, 1999; Lin *et al.*, 2000; Bolsi *et al.*, 2003; Baumert *et al.*, 2004; St. Clair *et al.*, 2004; Merchant *et al.*, 2008). However, the fractional volume of the brain receiving high dose ($V_{50Gy\text{-}RBE}$, $V_{52Gy\text{-}RBE}$, and $V_{56Gy\text{-}RBE}$) showed very little difference between planning modalities. These volume metrics were compared in a study by Murphy *et al.* (2012) and determined to be an indicator of risk for radiation necrosis. The volumes irradiated to the 50, 52, and 56 Gy levels were in most cases below the volume indicated by Murphy *et al.* (2012) to incur a 3.7% risk of necrosis. A more important indicator presented by that study was the infratentorial volumes irradiated and may be of interest in future studies for our ependymoma patients with assigned tumors located in the posterior fossa. Murphy *et al.*

(2012) found that the volume of the infratentorial brain that received 50, 52, and 54 Gy-RBE was a significant predictor for radiation necrosis.

4.2   Outcome for specific aim two

Specific aim two was to predict the risk of radiation necrosis for each treatment plan and the mean ratio of risk for a cohort of pediatric patients with ependymoma and glioma. This risk was calculated using LKB NTCP model. Result clearly showed that there is a reduction in the NTCP for both proton modalities relative to that for VMAT. However, the low level of risk calculated by the LKB model was largely unexpected. Previous studies have stated that the incidence of radiation necrosis is related to the total dose given, fraction size and irradiated volume (Ruben *et al.*, 2006; Lawrence *et al.*, 2010; Fink *et al.*, 2012). These studies reported an approximate incidence of 3% for prescribed dose of 50-60 Gy in 1.8-2.5 Gy/fraction for patients treated at their clinics. Our results were approximately 10% lower on average. Despite this discrepancy the mean rNTCP for PSPT and IMPT plans were 0.51 and 0.32, respectively, across the entire cohort. The Wilcoxon signed rank test was performed for these results confirming that both proton modalities (PSPT and IMPT) statistically significantly reduce the predicted risk of radiation-induced necrosis for our sample of pediatric patients.

4.3   Outcome of specific aim three

Specific aim three was to perform sensitivity analysis to determine if the baseline risk is dependent on setup error, proton range uncertainties and risk model selection. Simulated setup and range errors were performed by shifting the plan isocenter and introducing calibration curve errors, respectively, for 2 patients. Alternative risk model assessment was performed for all patients and compared to the baseline risk

Plan specific isocenter shifts resulted in a reduction of PTV coverage as seen by a reduction in the dose to 95% of the PTV ($D_{95\%}$) and the mean dose to the PTV for both patient 5 and 12. This result was expected for a simulated patient setup error since we are moving the isocenter away from the center of the PTV resulting in a slight miss in the target. The minimum and maximum dose to both the PTV and brain fluctuated with isocenter shift but tended to have much greater changes in the proton plans compared to VMAT plans. Overall the changes in the dose metric for isocenter shifts were minimal and resulted in minor variations in NTCP and the ratio of NTCP compared to the nominal plans. PSPT plans seemed to be slightly more susceptible to setup error, which is likely due to the single beam arrangement that was used in most of the PSPT plans.

Range errors from shifts in the CT calibration curve resulted in changes to the relative risk of necrosis (rNTCP) across proton planning modalities. An increase of 10% in the calibration curve resulted in reduction of the proton range within the target as well as within the brain and a reduction in the risk. A decrease in the calibration curve would have the opposite effect and an increase in the risk of necrosis was the result. This is in accordance with calibration reports for HU-proton stopping power in the literature.(Schneider *et al.*, 1996; Urie *et al.*, 1984; Schaffner and Pedroni, 1998; Moyers *et al.*, 2001) Additionally a 10% shift in the calibration curve is unlikely and is at the high end of what might be expected for actual range uncertainty. Even with such a large shift all of the proton NTCP values are still less than or equal to VMAT NTCP resulting in a rNTCP of less than 1 for all range errors.

The choice of risk model used can cause large variations in the NTCP results as seen with the alternate risk models chosen in this paper. Most alternative models we

considered showed a reduction in the predicted risk when PSPT or IMPT was used instead of VMAT. Unfortunately, there are very few models to choose from with necrosis as an endpoint that take all variables into account. Our findings clearly revealed that LKB, LNT, and LP models were strongly influenced by the volume of the brain irradiated at low dose. And although volumes receiving low dose may increase the chance of developing necrosis we believe that necrosis is likely a deterministic effect with a threshold dose and that the high dose region may strongly impact the initial necrotic incident. Additionally, the linear threshold (LT) model had a threshold at about 43 Gy-RBE and resulted in risks of necrosis of approximately 1-5% as seen in Table 3.20, which better agreed with retrospective studies of similar prescriptions and fractionation and had observed rates of necrosis of approximately 3-5%. (Ruben *et al.*, 2006; Murphy *et al.*, 2012; Lee *et al.*, 2011)

4.4   Implications of this study

The risk of radiation necrosis is of particular interest in pediatric patients with brain cancer because the current cure rates for these cancers are high and life expectancy is long. Additionally, with the second highest incidence among pediatrics, brain cancer is more prevalent than many other cancers and necrosis is severe side effect of treatment that is potentially fatal.

The findings of this study indicate that choosing either PSPT or IMPT over VMAT when treating some pediatric brain cancer patients can reduce the predicted risk of radiation necrosis. The ratio of risk was sensitive to proton range uncertainty but still showed significant risk reduction for proton plans over VMAT. Additionally the choice of risk model had little impact on the ratio of risk for necrosis except for the linear

threshold (LT) model, which in some cases resulted in ratios of risk greater than one. The LT model reduces the impact of the low dose volumes in risk calculation by instituting a threshold dose, which result in calculation of risk only in the high dose region.

4.5   Strengths and limitations of this study

This study had several strengths. Among them was the use of clinically realistic data from 13 pediatric patients. Additionally all plans were planned by a single individual and approved by a single board certified radiation oncologist to reduce bias between plans and give an accurate comparison. Patient plans were also investigated for uncertainties such as setup error and range error to determine if the rNTCP for radiation necrosis was sensitive to shifts and proton range errors compared to the nominal beam delivery. Finally the LKB NTCP model was used as a baseline measurement for risk of necrosis, and alternative risk models were examined too.

Some limitations of this study include the small patient cohort. Although we used real patient data the time resource constraints made it difficult include a larger pediatric patient population. However, with a cohort of 13 pediatric patients, statistical comparison was still applicable and largely overcome this limitation.

Another limitation was risk model selection. Little has been done to develop a model that accurately predicts radiation necrosis or improves upon the existing LKB NTCP model. Lawrence *et al.* (2010) in their recent study as part of a Quantitative Analyses of Normal Tissue Effects in the Clinic (QUANTEC) stated that the data used for the data that the LKB model is based off of was likely conservative but they did not propose a new model. Additionally, recent studies such as the one by Murphy *et al.* (2012) reported higher incidence than the risk predicted by the LKB model in this

research. For these reason, a sensitivity analysis was performed to determine the effects of risk model selection on the ratio of normal tissue complication probability (rNTCP).

4.6   Future work

Future studies should investigate in greater detail the effects of proton range error on clinical acceptability and its effect on necrosis. Additionally there are some clinical alternatives for treatment that may increase the potential risk of necrosis from protons therapy (i.e. patch beams). Maybe most importantly there is potential for development of a risk model that can better predict the risk of necrosis. An important step in this process would be a better understanding of the patient history, pediatric and otherwise, that have been diagnosed with necrosis across a large population. Currently there is little information, or little shared, on the population of patients that have developed necrosis post irradiation from any institution. From this information a new analytical model for necrosis could be developed that might better predict the risk of RIN.

Chapter 5   Conclusion

This study demonstrated that proton plans (PSPT and IMPT) were capable of reducing the predicted risk of necrosis. IMPT overall had improved conformity and similar homogeneity to VMAT plans with similar PTV coverage while PSPT had similar conformity to VMAT and worse homogeneity and typically worse coverage of the PTV compared to VMAT. VMAT plans delivered low dose to a considerably greater volume of the brain.

Calculated NTCP resulted in a fairly low risk of necrosis to the brain however the ratio of risk showed a considerable reduction when using either PSPT or IMPT over VMAT. The effects of setup and range uncertainties did have an effect on the calculated rNTCP but did not affect the qualitative findings that both proton modalities confer a reduced risk of necrosis. For all alternative models, except the linear threshold (LT) model, the ratio of risk was insensitive to the selection of risk model selection and upheld the findings that PSPT and IMPT confer a reduction in the risk of radiation necrosis. For these reasons we must reject the null hypothesis and conclude that, for our cohort of pediatric patients, proton plans resulted in a reduction in the predicted risk of radiation induced necrosis of the brain.

References

Ashamalla H L, Thom S R and Goldwein J W 1996 Hyperbaric oxygen therapy for the treatment of radiation-induced sequelae in children. The University of Pennsylvania experience *Cancer* 77 2407-12

Attix F H 2007 *Introduction to Radiological Physics and Radiation Dosimetry*: Wiley-VCH Verlag GmbH) pp 124-59

Baumert B G, Lomax A J, Miltchev V and Davis J B 2001 A comparison of dose distributions of proton and photon beams in stereotactic conformal radiotherapy of brain lesions *International Journal of Radiation Oncology*Biology*Physics* 49 1439-49

Baumert B G, Norton I A, Lomax A J and Davis J B 2004 Dose conformation of intensity-modulated stereotactic photon beams, proton beams, and intensity-modulated proton beams for intracranial lesions *International Journal of Radiation Oncology*Biology*Physics* 60 1314-24

Bennett M, Feldmeier J, Hampson N, Smee R and Milross C 2012 Hyperbaric oxygen therapy for late radiation tissue injury. *Cochrane Database of Systematic Reviews*

Bennett M H, Feldmeier J, Hampson N, Smee R and Milross C 2005 Hyperbaric oxygen therapy for late radiation tissue injury *The Cochrane database of systematic reviews* CD005005

Boehling N S, Grosshans D R, Bluett J B, Palmer M T, Song X, Amos R A, Sahoo N, Meyer J J, Mahajan A and Woo S Y 2012 Dosimetric comparison of three-dimensional conformal proton radiotherapy, intensity-modulated proton therapy, and intensity-modulated radiotherapy for treatment of pediatric craniopharyngiomas *International journal of radiation oncology, biology, physics* 82 643-52

Bolsi A, Fogliata A and Cozzi L 2003 Radiotherapy of small intracranial tumours with different advanced techniques using photon and proton beams: a treatment planning study *Radiotherapy and Oncology* 68 1-14

Burman C, Kutcher,G.J., Emami, B., Goitein, M. 1991 Fitting of Normal Tissue Tolerance Data to an Analytic Function *Int. J. Radiat. Oncol. Biol. Phys.* 21 123-35

Bushberg J T 2002 *The Essential Physics of Medical Imaging*: Lippincott Williams & Wilkins)

Chao S T, Ahluwalia M S, Barnett G H, Stevens G H, Murphy E S, Stockham A L, Shiue K and Suh J H 2013 Challenges with the diagnosis and treatment of cerebral

radiation necrosis *International journal of radiation oncology, biology, physics* 87 449-57

Chuba P J, Aronin P, Bhambhani K, Eichenhorn M, Zamarano L, Cianci P, Muhlbauer M, Porter A T and Fontanesi J 1997 Hyperbaric oxygen therapy for radiation-induced brain injury in children *Cancer* 80 2005-12

De Laney T F and Kooy H M 2008 *Proton and charged particle radiotherapy* (Philadelphia: Wolters Kluwer Health/Lippincott Williams & Wilkins)

Delanian S and Lefaix J L 2007 Current management for late normal tissue injury: radiation-induced fibrosis and necrosis *Seminars in radiation oncology* 17 99-107

Delsigne J 2012 Treatments May Alleviate and Reverse Central Nervous System Radiation Necrosis *OncoLog* 57

Dolecek T A, Propp J M, Stroup N E and Kruchko C 2012 CBTRUS statistical report: primary brain and central nervous system tumors diagnosed in the United States in 2005-2009 *Neuro-oncology* 14 Suppl 5 v1-49

Feuvret L, Noel G, Mazeron J J and Bey P 2006 Conformity index: a review *International journal of radiation oncology, biology, physics* 64 333-42

Fink J, Born D and Chamberlain M C 2012 Radiation necrosis: relevance with respect to treatment of primary and secondary brain tumors *Current neurology and neuroscience reports* 12 276-85

Fuss M, Hug E B, Schaefer R A, Nevinny-Stickel M, Miller D W, Slater J M and Slater J D 1999 Proton radiation therapy (prt) for pediatric optic pathway gliomas: comparison with 3d planned conventional photons and a standard photon technique *International Journal of Radiation Oncology*Biology*Physics* 45 1117-26

Gonzalez J, Kumar A J, Conrad C A and Levin V A 2007 Effect of bevacizumab on radiation necrosis of the brain *International journal of radiation oncology, biology, physics* 67 323-6

Haas-Kogan D A, Barani I J, Hayden M G, Edwards M S B and Fisher P G 2010 *Pediatric Central Nervous System Tumors*

Hall E J and Giaccia A J 2012 *Radiobiology for the radiologist* (Philadelphia: Wolters Kluwer Health/Lippincott Williams & Wilkins)

Halperin E C, Constine L S and Tarbell N J 2010 *Pediatric Radiation Oncology*: Lippincott Williams & Wilkins)

Hoppe R, Phillips T L and Roach M 2010 *Leibel and Phillips Textbook of Radiation Oncology: Expert Consult*: Elsevier Health Sciences)

Howell R, Giebeler A, Koontz-Raisig W, Mahajan A, Etzel C, D'Amelio A, Homann K and Newhauser W 2012 Comparison of therapeutic dosimetric data from passively scattered proton and photon craniospinal irradiations for medulloblastoma *Radiation Oncology* 7 116

Kozak K R, Adams J, Krejcarek S J, Tarbell N J and Yock T I 2009 A Dosimetric Comparison of Proton and Intensity-Modulated Photon Radiotherapy for Pediatric Parameningeal Rhabdomyosarcomas *International Journal of Radiation Oncology*Biology*Physics* 74 179-86

Kutcher G J and Burman C 1989 Calculation of complication probability factors for non-uniform normal tissue irradiation: The effective volume method gerald *International journal of radiation oncology, biology, physics* 16 1623-30

Lawrence Y R, Li X A, el Naqa I, Hahn C A, Marks L B, Merchant T E and Dicker A P 2010 Radiation dose-volume effects in the brain *International journal of radiation oncology, biology, physics* 76 S20-7

Lee A W, Foo W, Chappell R, Fowler J F, Sze W M, Poon Y F, Law S C, Ng S H, O S K, Tung S Y, Lau W H and Ho J H 1998 Effect of time, dose, and fractionation on temporal lobe necrosis following radiotherapy for nasopharyngeal carcinoma *International journal of radiation oncology, biology, physics* 40 35-42

Lee D-S, Yu M, Jang H-S, Kim Y-S, Choi B-O, Kang Y-N, Lee Y-S, Kim D-C, Hong Y-K, Jeun S-S and Yoon S-C 2011 Radiation-induced brain injury: retrospective analysis of twelve pathologically proven cases *Radiat Oncol J* 29 147-55

Li Z 2012 Toward robust proton therapy planning and delivery *Transl Cancer Res* 1 217-26

Lin R, Hug E B, Schaefer R A, Miller D W, Slater J M and Slater J D 2000 Conformal proton radiation therapy of the posterior fossa: a study comparing protons with three-dimensional planned photons in limiting dose to auditory structures *International Journal of Radiation Oncology*Biology*Physics* 48 1219-26

Louis D N, Ohgaki H, Wiestler O D, Cavenee W K, Burger P C, Jouvet A, Scheithauer B W and Kleihues P 2007 The 2007 WHO classification of tumours of the central nervous system *Acta neuropathologica* 114 97-109

Merchant T E, Hua C-h, Shukla H, Ying X, Nill S and Oelfke U 2008 Proton versus photon radiotherapy for common pediatric brain tumors: Comparison of models of dose characteristics and their relationship to cognitive function *Pediatric Blood & Cancer* 51 110-7

Moyers M F, Miller D W, Bush D A and Slater J D 2001 Methodologies and tools for proton beam design for lung tumors *International journal of radiation oncology, biology, physics* 49 1429-38

Murphy E S, Merchant T E, Wu S, Xiong X, Lukose R, Wright K D, Qaddoumi I, Armstrong G T, Broniscer A and Gajjar A 2012 Necrosis after craniospinal irradiation: results from a prospective series of children with central nervous system embryonal tumors *International journal of radiation oncology, biology, physics* 83 e655-60

Myrehaug S, Chan G, Craig T, Weinberg V, Cheng C, Roach M, 3rd, Cheung P and Sahgal A 2012 A treatment planning and acute toxicity comparison of two pelvic nodal volume delineation techniques and delivery comparison of intensity-modulated radiotherapy versus volumetric modulated arc therapy for hypofractionated high-risk prostate cancer radiotherapy *International journal of radiation oncology, biology, physics* 82 e657-62

Ostrom Q T, Gittleman H, Farah P, Ondracek A, Chen Y, Wolinsky Y, Stroup N E, Kruchko C and Barnholtz-Sloan J S 2013 CBTRUS statistical report: Primary brain and central nervous system tumors diagnosed in the United States in 2006-2010 *Neuro-oncology* 15 Suppl 2 ii1-56

Otto K 2008 Volumetric modulated arc therapy: IMRT in a single gantry arc *Medical physics* 35 310

Pasler M, Georg D, Wirtz H and Lutterbach J 2011 Effect of photon-beam energy on VMAT and IMRT treatment plan quality and dosimetric accuracy for advanced prostate cancer. *Strahlentherapie und Onkologie : Organ der Deutschen Rontgengesellschaft ... [et al]* 187 792-8

Pizzo P A and Poplack D G 1997 *Principles and practice of pediatric oncology* (Philadelphia: Lippincott-Raven)

Qi X S, Stinauer M, Rogers B, Madden J R, Wilkening G N and Liu A K 2012 Potential for improved intelligence quotient using volumetric modulated arc therapy compared with conventional 3-dimensional conformal radiation for whole-ventricular radiation in children *International journal of radiation oncology, biology, physics* 84 1206-11

Rechner L A, Howell R M, Zhang R, Etzel C, Lee A K and Newhauser W D 2012 Risk of radiogenic second cancers following volumetric modulated arc therapy and proton arc therapy for prostate cancer *Phys. Med. Biol.* 57 7117-32

Ries L, Smith M, Gurney J, Linet M, Tamra T, Young J and Bunin G e NIH Pub. No. 99-4649 Cancer Incidence and Survival among Children and Adolescents: United States
SEER Program 1975-1995, National Cancer Institute, SEER Program. (Bethesda, MD,1999

Ruben J D, Dally M, Bailey M, Smith R, McLean C A and Fedele P 2006 Cerebral radiation necrosis: incidence, outcomes, and risk factors with emphasis on

radiation parameters and chemotherapy *International journal of radiation oncology, biology, physics* 65 499-508

Schaffner B and Pedroni E 1998 The precision of proton range calculations in proton radiotherapy treatment planning: experimental verification of the relation between CT-HU and proton stopping power *Physics in medicine and biology* 43 1579

Schild S E, Nisi K, Scheithauer B W, Wong W W, Lyons M K, Schomberg P J and Shaw E G 1998 The results of radiotherapy for ependymomas: the Mayo Clinic experience *International journal of radiation oncology, biology, physics* 42 953-8

Schneider U, Pedroni E and Lomax A 1996 The calibration of CT Hounsfield units for radiotherapy treatment planning *Physics in medicine and biology* 41 111

St. Clair W H, Adams J A, Bues M, Fullerton B C, La Shell S, Kooy H M, Loeffler J S and Tarbell N J 2004 Advantage of protons compared to conventional X-ray or IMRT in the treatment of a pediatric patient with medulloblastoma *International Journal of Radiation Oncology*Biology*Physics* 58 727-34

Urie M, Goitein M and Wagner M 1984 Compensating for heterogeneities in proton radiation therapy *Physics in medicine and biology* 29 553

Whelan H T and Helms A K 2012 Hyperbaric oxygen for neurologic indications. Action plan for multicenter trials in: stroke, traumatic brain injury, radiation encephalopathy and status migrainosus *Pediatria Polska* 87 429-37

Wong E T, Huberman M, Lu X Q and Mahadevan A 2008 Bevacizumab reverses cerebral radiation necrosis *Journal of clinical oncology : official journal of the American Society of Clinical Oncology* 26 5649-50

Yoon M, Park S Y, Shin D, Lee S B, Pyo H R, Kim D Y and Cho K H 2007 A new homogeneity index based on statistical analysis of the dose-volume histogram *Journal of applied clinical medical physics / American College of Medical Physics* 8 9-17

Appendix A: Isodose Distributions

Isodose	Color
59.4 Gy-RBE	
56.7 Gy-RBE	
54 Gy-RBE	
51.3 Gy-RBE	
48.6 Gy-RBE	
30 Gy-RBE	
20 Gy-RBE	
10 Gy-RBE	
5 Gy-RBE	

ROI	Color
PTV	colorwash
Brain Stem	colorwash
Optic Chiasm	colorwash
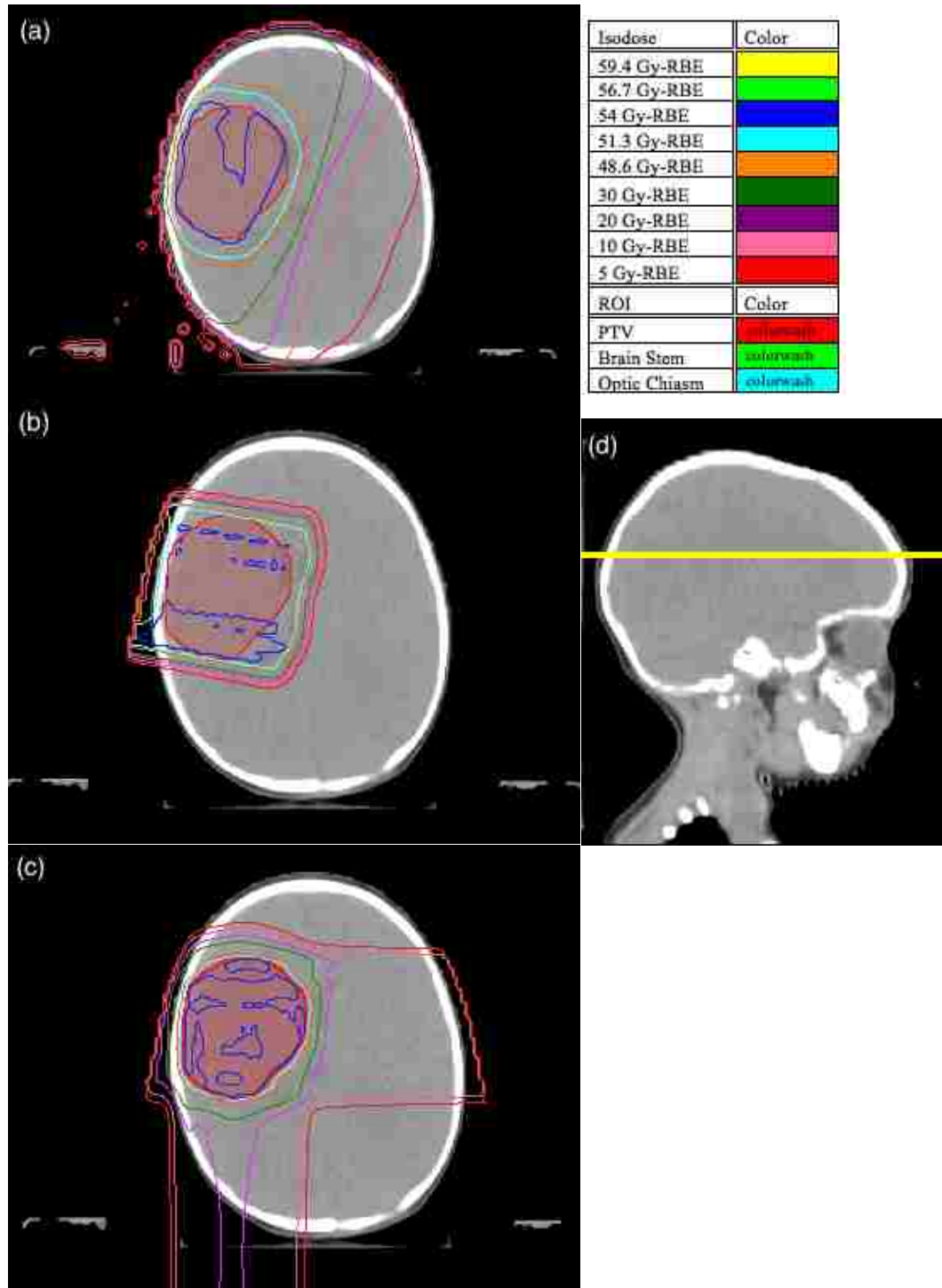
Figure A.1 Isodose distributions for VMAT(a), PSPT (b), and IMPT (c) for patient 1.
The slice location is through the planning isocenter and displayed on the sagittal view (d)
by a yellow line.

Isodose	Color
59.4 Gy-RBE	
56.7 Gy-RBE	
54 Gy-RBE	
51.3 Gy-RBE	
48.6 Gy-RBE	
30 Gy-RBE	
20 Gy-RBE	
10 Gy-RBE	
5 Gy-RBE	
ROI	Color
PTV	colorwash
Brain Stem	colorwash
Optic Chiasm	colorwash
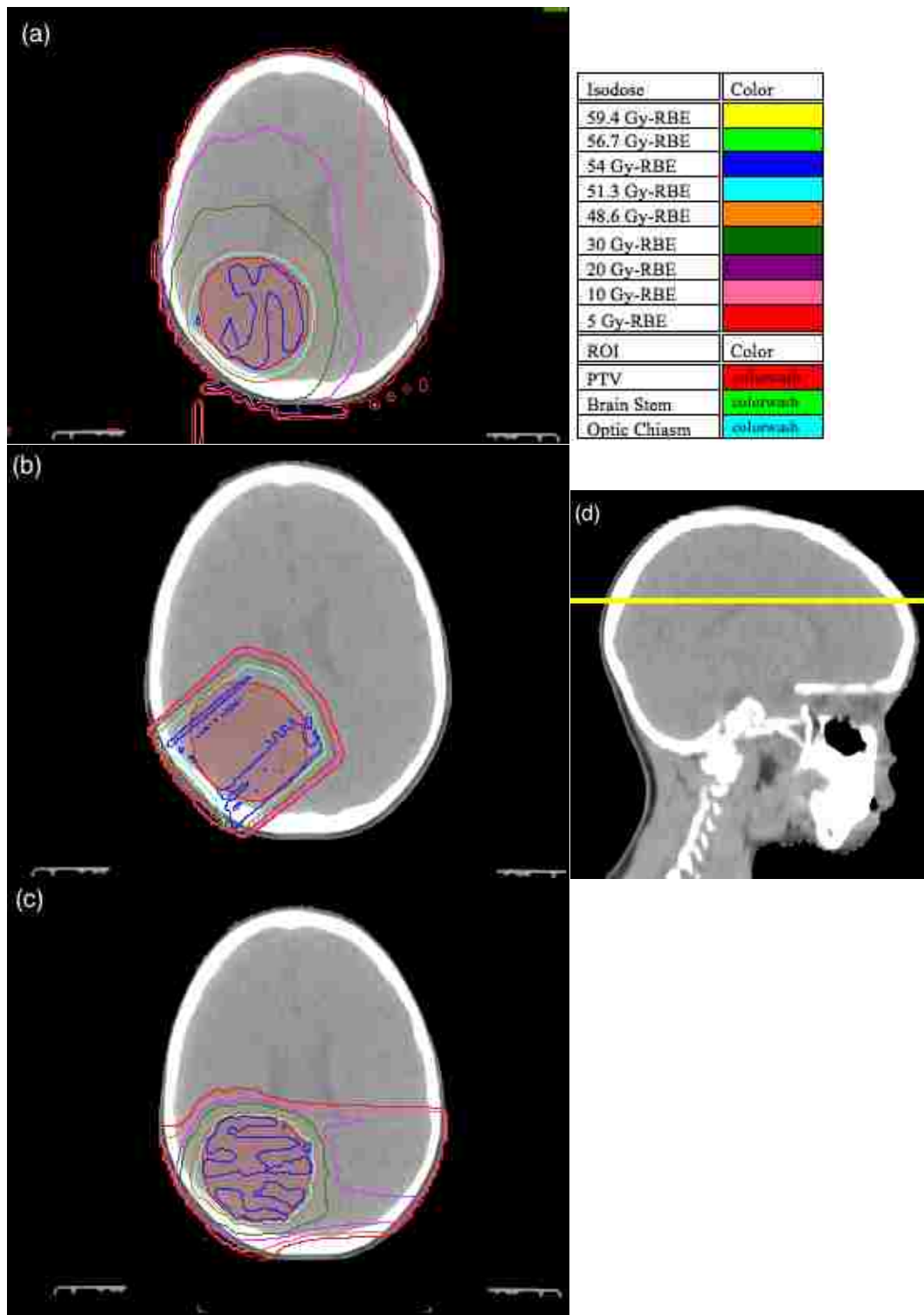
Figure A.2 Isodose distributions for VMAT(a), PSPT (b), and IMPT (c) for patient 2.
The slice location is through the planning isocenter and displayed on the sagittal view (d)
by a yellow line.
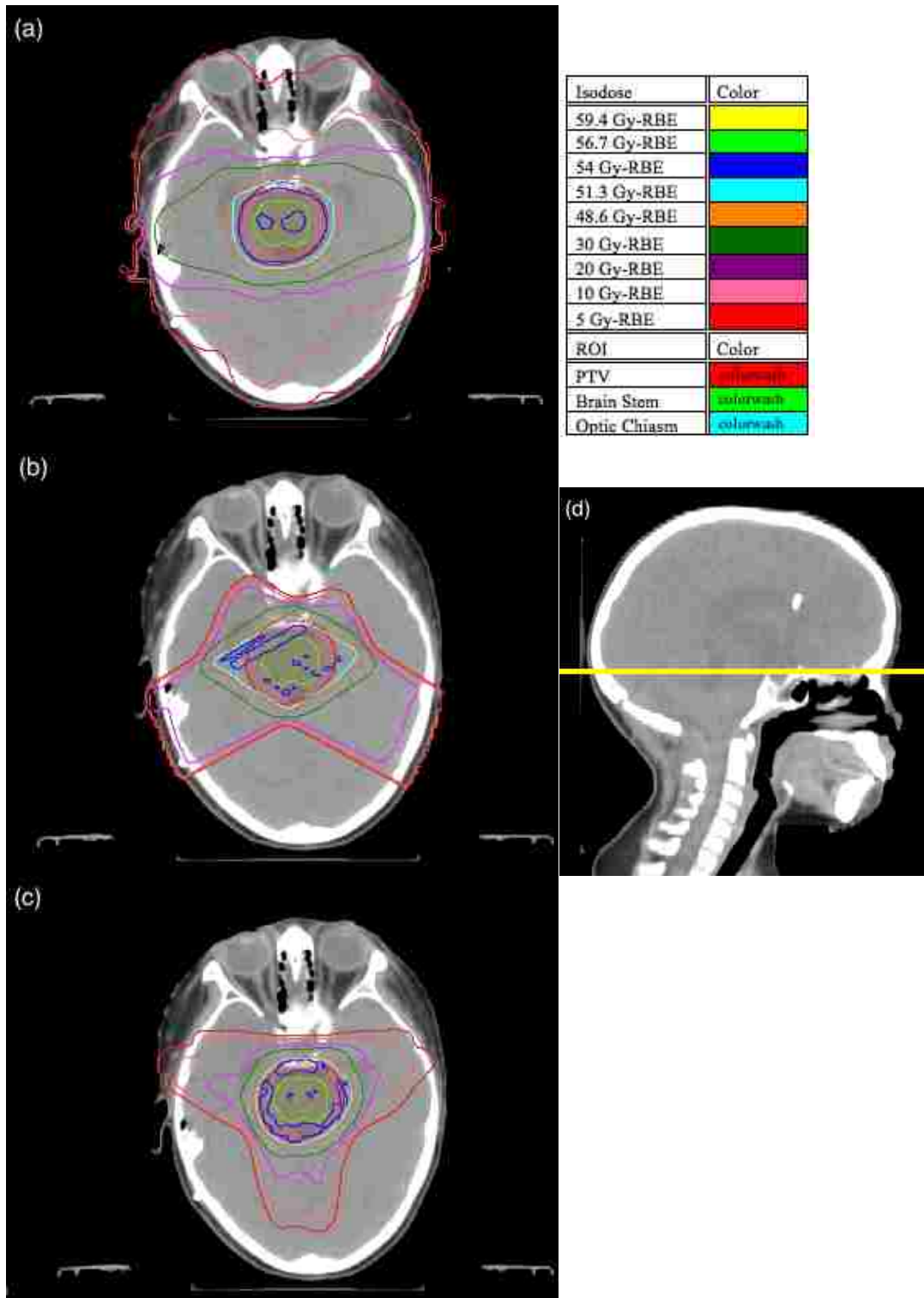
Figure A.3 Isodose distributions for VMAT(a), PSPT (b), and IMPT (c) for patient 3. The slice location is through the planning isocenter and displayed on the sagittal view (d) by a yellow line.
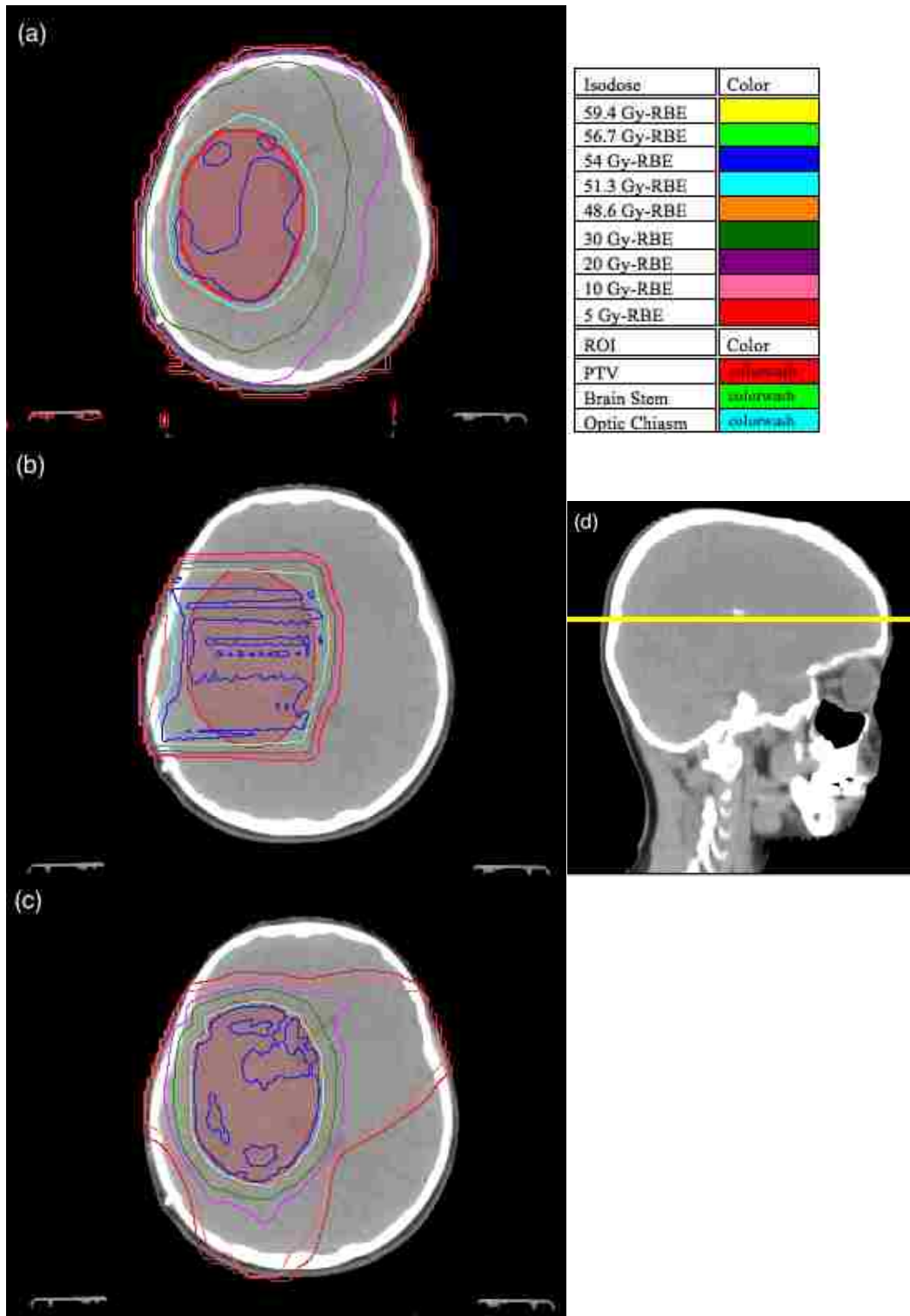
Figure A.4 Isodose distributions for VMAT(a), PSPT (b), and IMPT (c) for patient 4. The slice location is through the planning isocenter and displayed on the sagittal view (d) by a yellow line.
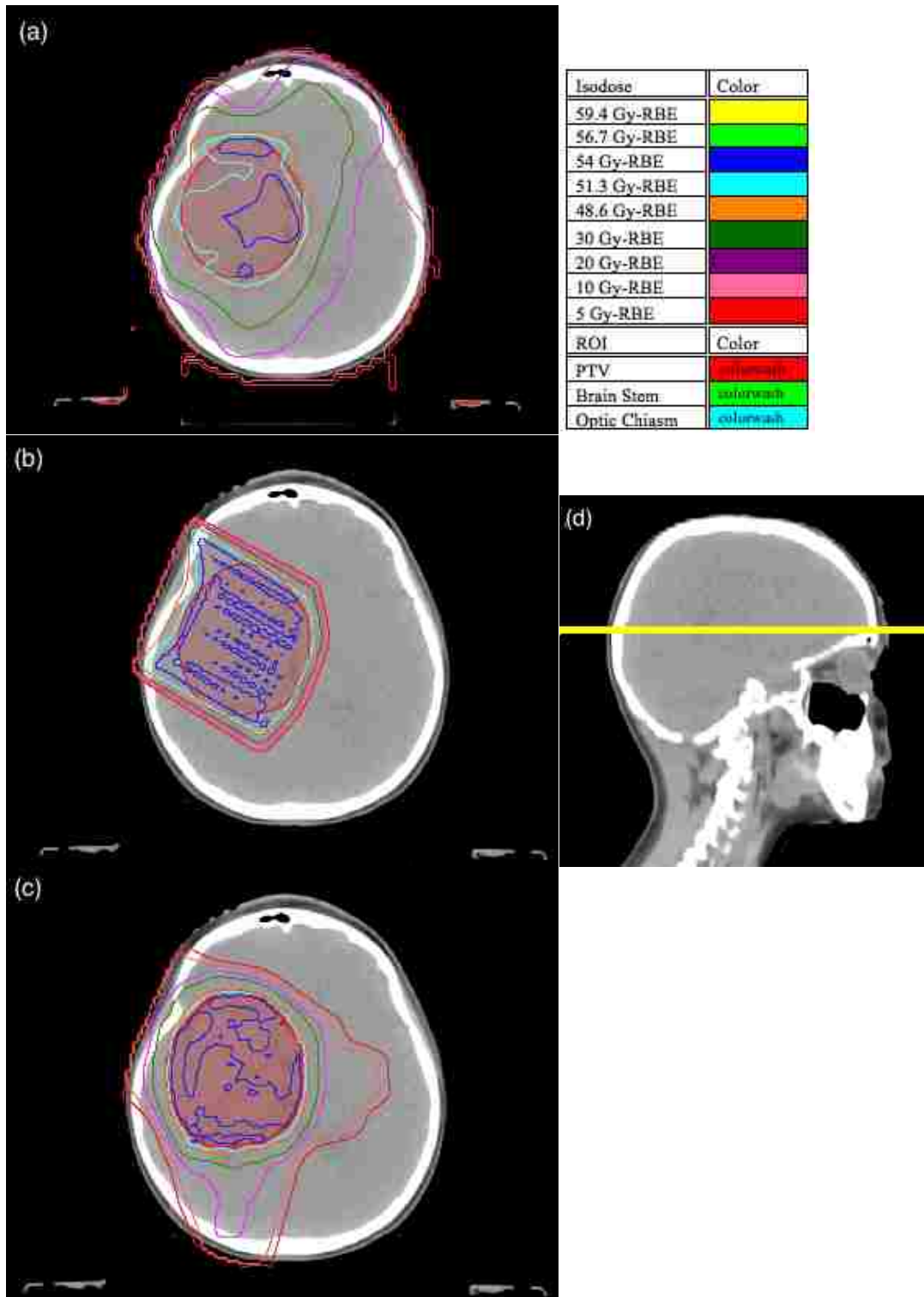
Figure A.5 Isodose distributions for VMAT(a), PSPT (b), and IMPT (c) for patient 5.
The slice location is through the planning isocenter and displayed on the sagittal view (d)
by a yellow line.

Isodose	Color
59.4 Gy-RBE	
56.7 Gy-RBE	
54 Gy-RBE	
51.3 Gy-RBE	
48.6 Gy-RBE	
30 Gy-RBE	
20 Gy-RBE	
10 Gy-RBE	
5 Gy-RBE	

ROI	Color
PTV	colorwash
Brain Stem	colorwash
Optic Chiasm	colorwash
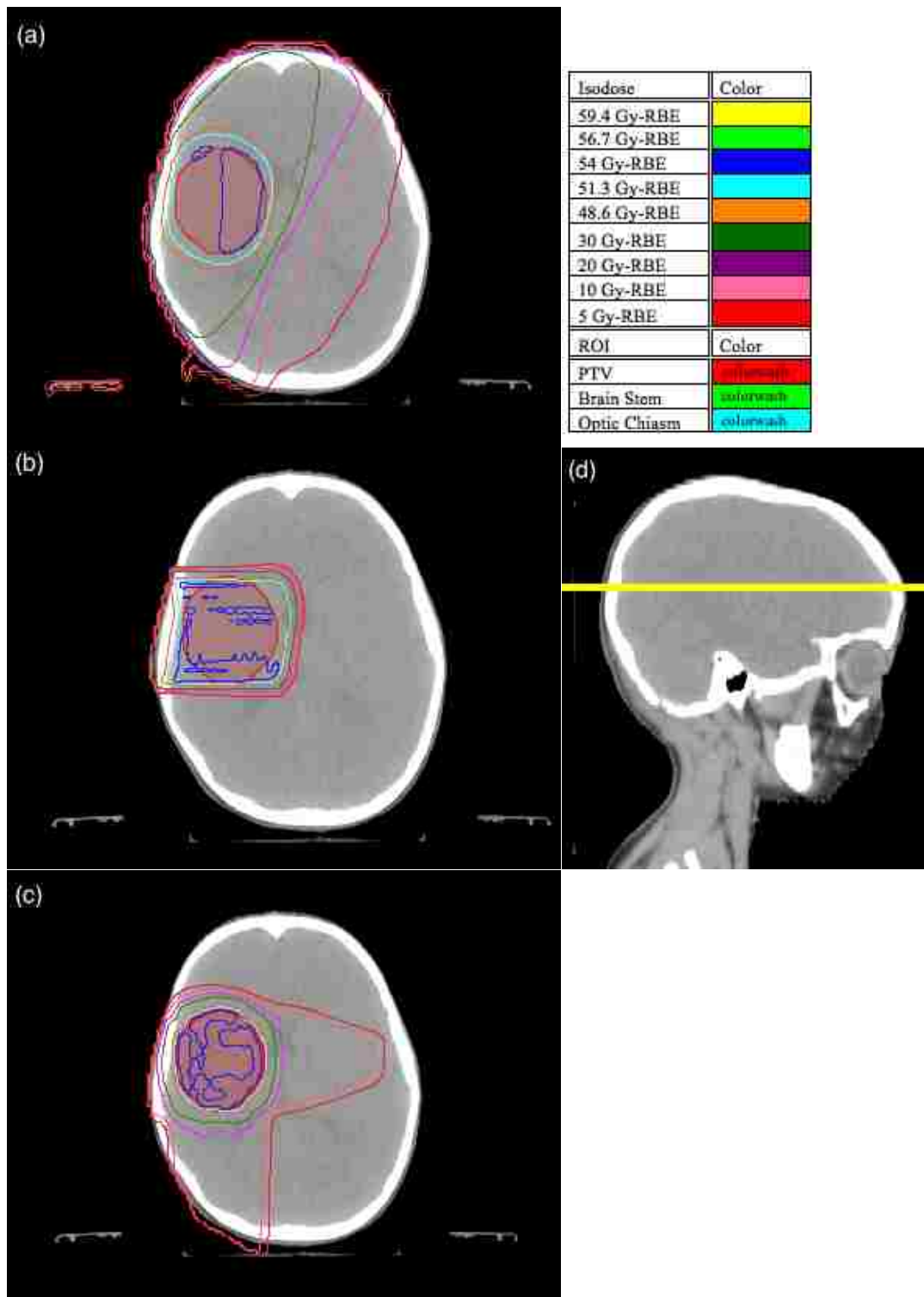
Figure A.6 Isodose distributions for VMAT(a), PSPT (b), and IMPT (c) for patient 6.
The slice location is through the planning isocenter and displayed on the sagittal view (d)
by a yellow line.

Isodose	Color
59.4 Gy-RBE	
56.7 Gy-RBE	
54 Gy-RBE	
51.3 Gy-RBE	
48.6 Gy-RBE	
30 Gy-RBE	
20 Gy-RBE	
10 Gy-RBE	
5 Gy-RBE	
ROI	Color
PTV	colorwash
Brain Stem	colorwash
Optic Chiasm	colorwash
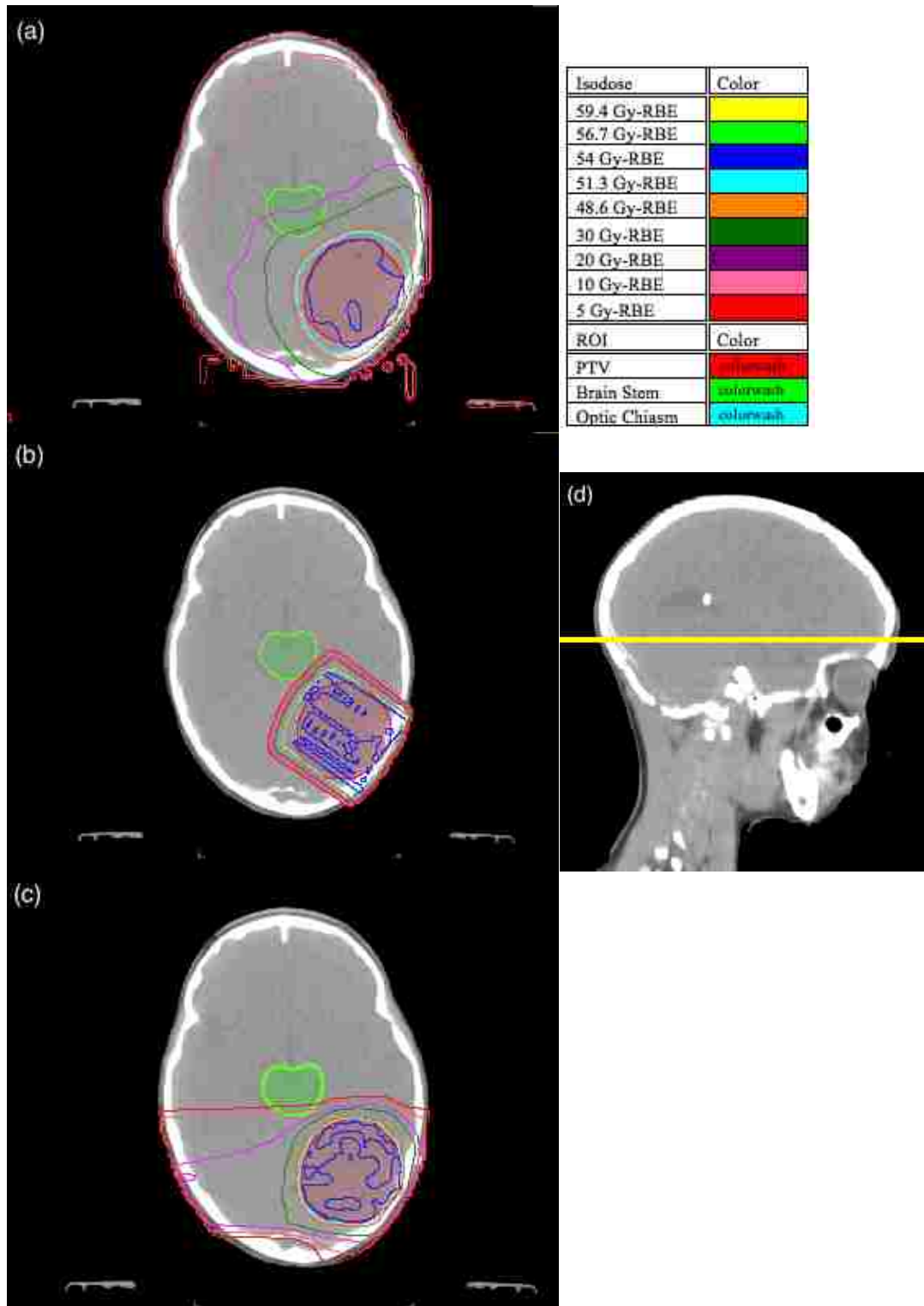
Figure A.7 Isodose distributions for VMAT(a), PSPT (b), and IMPT (c) for patient 7. The slice location is through the planning isocenter and displayed on the sagittal view (d) by a yellow line.

Isodose	Color
59.4 Gy-RBE	
56.7 Gy-RBE	
54 Gy-RBE	
51.3 Gy-RBE	
48.6 Gy-RBE	
30 Gy-RBE	
20 Gy-RBE	
10 Gy-RBE	
5 Gy-RBE	

ROI	Color
PTV	colorwash
Brain Stem	colorwash
Optic Chiasm	colorwash
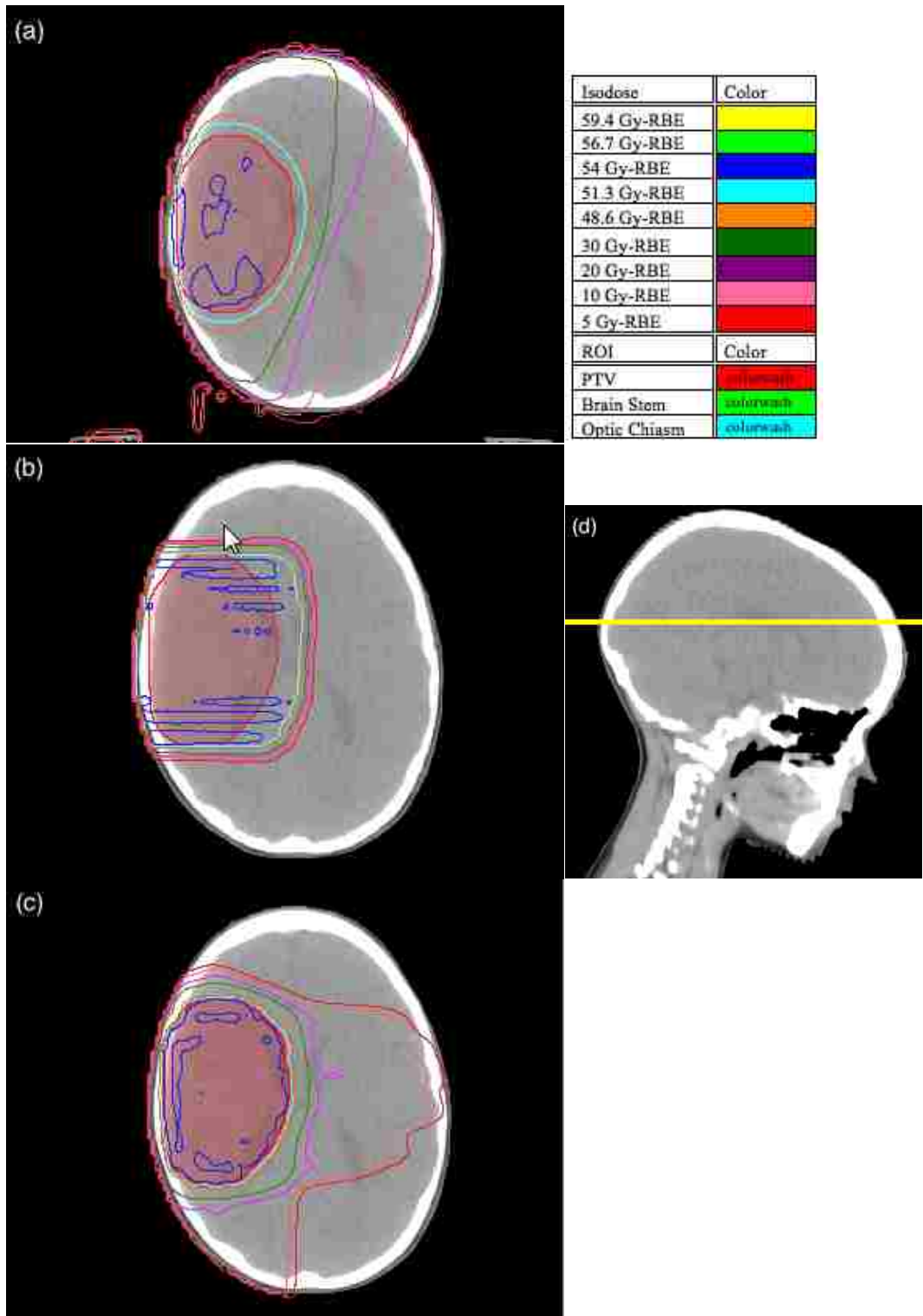
Figure A.8 Isodose distributions for VMAT(a), PSPT (b), and IMPT (c) for patient 8. The slice location is through the planning isocenter and displayed on the sagittal view (d) by a yellow line.
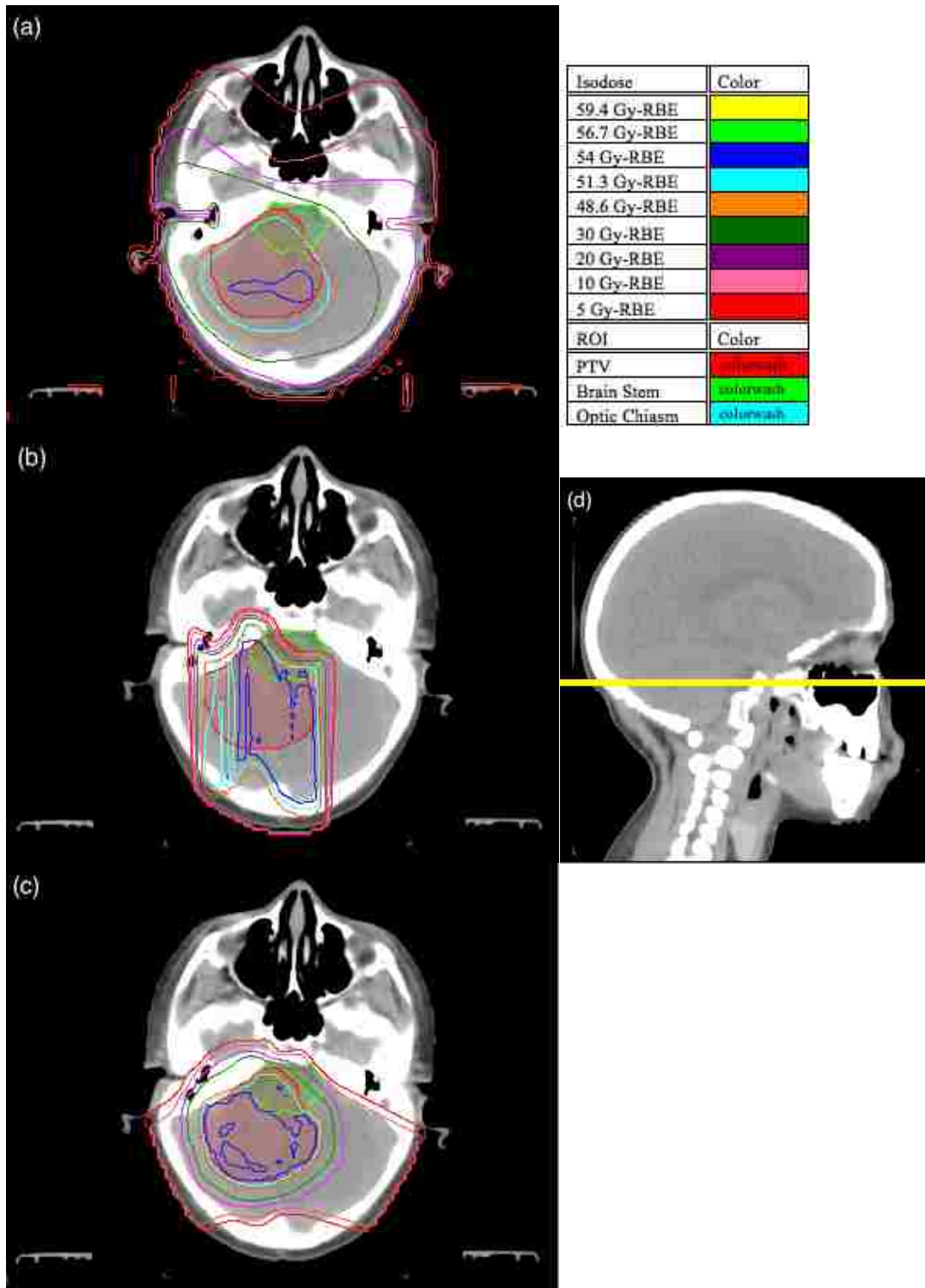
Figure A.9 Isodose distributions for VMAT(a), PSPT (b), and IMPT (c) for patient 9. The slice location is through the planning isocenter and displayed on the sagittal view (d) by a yellow line.
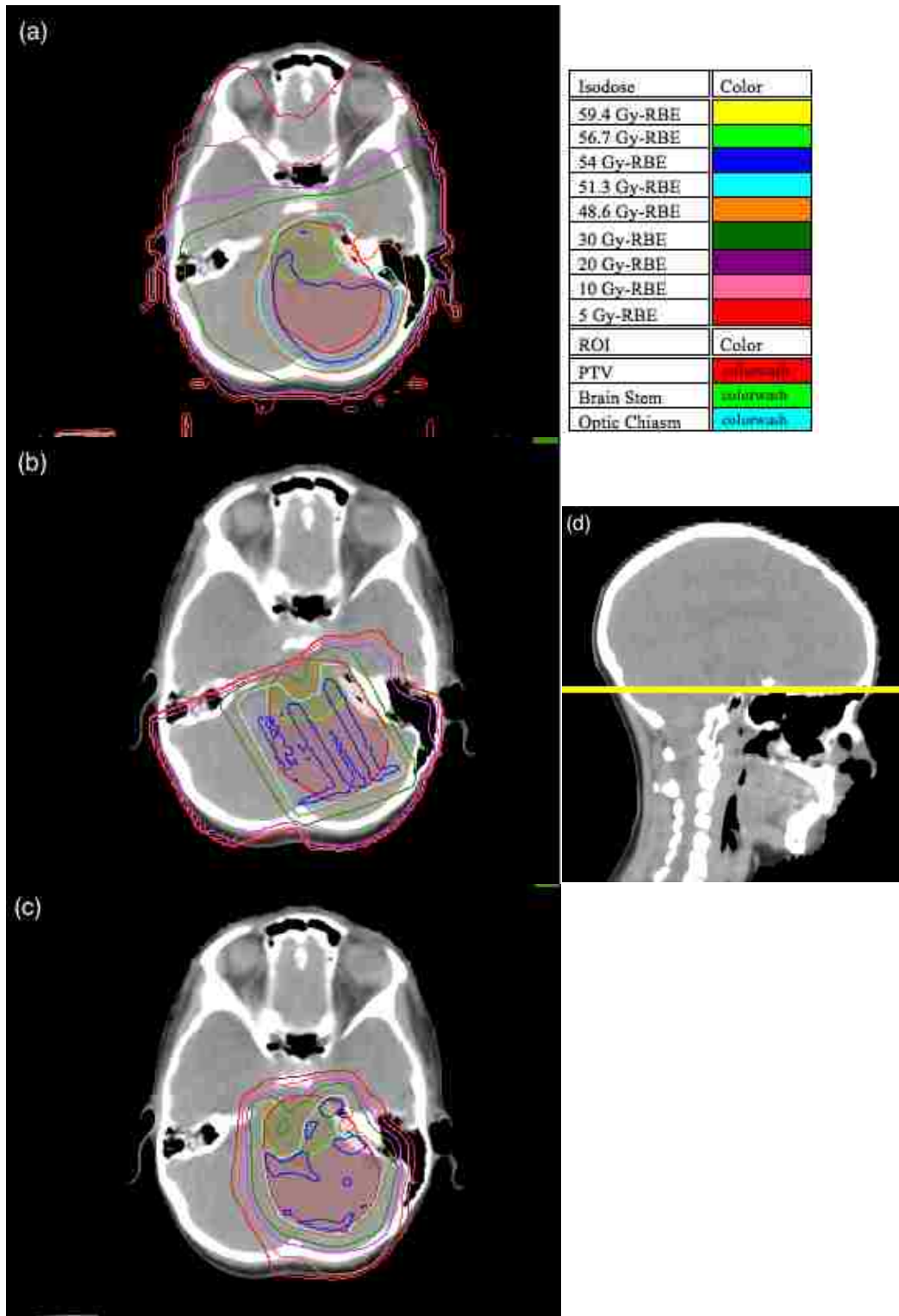
Figure A.10 Isodose distributions for VMAT(a), PSPT (b), and IMPT (c) for patient 10. The slice location is through the planning isocenter and displayed on the sagittal view (d) by a yellow line.
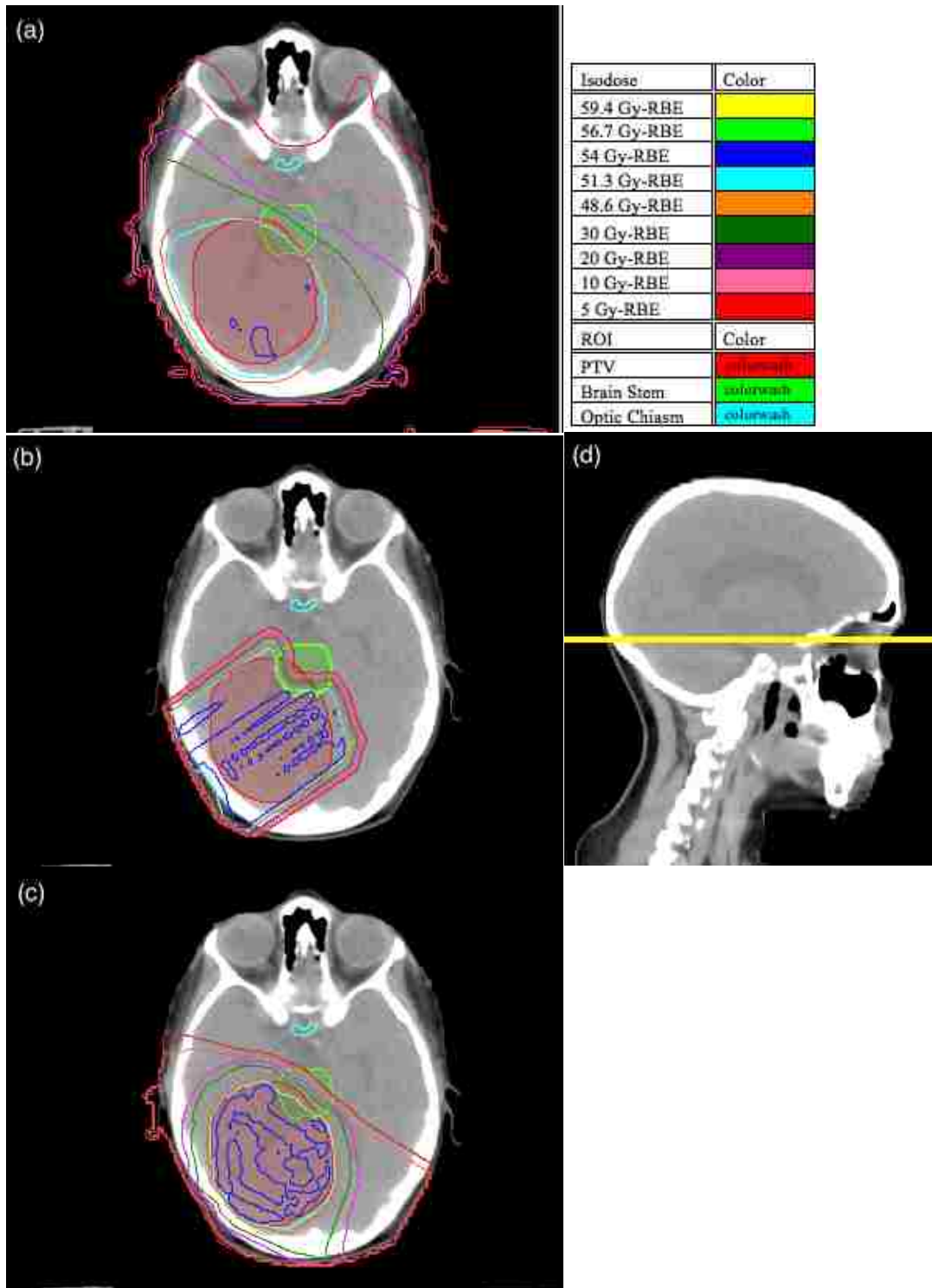
Figure A.11 Isodose distributions for VMAT(a), PSPT (b), and IMPT (c) for patient 11. The slice location is through the planning isocenter and displayed on the sagittal view (d) by a yellow line.

Isodose	Color
59.4 Gy-RBE	yellow
56.7 Gy-RBE	green
54 Gy-RBE	blue
51.3 Gy-RBE	cyan
48.6 Gy-RBE	orange
30 Gy-RBE	dark green
20 Gy-RBE	purple
10 Gy-RBE	pink
5 Gy-RBE	red

ROI	Color
PTV	colorwash
Brain Stem	colorwash
Optic Chiasm	colorwash
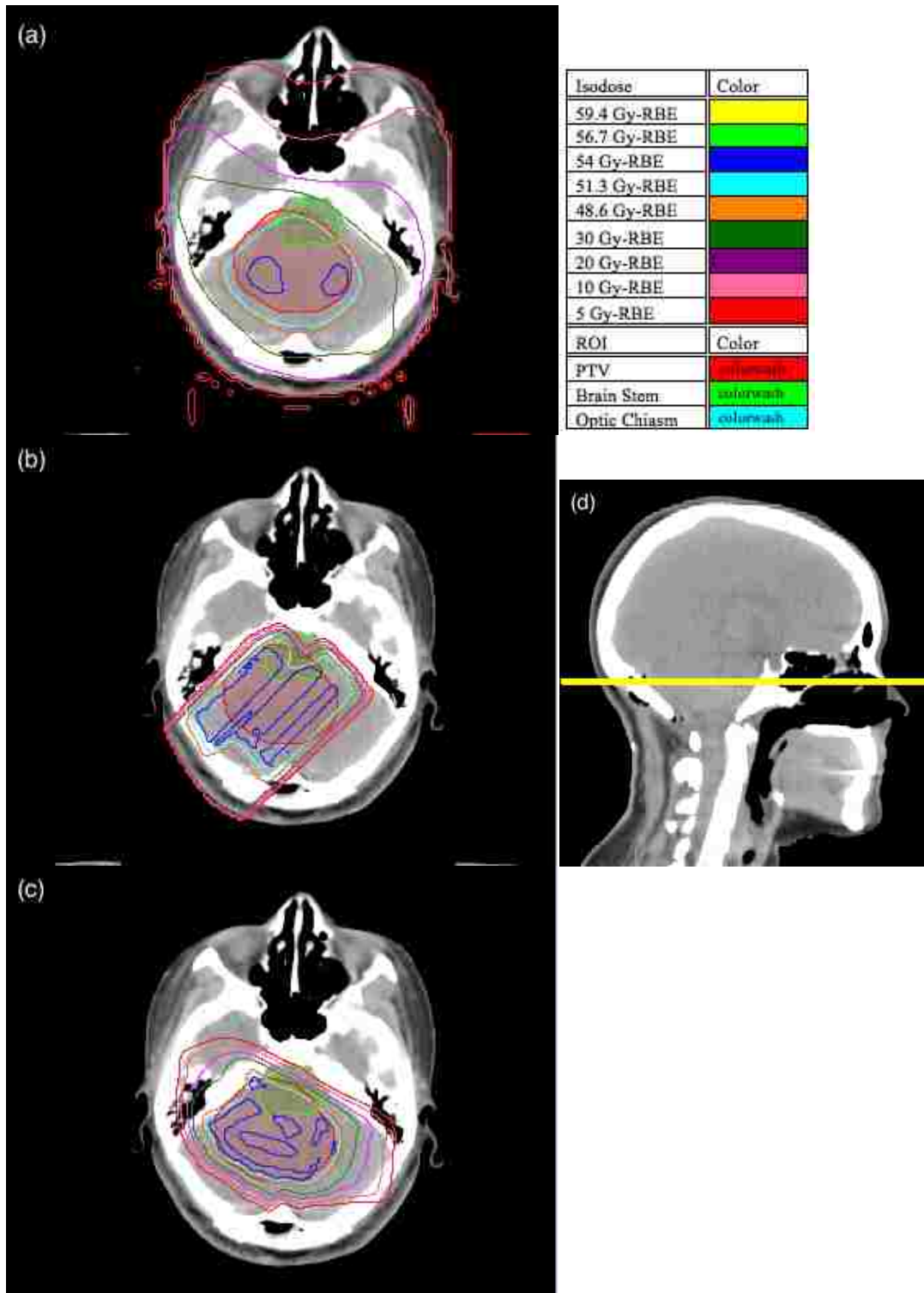
Figure A.12 Isodose distributions for VMAT(a), PSPT (b), and IMPT (c) for patient 12. The slice location is through the planning isocenter and displayed on the sagittal view (d) by a yellow line.

Isodose	Color
59.4 Gy-RBE	yellow
56.7 Gy-RBE	green
54 Gy-RBE	blue
51.3 Gy-RBE	cyan
48.6 Gy-RBE	orange
30 Gy-RBE	dark green
20 Gy-RBE	purple
10 Gy-RBE	pink
5 Gy-RBE	red

ROI	Color
PTV	colorwash
Brain Stem	colorwash
Optic Chiasm	colorwash
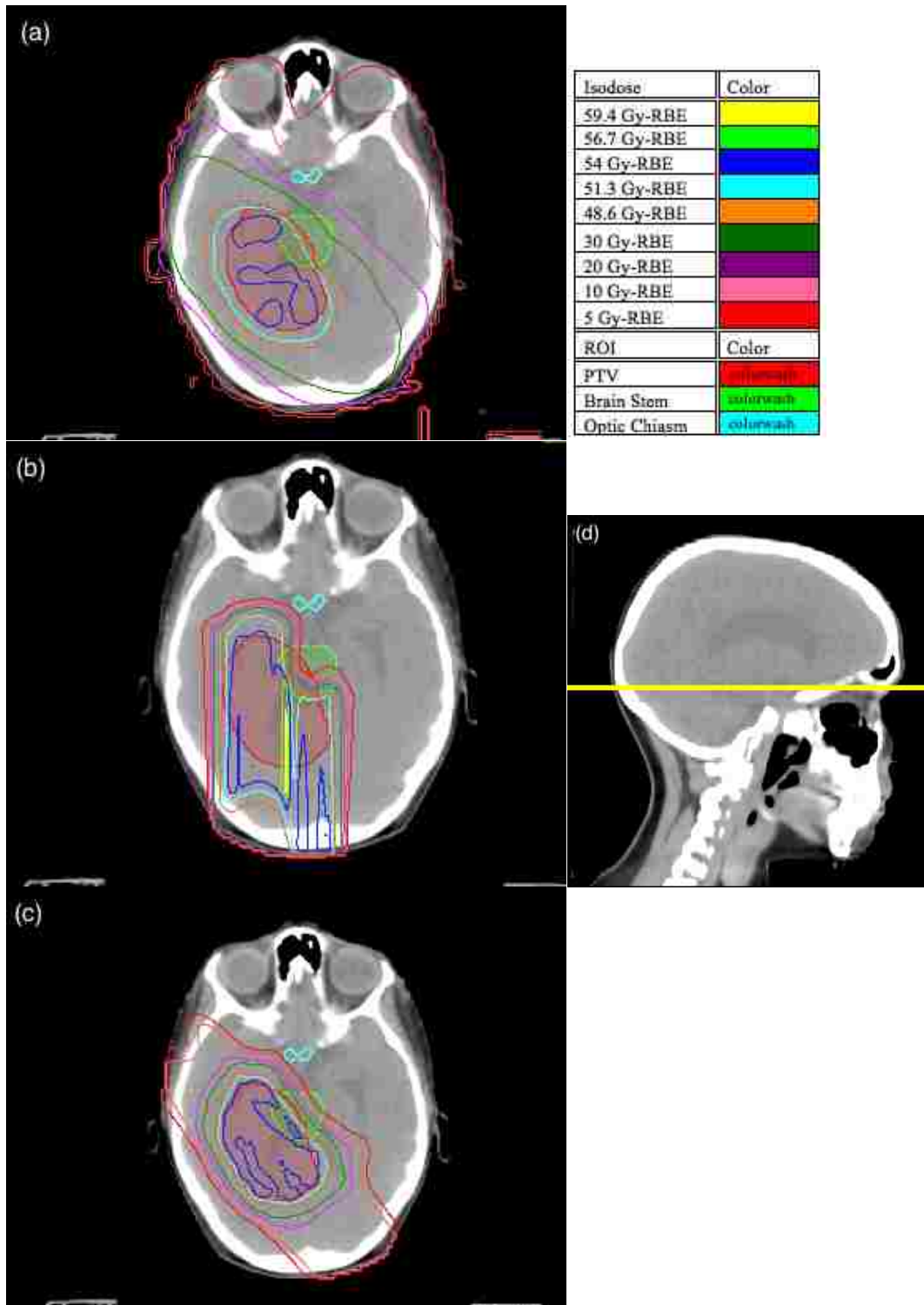
Figure A.13 Isodose distributions for VMAT(a), PSPT (b), and IMPT (c) for patient 13. The slice location is through the planning isocenter and displayed on the sagittal view (d) by a yellow line.

Appendix B: Patient DVH
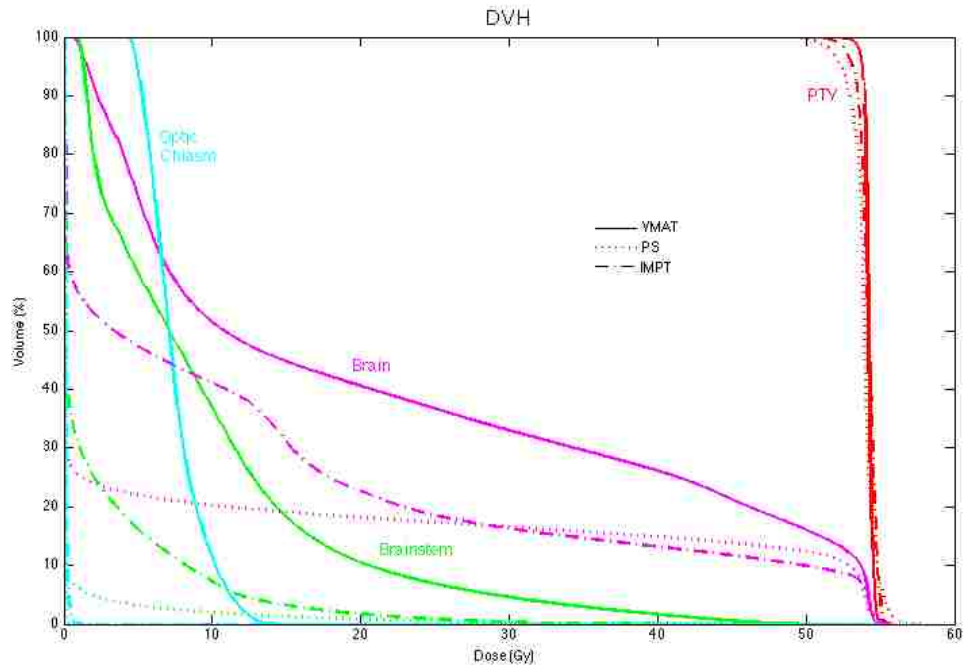
Figure B.1 DVH for patient 1
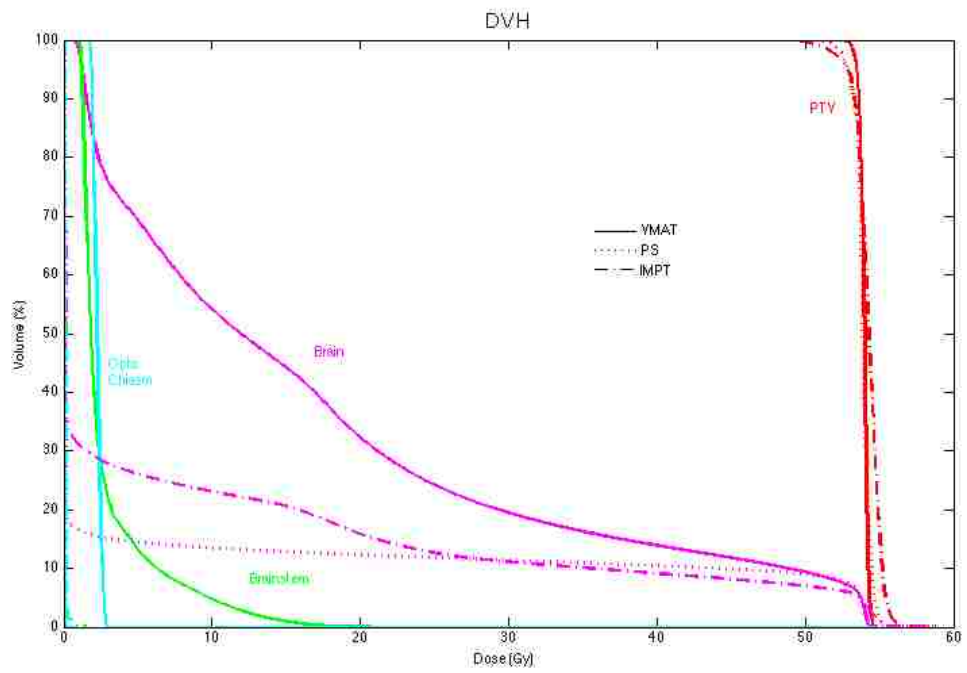
Figure B.2 DVH for patient 2
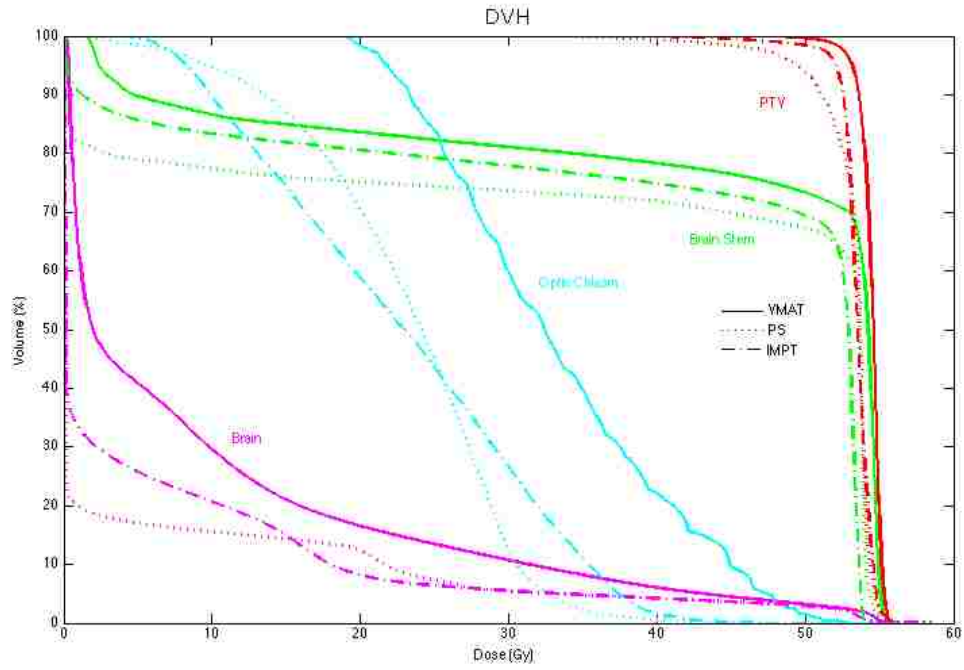
Figure B.3 DVH for patient 3
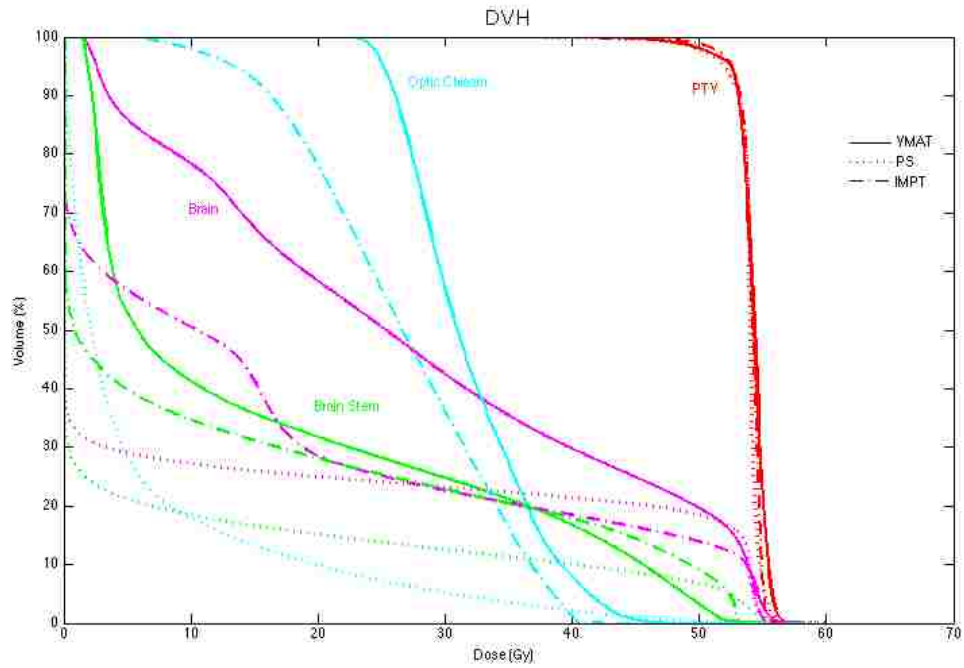
Figure B.4 DVH for patient 4
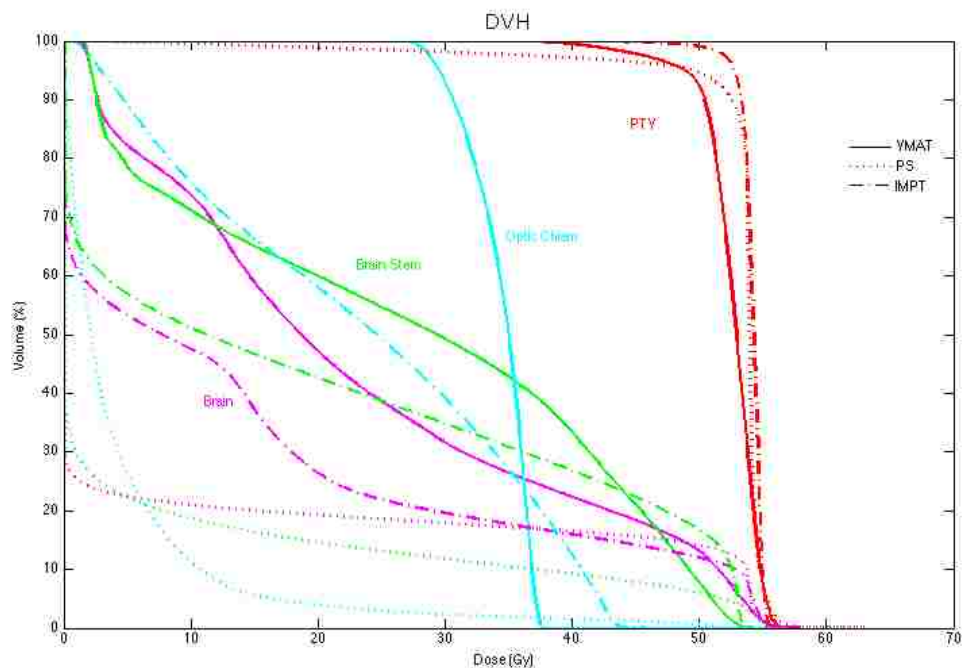
Figure B.5 DVH for patient 5
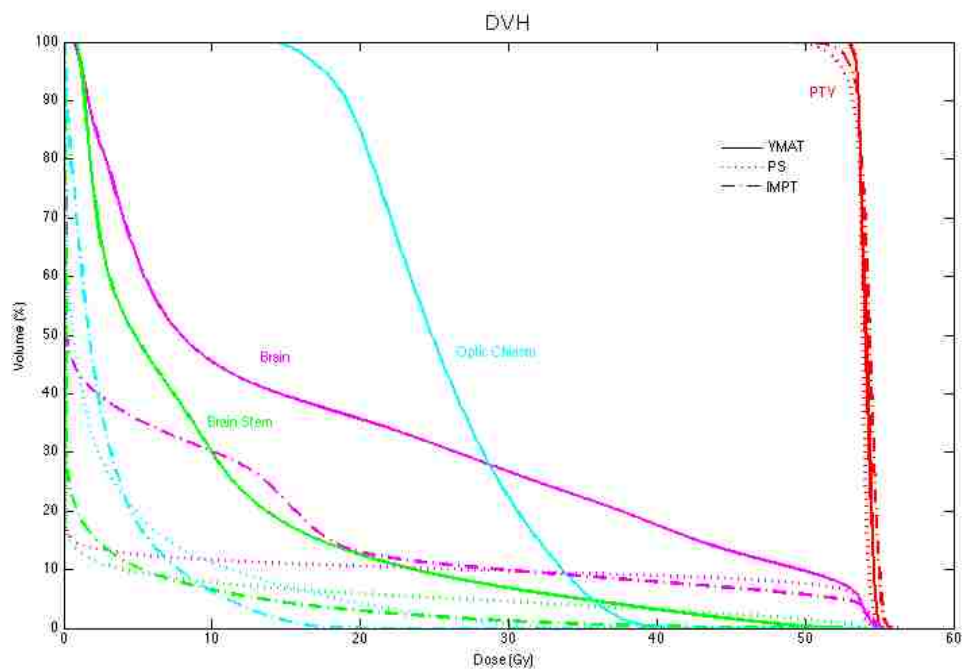
Figure B.6 DVH for patient 6
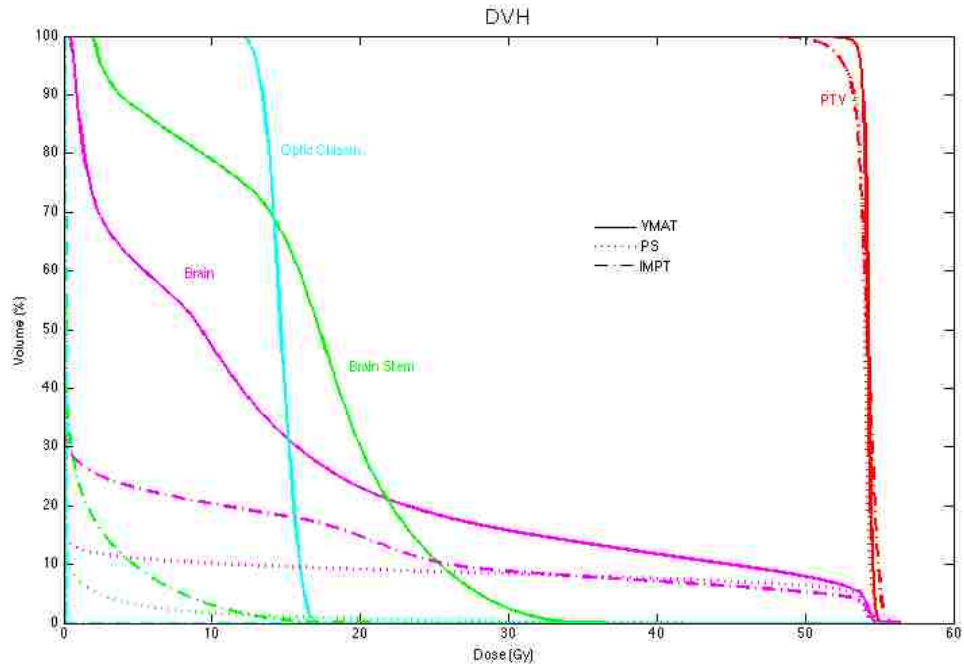
Figure B.7 DVH for patient 7
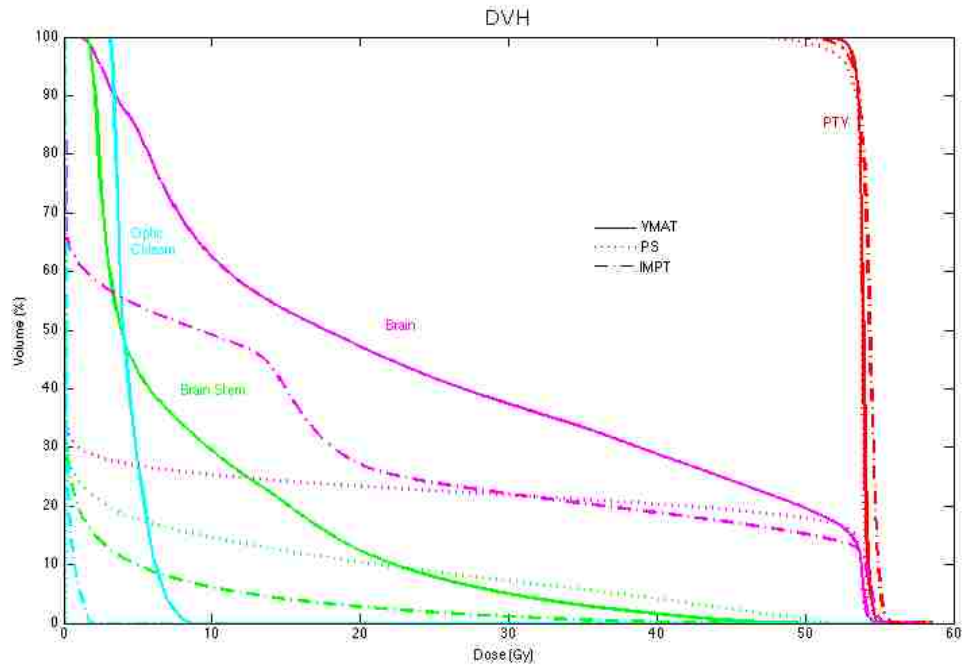
Figure B.8 DVH for patient 8
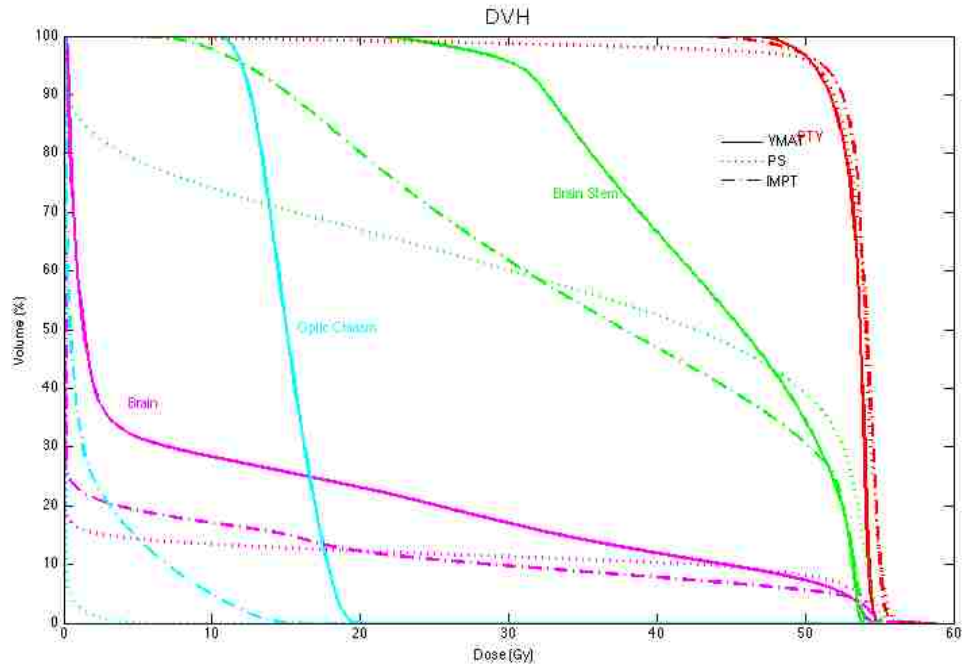
Figure B.9 DVH for patient 9
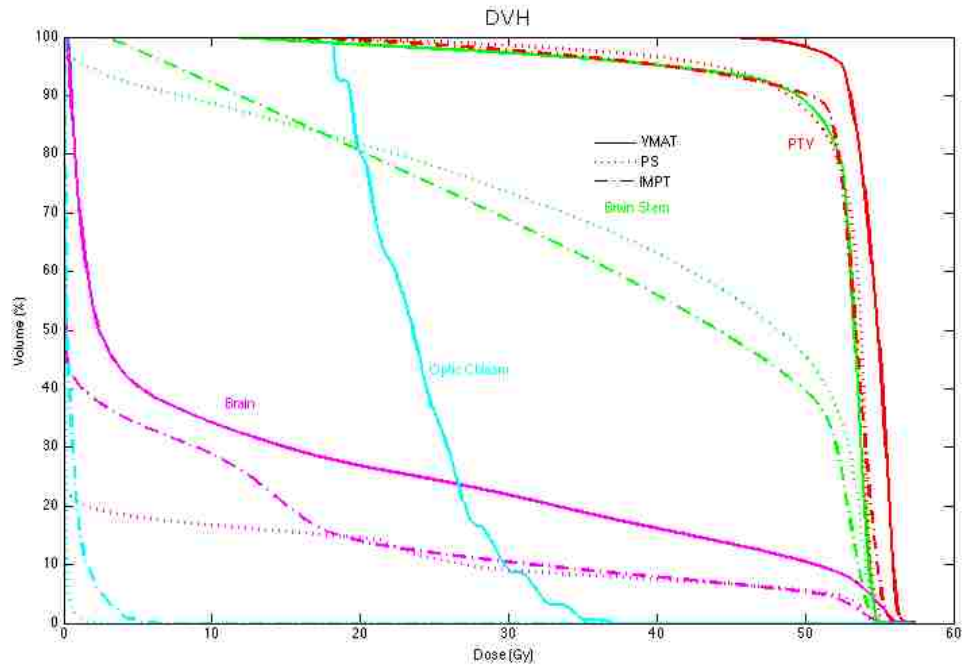
Figure B.10 DVH for patient 10
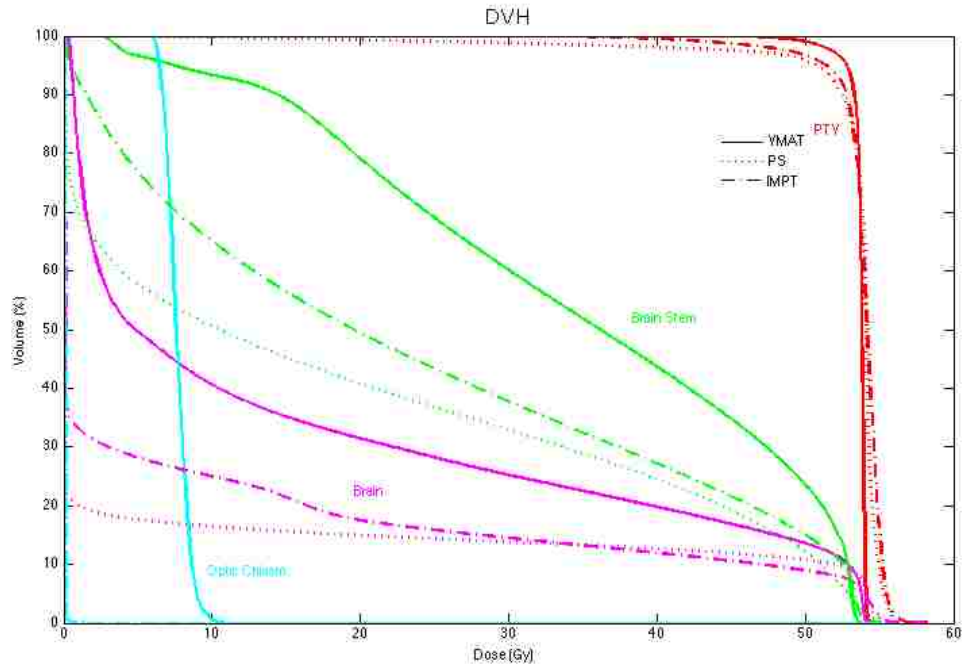
Figure B.11 DVH for patient 11
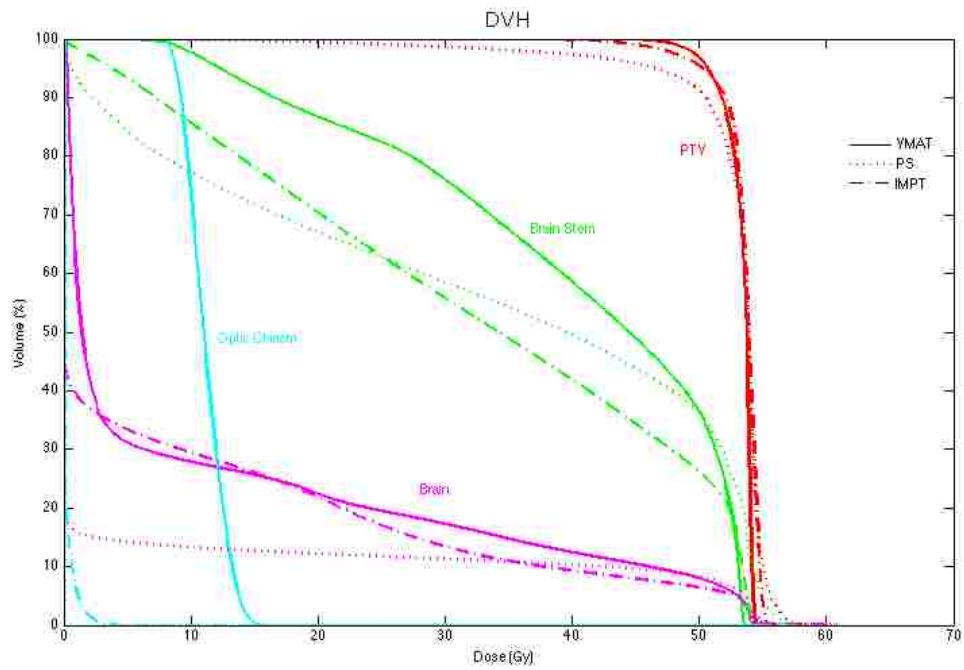
Figure B.12 DVH for patient 12
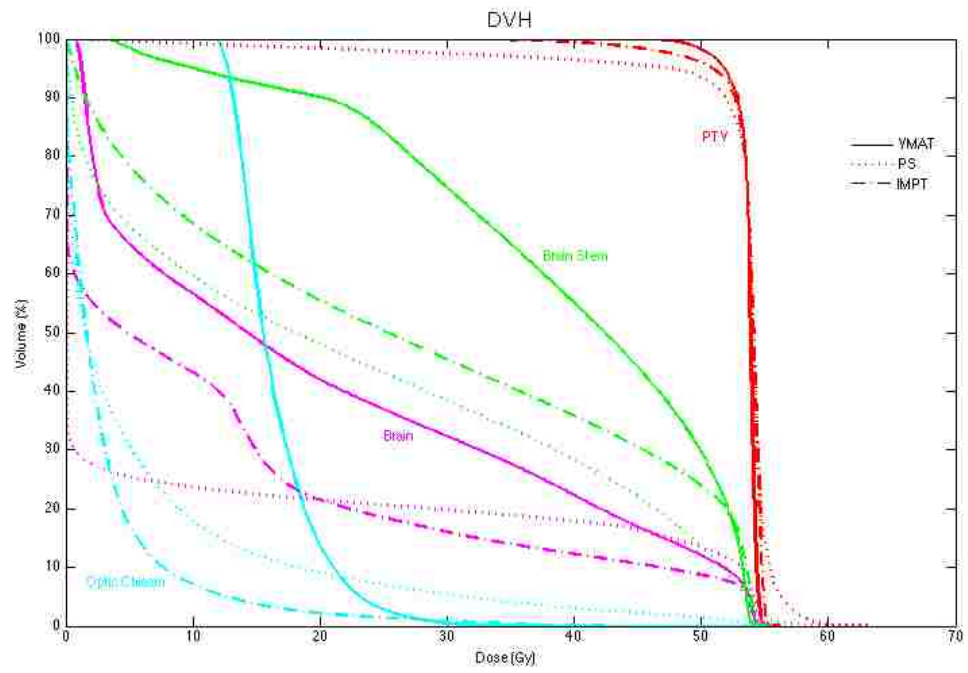
Figure B.13 DVH for patient 13

Appendix C: Isocenter shift DVH
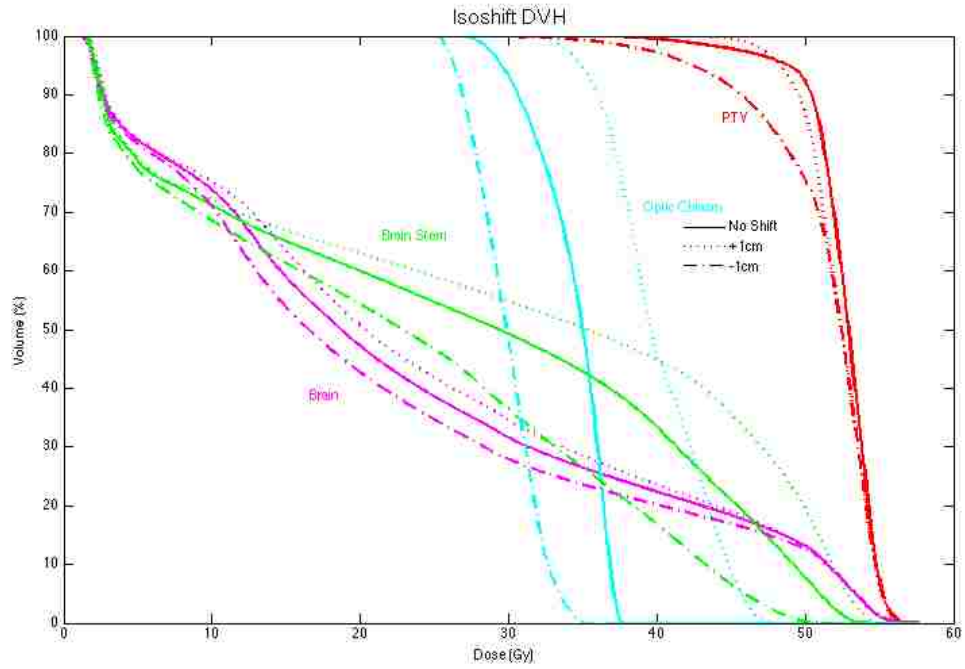
Figure C.1 DVH for patient 5 VMAT isocenter shift in the x direction
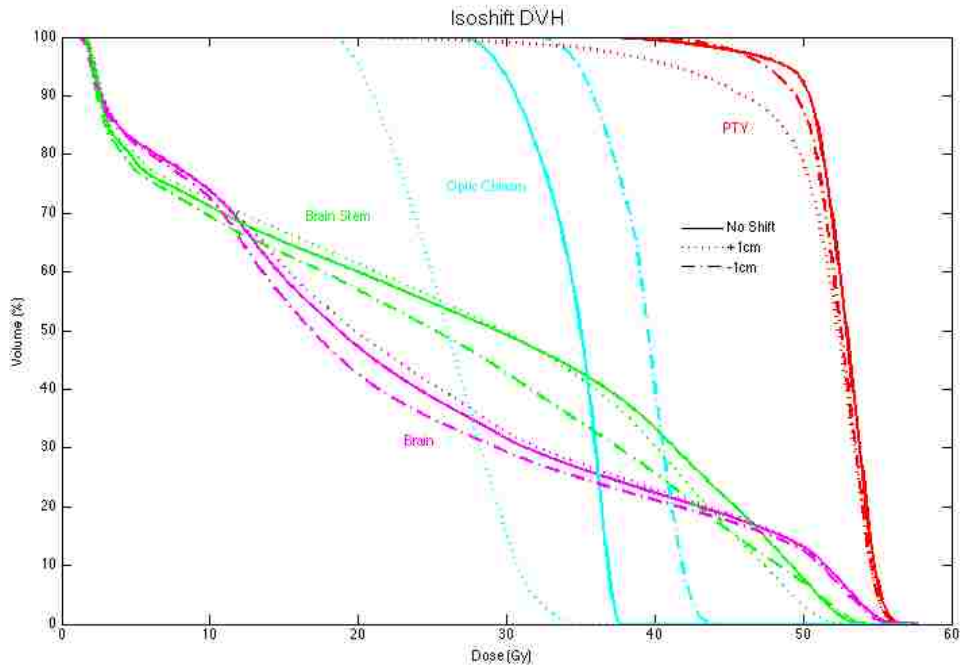
Figure C.2 DVH for patient 5 VMAT isocenter shift in the y direction
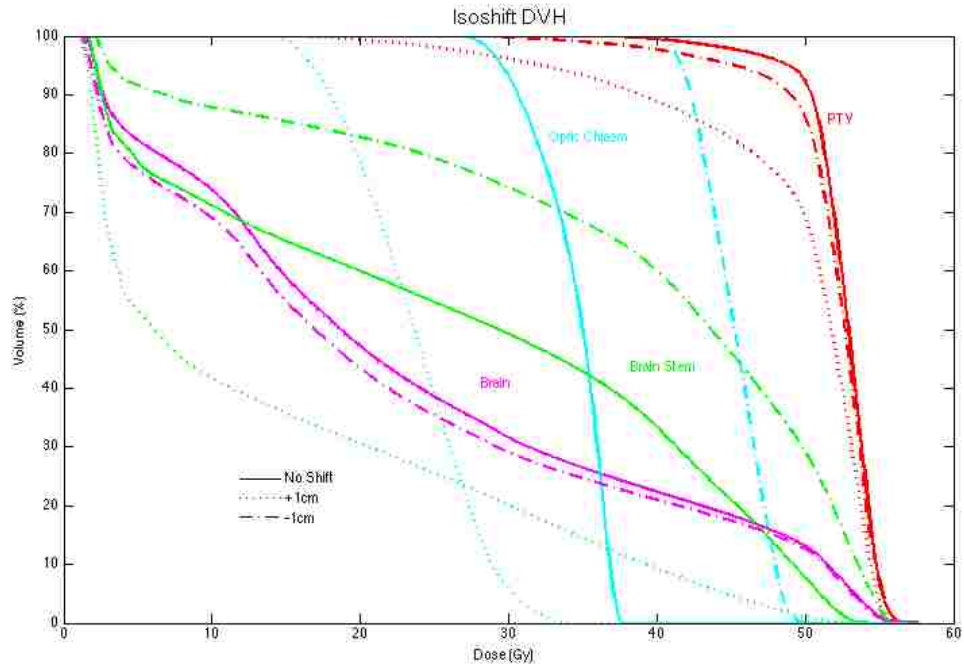
Figure C.3 DVH for patient 5 VMAT isocenter shift in the z direction

Table C.1 Mean, maximum and minimum doses to the PTV for VMAT isocenter shifts in patient 5

VMAT	D_{mean} (Gy-RBE)	D_{max} (Gy-RBE)	D_{min} (Gy-RBE)	$D_{95\%}$ (Gy-RBE)
nominal	52.5	57.5	31.7	48.8
x+1cm	52.2	57.3	40.4	48.3
x-1cm	51.2	57.7	25.1	42.4
y+1cm	51.0	57.4	15.1	41.3
y-1cm	52.1	57.2	37.5	47.4
z+1cm	49.2	57.6	14.0	32.1
z-1cm	51.9	57.2	24.2	45.2

Table C.2 The mean and maximum doses to the brain for VMAT isocenter shifts in patient 5.

VMAT	D_{mean} (Gy-RBE)	D_{max} (Gy-RBE)
Nominal	23.2	57.5
x+1cm	24.2	57.3
x-1cm	21.8	57.7
y+1cm	23.7	57.7
y-1cm	22.1	57.9
z+1cm	23.1	57.7
z-1cm	21.7	57.9

Table C.3 Percentage volume of the brain receiving 5, 10, 50, 52, and 56 Gy-RBE and normal tissue complication probability for VMAT isocenter shifts in patient 5.

VMAT	$V_{5Gy-RBE}$ (%)	$V_{10Gy-RBE}$ (%)	$V_{50Gy-RBE}$ (%)	$V_{52Gy-RBE}$ (%)	$V_{56Gy-RBE}$ (%)	NTCP(%)
Nominal	82.2	73.7	13.1	8.6	0.2	0.14
x+1cm	82.4	75.1	13.0	8.4	0.20	0.159
x-1cm	81.6	70.9	12.6	8.8	0.34	0.1163
y+1cm	82.2	73.9	13.2	8.7	0.29	0.155
y-1cm	81.7	72.4	12.4	7.7	0.08	0.1159
z+1cm	82.2	73.7	13.1	8.5	0.28	0.1434
z-1cm	77.1	69.0	12.6	8.1	0.10	0.1176
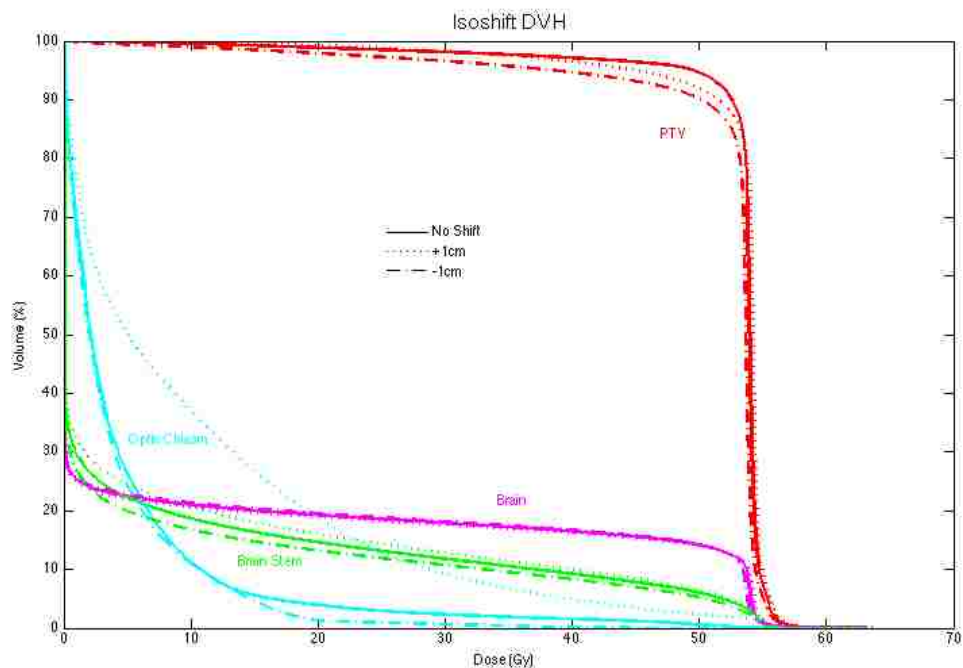
Figure C.4 DVH for patient 5 PSPT plans with an isocenter shift in the x direction.
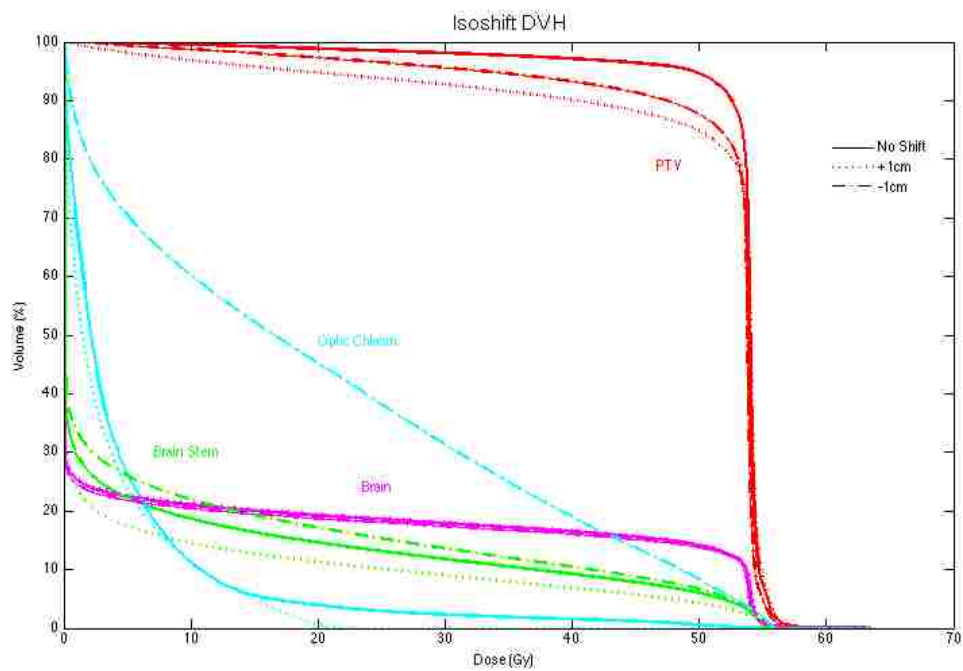
Figure C.5 DVH for patient 5 PSPT plans with an isocenter shift in the y direction.
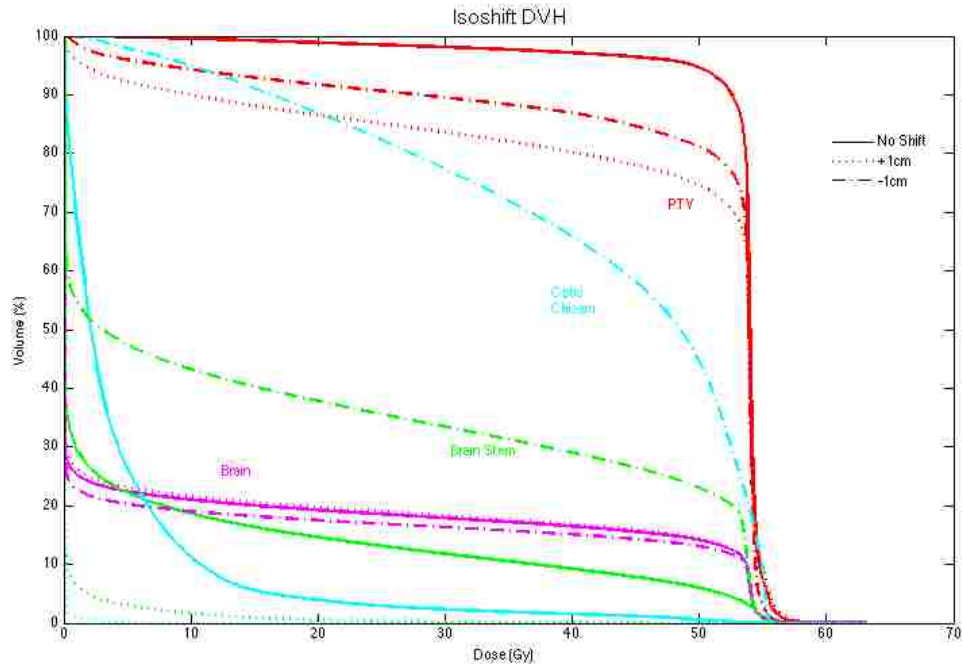
Figure C.6 DVH for patient 5 PSPT plans with an isocenter shift in the z direction.

Table C.4 PTV results for passively scattered proton therapy isocenter shifts for patient 5.

PSPT	D_{mean} (Gy-RBE)	D_{max} (Gy-RBE)	D_{min} (Gy-RBE)	$D_{95\%}$ (Gy-RBE)
nominal	52.9	63.2	0.5	49.5
x+1cm	52.9	63.7	2.1	44.9
x-1cm	51.7	62.5	0.1	38.4
y+1cm	50.2	63.2	0.0	18.8
y-1cm	51.3	61.8	0.5	33.0
z+1cm	45.6	62.7	0.0	1.6
z-1cm	48.4	59.2	0.1	7.7

Table C.5 Mean and maximum doses to the brain for PSPT isocenter shifts in patient 5.

PSPT	D_{mean} (Gy-RBE)	D_{max} (Gy-RBE)
Nominal	10.0	63.2
x+1cm	9.8	63.7
x-1cm	10.0	62.5
y+1cm	10.1	63.8
y-1cm	9.7	62.5
z+1cm	10.2	62.7
z-1cm	9.1	62.4

Table C.6 Percentage volume of the brain receiving 5, 10, 50, 52, and 56Gy-RBE for PSPT isocenter shifts in patient 5.

PSPT	$V_{5Gy-RBE}$ (%)	$V_{10Gy-RBE}$ (%)	$V_{50Gy-RBE}$ (%)	$V_{52Gy-RBE}$ (%)	$V_{56Gy-RBE}$ (%)	NTCP(%)
Nominal	22.4	21.0	14.1	13.0	0.3	0.10
x+1cm	22.0	20.6	14.0	13.0	0.45	0.107
x-1cm	22.8	21.3	14.2	12.9	0.23	0.098
y+1cm	22.8	21.3	14.2	13.1	0.39	0.109
y-1cm	21.8	20.4	13.8	12.6	0.22	0.092
z+1cm	23.1	21.6	14.3	13.1	0.34	0.108
z-1cm	20.3	19.0	13.1	12.1	0.25	0.081
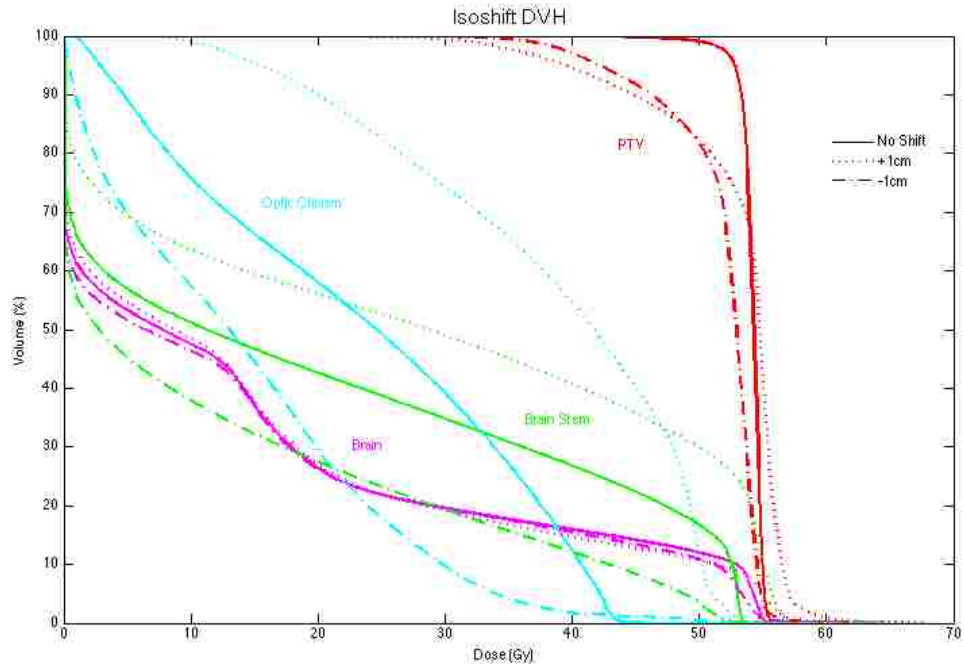
Figure C.7 DVH for patient 5 IMPT plan with a shift in the x direction
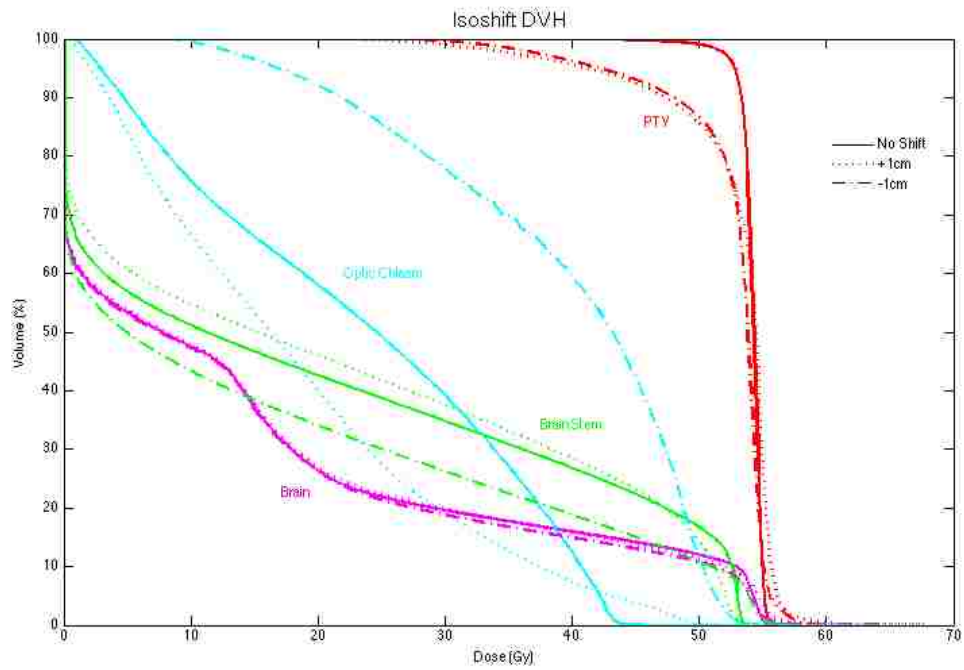
Figure C.8 DVH for patient 5 IMPT plan with a shift in the y direction.
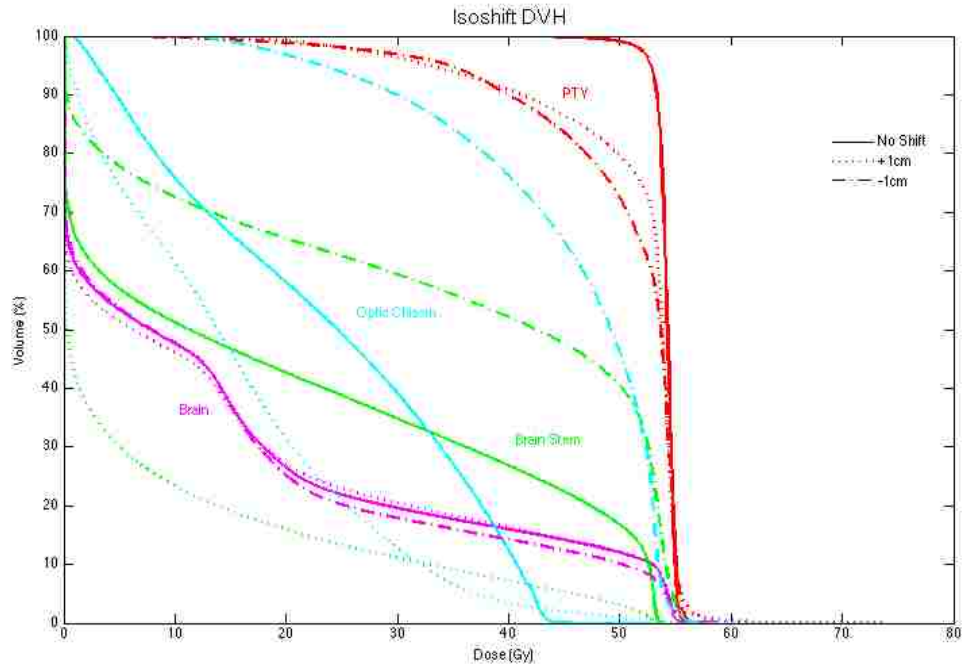
Figure C.9 DVH for patient 5 IMPT plan with a shift in the z direction.

Table C.7 PTV results for IMPT isocenter shift for patient 5.

IMPT	D_{mean} (Gy-RBE)	D_{max} (Gy-RBE)	D_{min} (Gy-RBE)	$D_{95\%}$ (Gy-RBE)
nominal	54.1	57.2	39.2	52.8
x+1cm	52.7	66.1	14.5	39.5
x-1cm	51.6	61.8	23.2	42.1
y+1cm	52.7	67.5	16.3	41.2
y-1cm	52.4	60.1	22.9	42.2
z+1cm	50.9	61.9	7.4	32.8
z-1cm	50.2	56.8	3.3	34.6

Table C.8 Mean and Maximum doses to the brain for IMPT isocenter shifts in patient 5.

IMPT	D_{mean} (Gy-RBE)	D_{max} (Gy-RBE)
Nominal	15.0	58.0
x+1cm	15.0	67.9
x-1cm	14.6	64.5
y+1cm	15.1	67.6
y-1cm	14.6	64.2
z+1cm	15.0	73.9
z-1cm	14.4	58.8

Table C.9 Percentage volume of the brain receiving 5, 10, 50, 52, and 56Gy-RBE for IMPT isocenter shifts in patient 5.

IMPT	$V_{5Gy-RBE}$ (%)	$V_{10Gy-RBE}$ (%)	$V_{50Gy-RBE}$ (%)	$V_{52Gy-RBE}$ (%)	$V_{56Gy-RBE}$ (%)	NTCP(%)
Nominal	53.3	47.5	12.0	10.8	0.0	0.08
x+1cm	54.6	48.4	10.6	9.6	2.22	0.082
x-1cm	51.6	46.4	10.9	8.8	0.30	0.059
y+1cm	53.7	47.9	11.4	9.9	1.11	0.087
y-1cm	52.9	47.2	10.8	9.4	0.60	0.064
z+1cm	51.4	46.0	12.1	10.9	1.71	0.108
z-1cm	53.6	47.6	10.1	8.7	0.20	0.055
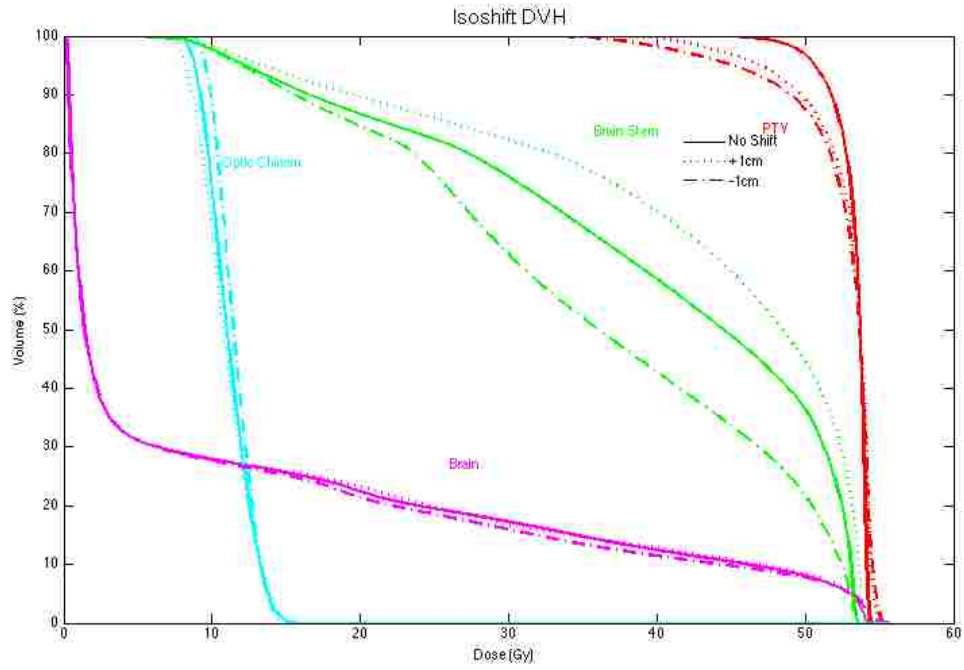
Figure C.10 DVH for patient 12 VMAT plans with an isocenter shift in the x direction.
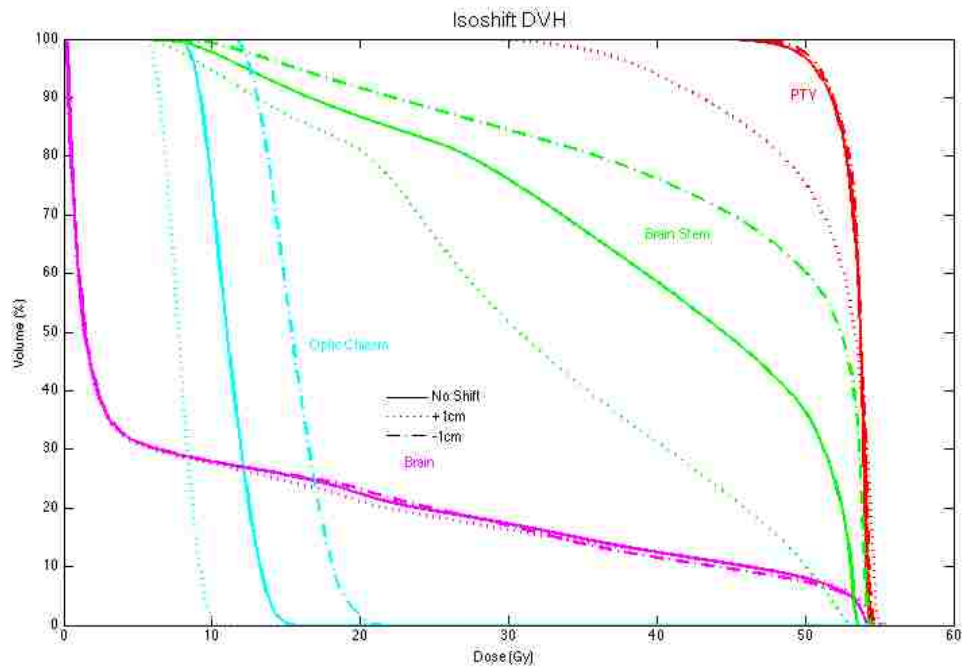
Figure C.11 DVH for patient 12 VMAT plans with an isocenter shift in the y direction.
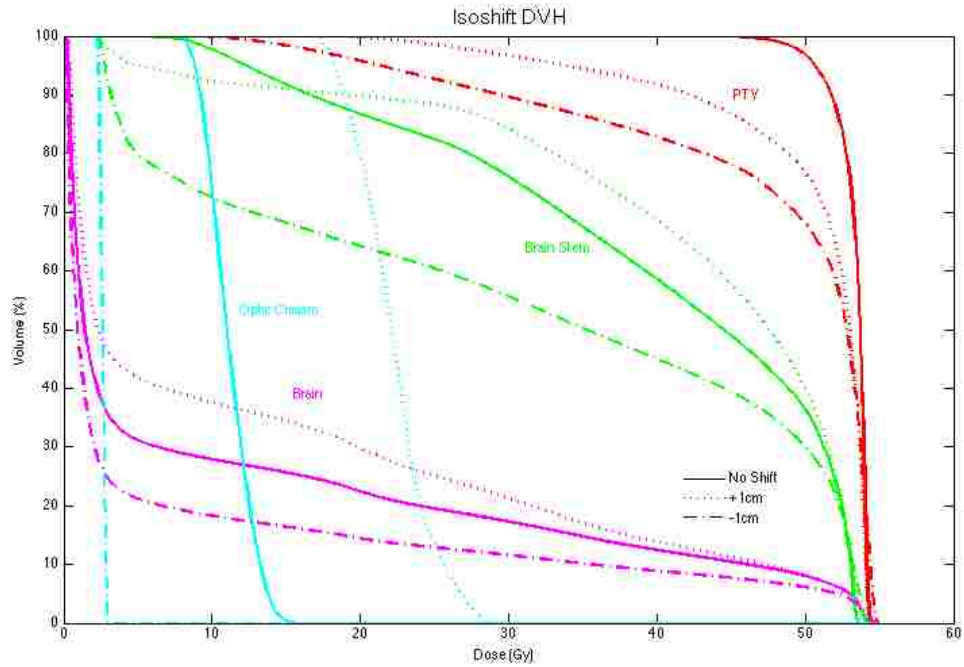
Figure C.12 DVH for patient 12 VMAT plans with an isocenter shift in the z direction.

Table C.10 PTV result for patient 12 VMAT isocenter shifts.

VMAT	D_{mean} (Gy-RBE)	D_{max} (Gy-RBE)	D_{min} (Gy-RBE)	$D_{95\%}$ (Gy-RBE)
Nominal	53.3	54.7	42.8	50.6
x+1cm	52.73	55.253	35.85	46.9
x-1cm	52.4	55.4	31.9	45.1
y+1cm	51.0	55.4	27.5	39.1
y-1cm	53.4	54.8	44.2	50.9
z+1cm	50.3	54.4	17.0	33.8
z-1cm	47.7	55.0	7.5	21.2

Table C.11 Mean and maximum doses to the brain for VMAT isocenter shifts in patient 12.

VMAT	D_{mean} (Gy-RBE)	D_{max} (Gy-RBE)
Nominal	11.1	54.7
x+1cm	11.2	55.5
x-1cm	10.7	55.8
y+1cm	10.8	55.4
y-1cm	11.0	54.8
z+1cm	13.8	54.4
z-1cm	7.7	55.0

Table C.12 Percentage volume of the brain receiving 5, 10, 50, 52, and 56Gy-RBE for PSPT isocenter shifts in patient 12.

PSPT	$V_{5Gy-RBE}$ (%)	$V_{10Gy-RBE}$ (%)	$V_{50Gy-RBE}$ (%)	$V_{52Gy-RBE}$ (%)	$V_{56Gy-RBE}$ (%)	NTCP (%)
Nominal	14.2	13.3	8.3	7.1	0.3	0.022
x+1cm	14.6	13.6	8.4	7.4	0.32	0.024
x-1cm	13.7	12.8	7.7	6.6	0.19	0.017
y+1cm	14.6	13.7	8.3	7.1	0.19	0.021
y-1cm	13.6	12.7	7.8	6.9	0.31	0.019
z+1cm	17.3	16.1	9.1	7.9	0.26	0.031
z-1cm	10.0	9.4	6.1	5.3	0.19	0.008
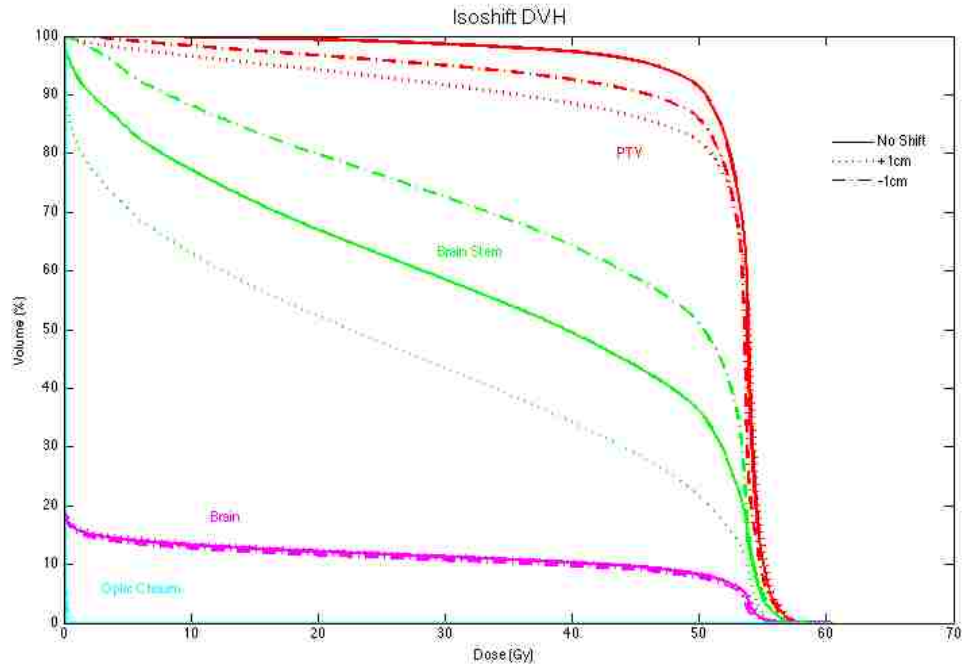
Figure C.13 DVH for patient 12 PSPT plans with an isocenter shift in the x direction.
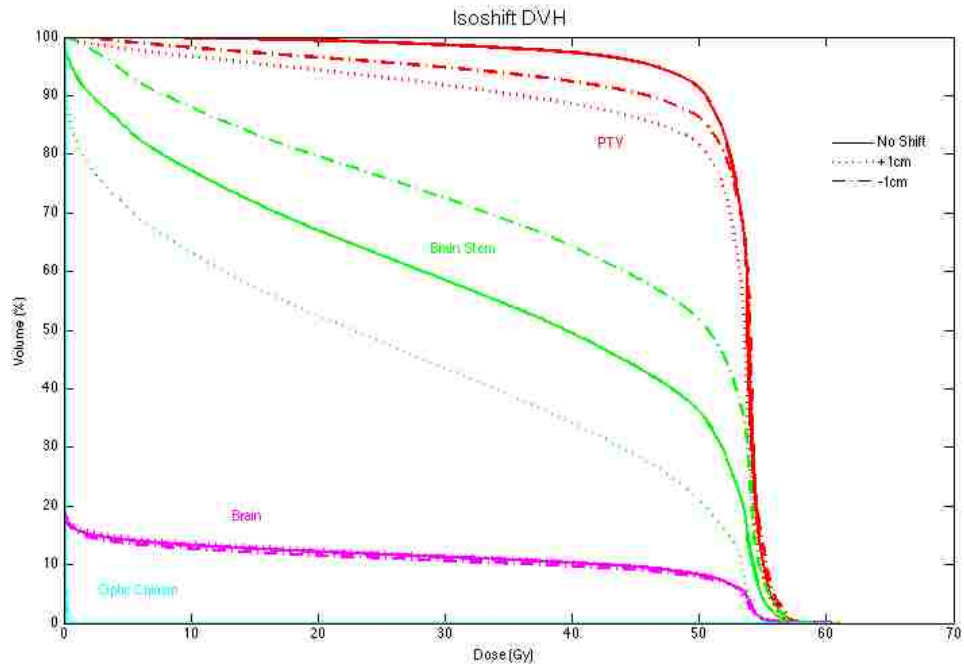
Figure C.14 DVH for patient 12 PSPT plans with an isocenter shift in the y direction.
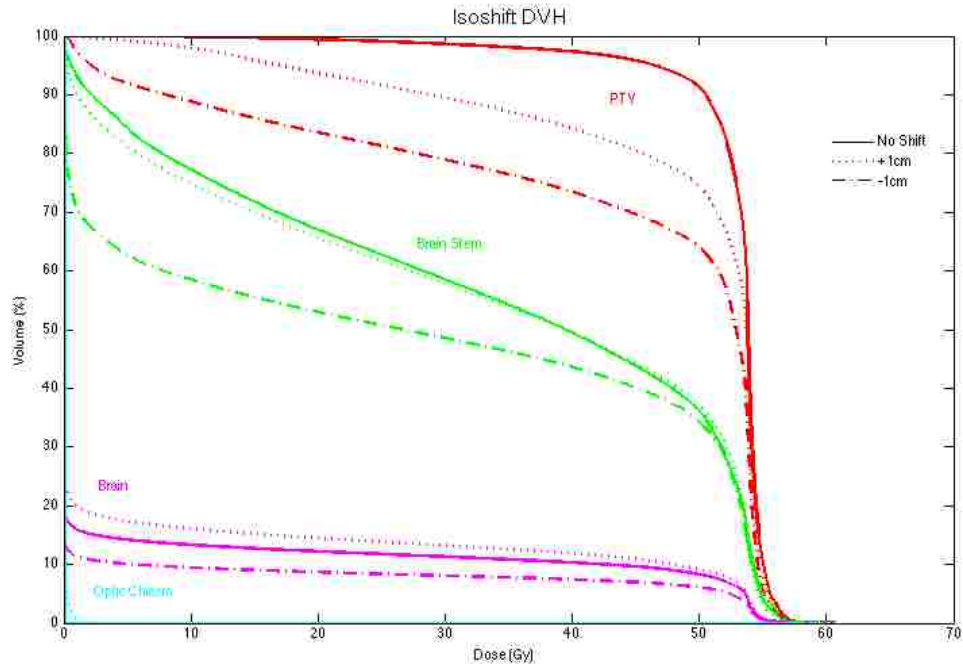
Figure C.15 DVH for patient 12 PSPT plans with an isocenter shift in the z direction.

Table C.13 Percentage volume of the brain receiving 5, 10, 50, 52, and 56Gy-RBE for PSPT isocenter shifts in patient 12.

VMAT	$V_{5Gy-RBE}$ (%)	$V_{10Gy-RBE}$ (%)	$V_{50Gy-RBE}$ (%)	$V_{52Gy-RBE}$ (%)	$V_{56Gy-RBE}$ (%)	NTCP
Nominal	31.2	27.9	8.0	6.4	0.0	0.027
x+1cm	31.2	28.0	8.3	6.8	0.00	0.031
x-1cm	31.1	27.6	7.7	6.4	0.00	0.0244
y+1cm	30.9	27.5	8.1	6.6	0.00	0.03
y-1cm	31.3	27.9	7.4	6.0	0.00	0.0228
z+1cm	41.8	37.5	8.1	6.1	0.00	0.0343
z-1cm	21.2	18.3	6.1	5.1	0.00	0.0112

Table C.14 PTV results for passively scattered proton therapy isocenter shifts for patient 12.

PSPT	D_{mean} (Gy-RBE)	D_{max} (Gy-RBE)	D_{min} (Gy-RBE)	$D_{95\%}$ (Gy-RBE)
Nominal	52.7	60.0	3.5	46.5
x+1cm	49.5	59.5	0.0	16.6
x-1cm	50.7	60.0	0.7	29.8
y+1cm	49.2	59.0	0.0	17.2
y-1cm	51.0	60.7	0.7	28.8
z+1cm	48.2	60.5	0.5	16.8
z-1cm	42.9	59.2	0.1	2.1

Table C.15 Mean and maximum doses to the brain for PSPT isocenter shifts in patient 12.

PSPT	D_{mean} (Gy-RBE)	D_{max} (Gy-RBE)
Nominal	6.2	60.3
x+1cm	6.4	60.2
x-1cm	5.9	60.5
y+1cm	5.9	61.2
y-1cm	6.3	59.6
z+1cm	7.3	60.5
z-1cm	4.4	60.7
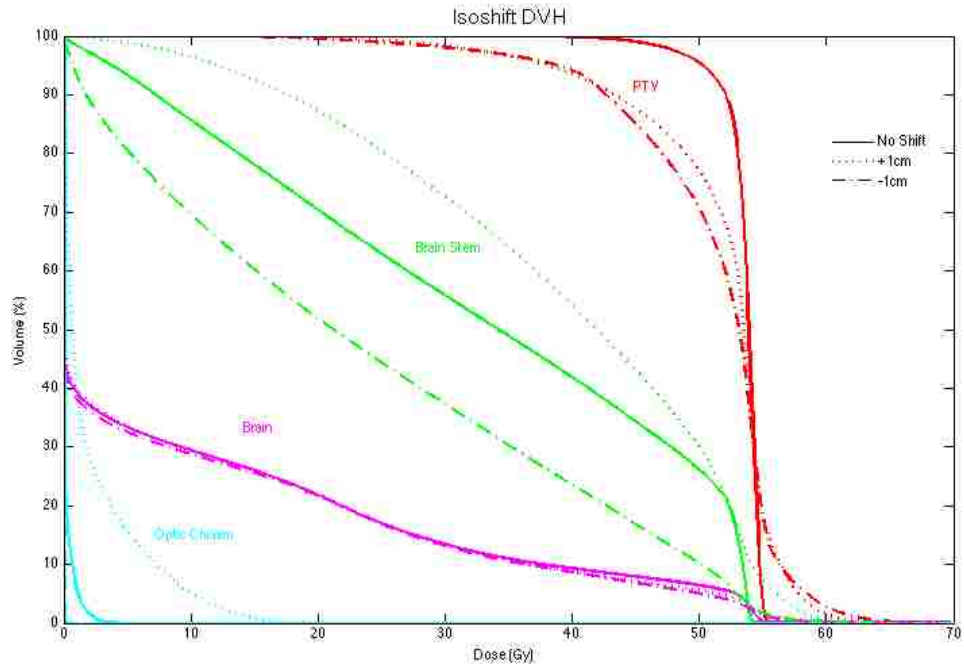
Figure C.16 DVH for patient 12 IMPT plans with an isocenter shift in the x direction.
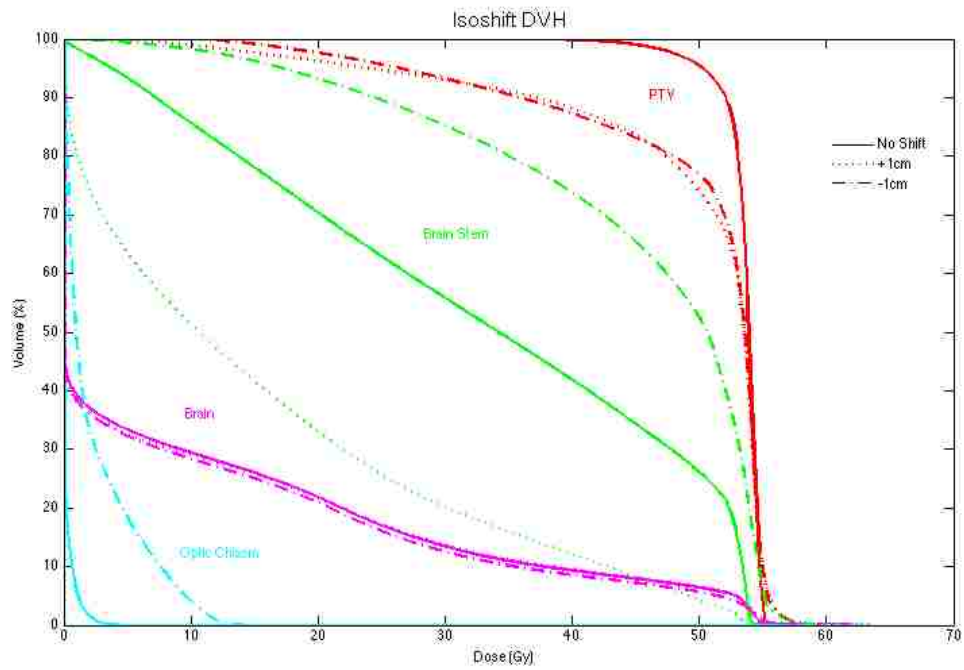
Figure C.17 DVH for patient 12 IMPT plans with an isocenter shift in the y direction.
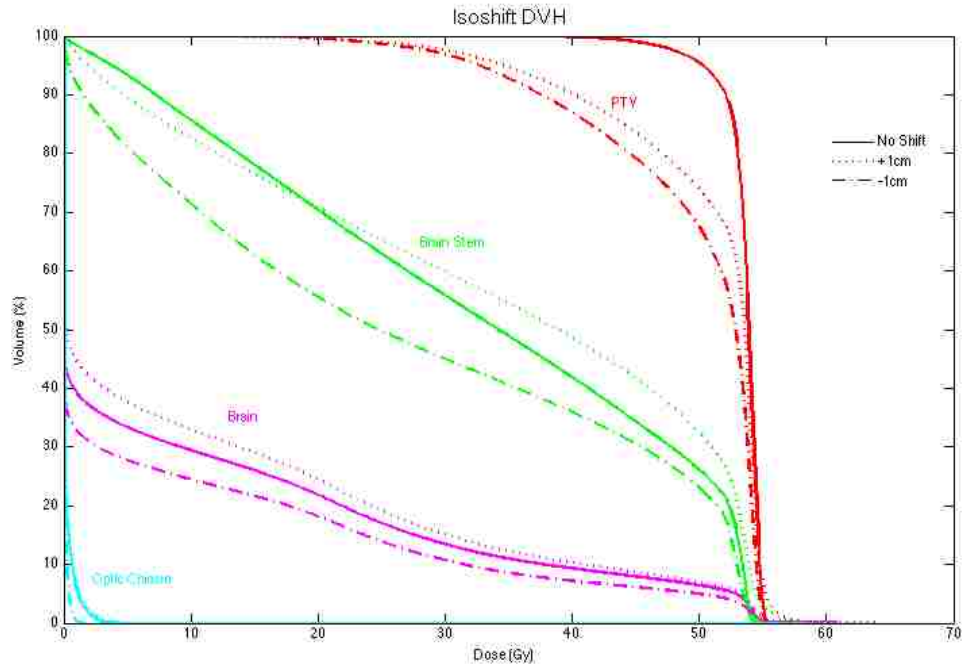
Figure C.18 DVH for patient 12 IMPT plans with an isocenter shift in the z direction.

Table C.16 PTV results for IMPT isocenter shifts in patient 12.

IMPT	D_{mean} (Gy-RBE)	D_{max} (Gy-RBE)	D_{min} (Gy-RBE)	$D_{95\%}$ (Gy-RBE)
Nominal	53.5	58.2	32.8	50.2
x+1cm	51.5	66.6	13.9	38.1
x-1cm	51.0	69.6	9.1	38.8
y+1cm	49.4	60.4	2.2	23.9
y-1cm	49.7	59.9	7.9	26.4
z+1cm	50.4	60.6	9.0	34.6
z-1cm	49.2	55.9	10.1	32.7

Table C.17 Mean and maximum doses to the brain for IMPT isocenter shifts in patient 12.

IMPT	D_{mean} (Gy-RBE)	D_{max} (Gy-RBE)
Nominal	9.9	60.9
x+1cm	9.8	69.0
x-1cm	9.5	69.8
y+1cm	9.8	63.6
y-1cm	9.4	62.8
z+1cm	11.1	64.1
z-1cm	8.1	58.4

Table C.18 Percentage volume of the brain receiving 5, 10, 50, 52, and 56Gy-RBE for IMPT isocenter shifts in patient 12.

IMPT	$V_{5Gy-RBE}$ (%)	$V_{10Gy-RBE}$ (%)	$V_{50Gy-RBE}$ (%)	$V_{52Gy-RBE}$ (%)	$V_{56Gy-RBE}$ (%)	NTCP
Nominal	33.4	29.4	6.4	5.6	0.0	0.015
x+1cm	33.6	29.5	5.6	4.7	1.06	0.014
x-1cm	32.5	28.8	5.0	4.1	0.81	0.012
y+1cm	32.7	29.0	6.4	5.5	0.35	0.016
y-1cm	32.2	28.4	5.7	4.7	0.35	0.012
z+1cm	37.6	33.0	6.9	6.1	0.39	0.021
z-1cm	27.7	24.5	5.0	4.2	0.02	0.007

The Vita

The son of Jack Freund and Cathy Scroggs, Derek Freund was born in Oklahoma City, OK in December of 1978. Following his graduation from Camdenton High school in Camdenton, Missouri, in 1997, Derek briefly attended Kansas State University before finally graduating from the University of Missouri-Columbia, Missouri in 2001 where he received a Bachelor of Science in Biology. After a brief stint as a personal trainer and bicycle mechanic Derek enrolled at the University of Missouri-St. Louis, Missouri where he studied physics.

After graduating with Bachelor of Arts in physic from MU-STL in 2009, Derek and his wife, Andrea Freund, moved to Louisiana to begin his studies in medical physics at Louisiana State University in 2011. In 2013, they celebrated the birth of their son, Liam, to add to their happy home. Derek will continue his training and education in medical physic in the medical physics residency program at Willis Knighton Cancer Center in Shreveport, Louisiana.